MODELING, SIMULATION AND MULTI-OBJECTIVE OPTIMIZATION OF AN INDUSTRIAL, LOW-DENSITY POLYETHYLENE REACTOR

NAVEEN AGRAWAL

NATIONAL UNIVERSITY OF SINGAPORE

2008

MODELING, SIMULATION AND MULTI-OBJECTIVE OPTIMIZATION OF AN INDUSTRIAL, LOW-DENSITY POLYETHYLENE REACTOR

NAVEEN AGRAWAL

(B.Tech, Indian Institute of Technology, Roorkee, India)

A THESIS SUBMITTED

FOR THE DEGREE OF DOCTOR OF PHILOSOPHY

DEPARTMENT OF CHEMICAL AND BIOMOLECULAR ENGINEERING

NATIONAL UNIVERSITY OF SINGAPORE

2008

Acknowledgements

I wish to express my deepest gratitude to Gurumata Bijaya. By her blessings, I always felt enlightened and peace of mind to face the challenges.

With all respect and gratitude, I wish to express my sincere thanks to my research advisors, *Prof. G. P. Rangaiah* and *Prof. A. K. Ray*. They have provided me the excellent guidance to work diligently and enthusiastically. I am overwhelmed with their constant encouragement and providing greater insights, invaluable suggestions and kind support for the last few years. I greatly respect their inspiration, unwavering examples of hard work and professional dedication.

I would like to convey my sincere thanks to Prof. S. K. Gupta, IIT Kanpur, India under whom I pursued part of my research. His mathematical expertise and wide range of knowledge and expertise were always instrumental in providing me the constant thrust to excel in research.

I would like to thank my parents and brothers for their affection, love and support at every stage of my life.

I am extremely thankful to my loved one – Monu who always encouraged and supported me with her deepest love and ideas.

I gratefully acknowledge the *National University of Singapore* which has provided me excellent research facilities and financial support in the form of scholarship.

Many thanks to Mr. Boey and non-technical staff of the department for their kind assistance in providing the necessary laboratory facilities and computational resources.

Last but not the least, I am lucky to have many friends who always kept me cheerful. I would like to thank Nidhi, Amit Gupta, Avinash Singh, Chand

Vishwakarma, Raju Gupta, Lee Nick, Yelneedi Sreenivas, Mekapati Srinivas, N. V. S. Murthy Konda, M. K. Saravanan, Ankur Dhanik, Manish Mishra, Naveen Bhutani, Bhupendra Singh, Lokesh B. Thiagarajan, G. Sundar, Ashok M. Prabhu, Desingh D. Balasubramaniam, Neha Tripathi and Koh Niak Wu for the good times spent together.

Table of Contents

Summary

Products made from polyethylene are very common in everyday life; these include kitchenware, containers for pharmaceutical drugs, wrapping materials for food and clothing, high frequency insulation, and pipes in irrigation systems. A very flexible and branched low density polyethylene (LDPE) is obtained commercially by high-pressure polymerization of ethylene, in the presence of chemical initiators (i.e., peroxides, oxygen, azo compounds), in long tubular reactors or well-stirred autoclaves. The polymerization in tubular reactors involves very severe processing conditions such as pressures from 150 – 300 MPa and temperatures from 325 – 625 K. No work in the open literature discusses multi-objective optimization (MOO) of LDPE tubular reactors even though multiple objectives are essential for overall optimum operation. Also, understanding the dynamic behavior of tubular reactor is essential in order to produce optimally thirty to forty grades of polymer in a single plant. Hence, this study focuses on modeling and simulation of LDPE tubular reactor and its optimization for multiple objectives for operation, design and grade-change policies.

A detailed survey of modeling studies on LDPE tubular reactors in the literature showed significant discrepancies in the kinetic rate parameters from different sources. Therefore, these kinetic data can not be relied on for simulation and optimization. Some authors have obtained these parameters by validating industrial results but they did not reveal the values of some parameters due to proprietary reasons. Thus, in our study, best-fit values of the model parameters are obtained by comparing the predictions with the available industrial data. This steady-state model is then used for

multi-objective optimization of an industrial LDPE reactor. Further, the reactor model with all parameter values, developed in this study, is available for any one to use.

Multiple objectives are important to the industry for best utilization of resources. The productivity of LDPE using high-pressure technology in industrial tubular reactor is reported to be 30 – 35% per pass which is quite low. At the same time, severe operating conditions deteriorate quality of the polymer due to formation of undesired side products (short chain branching and unsaturated groups). Therefore, reactors should be operated so as to minimize these side products and maximize the monomer conversion for a given feed flow rate, while the LDPE produced should have the desired properties defined in terms of number-average molecular weight. All these lead to constrained, multi-objective optimization problem.

In this study, the multi-objective problem for an industrial LDPE reactor is solved at both operation and design stage, using a binary-coded elitist non-dominated sorting genetic algorithm (NSGA-II) and its jumping gene (JG) adaptations. The difficulty in finding appropriate penalty parameter in penalty function approach led us to implement a systematic approach of constrained-dominance principle for handling the constraints in the binary-coded NSGA-II-JG and NSGA-II-aJG. The effectiveness of this approach is evaluated for the design stage MOO of the industrial LDPE reactor. The Pareto-optimal sets for both operation and deign problems are obtained. The results show that much higher monomer conversion at relatively lower side products can be obtained compared with the current industrial operating condition. The Pareto-optimal set gives many equally good points (non-dominated solutions) to the decision maker so that s/he can use her/his industrial experience and intuition to select one of these points for process design and/or operation.

A multitude of LDPE grades is usually produced from a single reactor. The major task in the operation of a tubular LDPE reactor is the minimization of off-spec polymer production during a grade transition. Hence, a comprehensive dynamic model is developed and used for optimizing the grade-change policies so as to minimize the grade change-over time and off-spec polymer defined in terms of polymer properties. The Pareto-optimal solutions of this dynamic optimization problem are successfully obtained using NSGA-II-aJG. The resulting optimal grade-change policies are better in terms of reaching the new steady-state faster with relatively less off-spec product.

Considering the unavailability of complete details of an LDPE tubular reactor model in the open literature and lack of MOO studies on LDPE reactors for industrially important objectives, the present work, its approach and results are of significant interest to both researchers and practitioners.

Nomenclature

A	frequency factor (1/s; m^3/kmol-s; $m^{3.3}$/$kmol^{1.1}$-s)
C_i	concentration of the i^{th} component (kmol/m^3)
C_P	specific heat of the reaction mixture (kJ/kg-K)
D_e	equivalent diameter of the jacket (m)
D_{int}	inside diameter of reactor (m)
D_{jacket}	inner diameter of jacket wall (m)
D_o	outer diameter of the inner (reactor) pipe (m)
E	activation energy (kJ/kmol)
E_v	activation energy for viscous flow (kJ/kmol)
F_i	flow rate of the i^{th} component (kg/s)
f_m	initiator efficiency
f_r	friction factor
G_i	i^{th} objective function in multi-objective optimization problem
J_i	i^{th} objective function
ΔH	heat of polymerization (kJ/kmol)
h_i	inside (the reactor) film heat transfer coefficient (W/m^2-K)
h_o	outside (jacket side of reactor) film heat transfer coefficient (W/m^2-K)
h_w	wall (reactor) heat transfer coefficient (W/m^2-K)
I_i	i^{th} initiator
K	thermal conductivity of the reaction mixture (W/m-K)
k	kinetic rate constant (1/s; m^3/kmol-s; $m^{3.3}$/$kmol^{1.1}$-s)
L	reactor length (m)
l_{aJG}	length of the replacing jumping gene

l_{chrom}	total length (number of binaries) of a chromosome
l_{substr}	length (number of binaries) of a substring representing a decision variable
L_t	total reactor length (m)
L_{zi}	axial length of i^{th} zone (m)
M	monomer
M'	molecular weight of ethylene (kg/kmol)
M_e	methyl end group (short-chain branches)
M_n	number-average molecular weight
N_{gen}	generation number
N_{pop}	total number of chromosomes in the population
Nu	Nusselt number
o	oxygen (initiator)
P	reactor pressure at any axial position (MPa)
Pr	Prandtl number
P_c	critical pressure (MPa)
$P_i(x)$	dead polymer molecule with x monomer units and i long-chain branches
p_c	crossover probability
p_{JG}	jumping probability for the JG operator
p_m	mutation probability
R	ideal gas constant (kJ/kmol-K)
Re	Reynolds number
$R_i(x)$	growing macro-radical with x monomer units and i long-chain branches

S	solvent (telogen)
S_r	seed for random number generator
T	temperature of the reaction mass (K)
T_c	critical temperature (K)
$T_{J,i}$	jacket fluid temperature in the i^{th} jacket (K)
T_r	reduced temperature
U	overall heat transfer coefficient (W/m^2-K)
ΔV	activation volume (m^3/kmol)
V_i	vinyl group
V_{id}	vinylidene group
$V_{J,i}$	flow rate of jacket fluid in i^{th} jacket (m^3/s)
V_M	specific volume of monomer (kg/m^3)
V_p	specific volume of polyethylene (kg/m^3)
v	velocity of the reaction mixture (m/s)
$v_{J,i}$	velocity of coolant in the i^{th} jacket (m/s)
w_i	weighting factor in the i^{th} objective function
W_M	monomer weight fraction
W_p	polymer weight fraction
X_M	monomer conversion at any axial position
z	axial distance (m)

Greek symbols

ΔP	pressure drop (MPa)
$\underline{\delta}_{ij}$	delta of Kronecker
η	dense gas viscosity of the monomer (Pa-s)

η^o	low-pressure monomer viscosity (Pa-s)
η_s	viscosity of the ethylene-polyethylene solution (Pa-s)
λ_{np}	n, p order moments for the chain length distribution of macro-radicals (kmol/m^3); n = 0, 1; p = 0, 1, 2
μ_J	viscosity of the jacket fluid (Pa-s)
μ_{np}	n, p order moments for the chain length distribution of the dead polymer molecules (kmol/m^3); n = 0, 1; p = 0, 1, 2
ξ	defined in Eq. 4.6b in Table 4.2 (Pa-s)$^{-1}$
ρ	density of the reaction mixture (kg/m^3)
ρ_J	density of the jacket fluid (kg/m^3)
ρ_M	monomer density (kg/m^3)
ρ_r	reduced density

Subscripts

b	β-scission of a secondary radical
bb	backbiting
b1	β-scission of a tertiary radical
d	desired value
dm	decomposition of m^{th} peroxide (initiator); m = 1, 2
f	(final) reactor exit
I,m	m^{th} initiator; m = 1, 2
in	inlet of reactor
J	jacket
M	monomer
M_e	methyl end group

max	maximum
o	oxygen (initiator)
p	propagation
S	solvent
tc	termination by combination
tdt	thermal degradation
trm	chain transfer to monomer
trp	chain transfer to polymer
trs	chain transfer to telogen or solvent
V_i	vinyl group
V_{id}	vinylidene group

List of Figures

List of Tables

Chapter 1

Introduction

1.1 Polyethylene and its Significance

Products made from polyethylene (PE) are very common in everyday life. The prevalence of polyethylene can be noted by the variety of products made form polyethylene such as kitchen utility ware, containers for pharmaceutical drugs, wrapping materials for food and clothing, high frequency insulation, and pipes in irrigation systems. PE is the largest production polymer with annual worldwide output of almost 84 millions tonnes (Kondratiev and Ivanchev, 2005). 25% of this is low-density polyethylene (LDPE) produced in auto-clave and tubular high-pressure reactors and remaining comprises of high-density polyethylene (HDPE) and linear low-density polyethylene (LLDPE) in low pressure reactors. The production of LDPE at high-pressure using tubular reactors is an important commercial process despite many developments in low-pressure processes such as gas phase and slurry polymerization.

Density and degree of branching are the most important physical and molecular characteristics of PE, respectively. In the past, the PE industry was conveniently classified by product density and process type. LDPE, in the density range of 910 to 925 kg/m^3, is manufactured by a high-pressure process. Medium density polyethylene lies in the range of 926 to 940 kg/m^3. HDPE (Linear Polyethylene), synthesized by a low pressure process, has a density in the range of 941 to 961 kg/m^3 (Kiparissides et al., 1993a). Low pressure processes are further classified into three categories namely suspension process, solution process, and gas process. LLDPE comprising a wide density range of 880 to 950 kg/m^3 is produced at low pressure by copolymerization of

ethylene with an alpha-olefin, such as 1-butene, 1-hexene or 1-octene. Polymer chains are branched at high temperature due to occurrence of side reactions. The density of PE is determined by the degree of short chain branching (SCB). The density and crystallinity are inversely proportional to the SCB. Today, PEs are more appropriately described as branched PEs and linear PEs.

Branched PE is made with a free-radical catalyst and contains long-chain branches (LCB). Linear PE is made with a transition metal catalyst and copolymerization of ethylene with an alpha-olefin and contains no long-chain branching. Both branched and linear PE may contain SCB as shown in Figure 1.1. The range of SCBs (CH_3 per 1000 C) for the three common PEs are:

LDPE: 10 – 50 [SCB = 30 per 1000 C (Gupta et al., 1985) for typical LDPEs]

HDPE: 2 – 3

LLDPE: 3 – 30

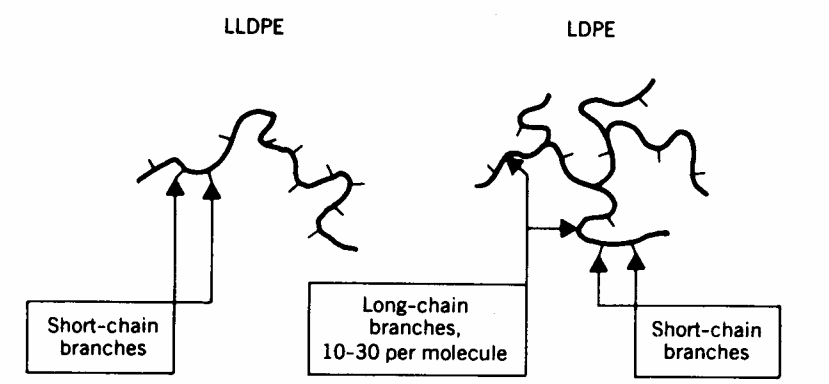

Figure 1.1 Molecular Structure: Branched Vs Linear Polyethylene

The molecular weight of LDPE ranges from waxy products at about 500 kg/kmol to very tough products at about 60,000 kg/kmol. One unique feature of LDPE, as opposed to HDPE or LLDPE, is the presence of both LCB and SCB along the

polymer chain. Another important feature of LDPE is its ability to incorporate a wide range of comonomers that can be polar in nature along the polymer chain.

1.2 LDPE Process Technology

A very flexible and branched LDPE, typically in the range of 915 – 925 kg/m^3, is obtained commercially by high-pressure polymerization of ethylene, in the presence of chemical initiators (i.e. peroxides, oxygen, azo compounds), in long tubular reactors (Figure 1.2) or well-stirred autoclaves. This process in tubular reactors involves extreme process conditions, namely, 150 – 300 MPa and 325 – 625 K.

A tubular reactor typically consists of several hundred meters of jacketed high-pressure tubing as long as 1.6 km arranged as a series of straight sections connected by 180 degree bends. Inner diameters of 25 – 75 mm have been quoted, but 60 mm or somewhat larger is probably typical of modern tubular reactors. Wall thickness equal to inner diameter is used to provide the necessary strength for the high-pressure involved. The first section of the tubular reactor behaves as a preheater to raise ethylene to a sufficiently high temperature for polymerization to start. This temperature depends on initiator employed, ranging from 190 °C for oxygen to 140 °C for a peroxydicarbonate. The latter part of the tubular reactor acts as a product cooler.

The heat of polymerization and specific heat of ethylene are 89.57 kJ/mol (3199 kJ/kg) and 2168 J/kg-K (Chen et al., 1976), respectively. Thus, adiabatic temperature rise in the gas phase is around 15 °C for each 1% conversion of monomer to polymer. Therefore, heat removal is a key factor in a commercial polymerization process. This heat of reaction is partially transferred to water flowing co- or counter-currently through the reactor jacket. But it is not possible to maintain isothermal conditions, and temperature peaks occur.

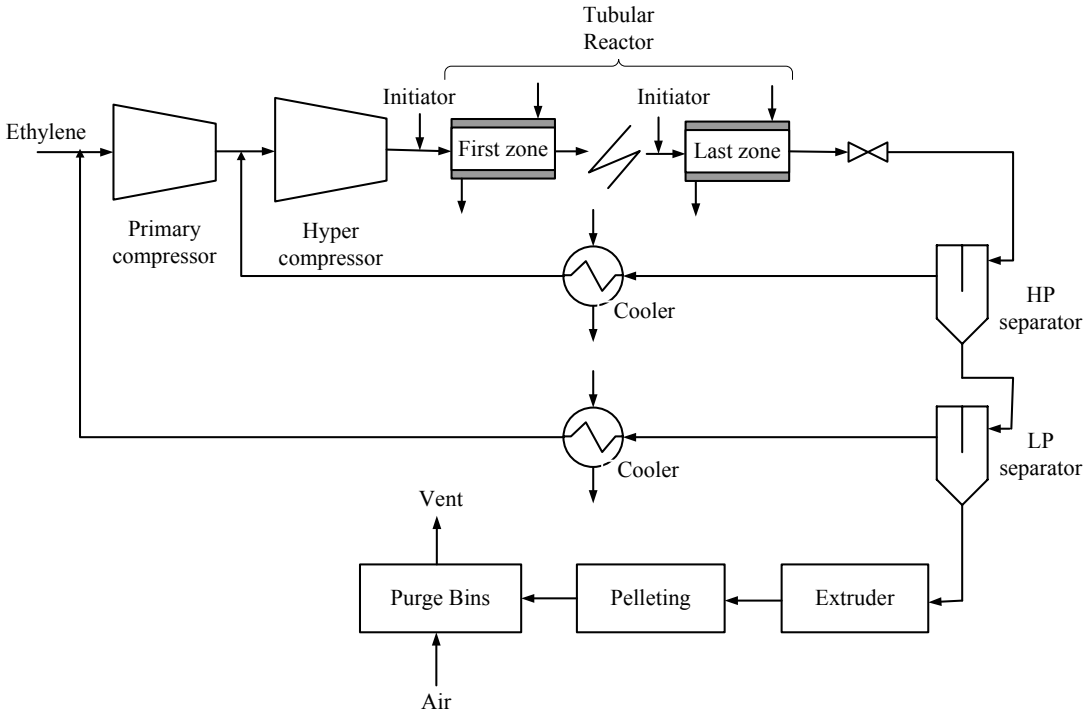

Figure 1.2 Simplified Diagram of the High-pressure Polyethylene Process

Reactor feed includes ethylene, oxygen and/or initiators and chain transfer agents. A commercial reactor may be divided into multiple reactor zones, heating and cooling zones. However, multiple temperature peaks, responsible for increasing the conversion, are obtained by injecting initiators, monomer, and solvents in different tubular reactor zones. Conversion of ethylene is reported in the range of 20-35% in the literature. PE is precipitated in the boundary layer (near to any relatively cold surfaces in the reactor or downstream lines) due to its solubility in ethylene at very high pressure. The build up of the polymer on the wall, if not removed, can lead to the runaway reaction due to decreased heat transfer from the hot gas-polymer solution. The precipitated PE from the wall is eliminated by opening the expansion valve more fully than required, about once every 2 – 3 seconds, causing a decrease in pressure by as much as 300 – 600 atm. The concomitant rapid increase in velocity of the gas

phase shears the walls and strips off any deposited PE so that a reasonably steady-state heat transfer situation exists.

The product mixture containing unconverted ethylene and PE is sent to a series of high- and low- pressure separators where polymer is obtained. These are also termed as primary- and secondary separators. The unconverted ethylene is cooled and de-waxed prior to being recycled to primary- and hyper- compressors, whereas molten polyethylene obtained from the low pressure separator is fed into an extruder to be pelleted, cooled and finally sent to storage.

1.3 LDPE Reactor Modeling and Optimization

In the past 30 years, various complex mathematical models have been developed to produce LDPE in high-pressure tubular reactors. These models are reviewed in detail in chapter 2 of this thesis. These models provide a sound basis for mathematical description of production of LDPE in commercial plants. But, they sometimes present complexities in the system. Thus, some assumptions are made to simplify the model without loosing its validity in commercial processes. In particular, the following model assumptions should be emphasized while studying a mathematical model in LDPE tubular reactor.

1. Physical state of the reaction mass mixture – one phase versus two phase system.
2. Kinetic mechanism and selection (estimation) of the kinetic parameters
3. Reactor flow conditions and mixing effects
4. Variation of the physical properties of the reaction mixture
5. Average jacket fluid temperature

6. Heat of reaction due to chain initiation, termination and transfer reactions is negligible.
7. Constant initiator efficiency

In general, a mathematical model for a tubular reactor includes a set of non-linear differential equations coupled with algebraic equations. These model equations take into account the conservation of various molecular species, total mass, energy, and momentum in the reactor and variation of kinetic, physical, and transport parameters with respect to operating variables.

A comprehensive mathematical model for LDPE production in tubular reactor should be able to predict the profiles of monomer conversion, initiator conversion, reaction mass temperature, pressure, the moments of free-radical and polymer chain length distribution, the SCB and LCB, and the number of unsaturated bonds (vinyl and vinylidene content) in the polymer chains. These quantities are affected by initiator concentration, inlet temperature and pressure, concentration of chain transfer agent, heat transfer coefficient, and other design and operating variables in the process.

Out of LDPE's annual production of almost 84 million tonnes worldwide, 22 million tonnes is produced by high-pressure technology (Kondratiev and Ivanchev, 2005). Therefore, even small improvement in the economic performance (polymer production) can generate huge revenues for the polyolefin industry. Various grades of LDPE are required due to its commercial application in diverse polymer products. These grades require different physical, chemical, and mechanical properties which are difficult to express in a single objective function. The end properties of polymer, viz. tensile strength, stiffness, tenacity etc. are related to molecular parameters. These parameters include average molecular weight, polydispersity index, SCB and LCB, distribution of functional groups etc. Therefore, the end properties of a polymer will

depend on the precise control of these variables. However, the end properties are generally experimentally measured, and define the quality and strength of the polymer. The operating and design variables often influence the molecular parameters in non-commensurable ways. Therefore, these applications are perfect scenarios for multi-objective optimization (MOO).

The LDPE, which is produced in the tubular reactor at high pressure conditions, consists of several short chain branches, primarily, ethyl and butyl groups. These branches deteriorate quality and strength of the polymer by lowering crystallinity, density, melting point, tensile strength, etc. (Luft et al., 1982). Therefore, these groups should be minimized to enhance quality and strength of the product. Also, some unsaturated groups (vinyl and vinylidene) are present in the LDPE chains, which make the product susceptible to cracking due to oxide formation. Hence, the minimization of these groups enhances the strength of the polymer product. Another important objective is to maximize the monomer conversion per pass for the constant monomer feed to the reactor. Indeed, any amount of improvement in the production by such studies leads to significant profits to the PE industry.

Various polymer grades are required in the industry for different end-uses. These grades are defined by the number-average molecular weight, $M_{n,f}$, of the polymer product. Therefore, an end-point equality constraint on the $M_{n,f}$ is imposed to meet the market requirements. Reaction mixture temperature may shoot up to a very high value due to exothermic polymerization reactions. Therefore, safe operation of the reactor is ensured by putting an inequality constraint on reactor temperature, locally, to avoid run-away condition.

1.4 Motivation and Scope of Work

Several publications (Asteasuain et al., 2001a, Asteasuain et al., 2001b; Asteasuain et al., 2001c; Cerventes et al., 2000; Iedema et al., 2000; Zhou et al., 2001; Bokis et al., 2002 etc.) were coming out on improving the modeling approach of tubular reactor. These mathematical models were reviewed by Kim and Iedema (2004), Kiparissides et al. (1993a), and Zabisky et al. (1992). The economic importance of the process and the necessity of studying safely and economically the influence of the different design and operating variables, have motivated us the development of a mathematical model for the LDPE tubular reactor. Also, no work was done on multi-objective optimization of these reactors which motivated us to choose this process. In fact, in the recent past, there are several studies published on the tubular reactor processes, which show the interest and development of this process in industrial and research community (Kim and Iedema, 2004; Kiparissides et al., 2005; Buchelli et al., 2005a; Buchelli et al., 2005b; Buchelli et al., 2005c; Hafele et al., 2005; Hafele et al., 2006; Asteasuain and Brandolin, 2008). In fact, SABIC UK Petrochemicals is commissioning soon the new LDPE plant based on tubular reactor technology (www.**sabic**.com/corporate/en/binaries/Annual%20Report-2006_tcm4-3241.pdf). Similarly, three new plants in People's Republic of China have been started earlier in this year and one more plant in Bangkok is starting-up in the 4th quarter of 2008 (http://www.azom.com/news.asp?newsID=3610); all these use high-pressure tubular reactor technology. There may be more plants coming in the near future using tubular reactor technology which justifies its continuous development and application in the industrial sector.

Several detailed studies have been reported on the modeling of LDPE tubular reactor in the literature. The most interesting observation that can be made from these

studies is the significant discrepancies in the values of the rate constants. Therefore, these data can not be relied on to simulate the industrial LDPE tubular reactor. In more recent studies, the kinetic parameters are estimated using industrial data but, again, they did not provide the complete details due to proprietary reasons. Therefore, it gives motivation to develop a sufficiently complex model using industrial data available in the literature and tune the model to estimate the kinetic parameters and provide the reasonable values for all the missing information. Therefore, we provided a descriptive steady-state model which is quite complete and useful for researchers. Best-fit values of several model parameters are obtained using the reported industrial data. This model is then used to optimize the steady-state operation and design of LDPE tubular reactor.

Even though the process of LDPE production in tubular reactor is well established but there are few studies, available in the literature, which deal with dynamic behavior of this process. Also, relatively simpler models have been presented in the literature for analysis of dynamic behavior. Thus, we developed a comprehensive dynamic model which comprises the time and spatial variations of all the physical and transport parameters. Also, it includes the detailed reaction kinetic mechanism which provides SCB, and the number of unsaturated bonds (vinyl and vinylidene content) in the polymer chains. Thereafter, this dynamic model is used in minimizing the amount of off-specification polymer for a grade change-over problem, using dynamic optimization methods.

A detailed literature review shows that a very limited work on MOO of LDPE tubular process is carried out. In these studies, MOO problems were solved using a single scalar objective function, which was a weighted average of several objectives ("scalarization" of the vector objective function). This process allows a simpler

algorithm to be used, but unfortunately, the solution obtained depends largely on the values assigned to the weighting factors used, which is done quite arbitrarily. An even more important disadvantage of the scalarization of the several objectives is that the algorithm may miss some optimal solutions, which can never be found regardless of the weighting factors chosen (Zhou et. al., 2000).

In recent years, a robust technique, genetic algorithm (GA), and its adaptations have become very popular for complex processes (MOO of steam reformers by Rajesh et al., 2000; and PMMA reactors by Zhou et al., 2000). These do not need any initial guesses. It uses a population of several points simultaneously, and it works as well with probabilistic (instead of deterministic) operators. In addition, it uses the information on the objective function and not its derivative, nor does it require any other auxiliary knowledge. An elaborate description of GA is available in Holland (1975), Goldberg (1989) and Deb (2001). One of its recent adaptations, the elitist non-dominated sorting genetic algorithm (NSGA-II; Deb et al., 2002) can be used to solve MOO problems. The performance of NSGA-II has been further enhanced by incorporating one of several recent jumping gene (JG) adaptations. Kasat and Gupta (2003) observed that the JG concept borrowed from nature provides the genetic diversity in the pool thus counteracting the negative effect of elitism; overall, it decreases computational time (number of generations) required for solving the multi-objective problem. In this study, constrained MOO problems at operation and design stage are solved using binary-coded NSGA-II and its JG adaptations.

Multiple objectives are important to the industry for the best utilization of resources and maximization of productivity while minimizing the side products which are responsible for degradation of polymer quality and strength. Different polymer grades are required for various applications in the downstream products. These results

in constraints on polymer properties which are defined in terms of easily measurable quantities such as M_n. Reactor should also be operated in the safer region to avoid run-away situation due to decomposition of ethylene. All these lead to constrained MOO problems. The correct global optimal solutions could not be obtained when equality constraint on $M_{n,f}$ is placed. But, the Pareto-optimal sets are obtained when softer constraints on $M_{n,f}$ are used. A Penalty function method is used to handle the constraints.

Although binary-coded NSGA-II-JG and NSGA-II-aJG performed better than NSGA-II in multi-objective operation optimization of an industrial LDPE tubular reactor near the hard-end point constraints, but constraints in these JG variants of NSGA-II are dealt with penalty function method. Deb (2001) showed that the penalty parameter for handling constraints plays an important role in multi-objective evolutionary algorithms. If the parameter is not chosen properly then it may create a set of infeasible solutions or a poor distribution of solutions. Therefore, a systematic approach of '*constrained-dominance principle*' for handling the constraints was proposed by Deb et al. (2002) for MOO. This shows the need for further improving JG variants of NSGA-II for handling the constraints. The current study also presents successful application of *constrained-dominance principle* in the binary-coded NSGA-II-aJG and NSGA-II-JG for handling the constraints for the first time.

1.5 Organization of Thesis

This dissertation is organized into seven chapters. Following this introduction to the high-pressure technology to produce LDPE in tubular reactors, in the subsequent chapter, several reaction kinetic schemes, various modeling and optimization work and recent developments of LDPE production in tubular reactor are reviewed. This is

followed by a review on multi-objective evolutionary algorithms and their applications in chemical engineering problems.

In Chapter 3, the methodology of NSGA-II and its JG variants is described in detail. Their implementation for MOO of industrial LDPE tubular is discussed. Thereafter, working principles of two constraint handling technique, i.e., penalty function method and *constrained-dominance principle* are given for handling the constraints. The implementation of *constrained-dominance principle* in JG variants of binary-coded NSGA-II is narrated and its performance is investigated on several test problems.

Chapter 4 includes the process description, detailed reaction kinetic scheme, and model assumptions required in modeling and simulation of industrial LDPE tubular reactor. Then, the steady-state model is tuned with the available industrial data and it is used in multi-objective operation optimization of tubular reactor. The objective functions: maximization of monomer conversion and minimization of normalized side products at the reactor exit, are optimized simultaneously using binary-coded NSGA-II and its JG adaptations. A four-objective optimization problem (with each of the three normalized side products concentrations taken individually as objective functions) is also formulated.

In Chapter 5, a brief introduction to modeling and simulation of LDPE tubular reactor is provided. Thereafter, MOO problem at design stage is formulated which includes reactor design variables and therefore increases the complexity of the problem by expanding the decision variable space. The two objectives were similar to what were used in operation stage optimization. The constraints are handled by penalty function method and *constrained-dominance principle* and the results obtained using these methods are compared. A three-objective optimization problem

with the compression power (associated with the compression cost) as the third objective along with the aforementioned two objectives, is also studied.

In Chapter 6, the steady-state model of Agrawal et al. (2006) is modified to study the dynamic behavior of an industrial tubular reactor. The dynamic model contains differential, partial differential and algebraic equations inclusive of the detailed reaction mechanism and kinetics. The dynamic model is used to study the effects of the disturbances in inlet pressure and concentrations of initiators and telogen on transient profiles of polymer properties, monomer conversion, and reactor temperature. Thereafter, the dynamic model is used to optimize the grade transition policies.

All the inferences and conclusions made from this research work and the directions for the future work are summarized in the Chapter 7.

Chapter 2

Literature Review

2.1 Introduction

This chapter starts with the reaction mechanism used in production of LDPE. Note that LDPE can be produced in tubular and autoclave reactors using high-pressure technology. However, we are referring to LDPE production in tubular reactors using high-pressure technology in entire work. LDPE is produced by free-radical polymerization in presence of initiators and ethylene. The detailed literature on various possible reactions is provided in this chapter.

LDPE is produced in tubular reactor at extremely critical conditions, namely, in the range of 325 – 625 K and 150 – 300 MPa. Thus, it poses safety and other associated constraints on experimentation of this process. This gave an impetus to research community to work on mathematical model which could alleviate the need of experimentation and describes the complex behavior of the process. The modeling of this process started in late sixties and plethora of steady-state models are now available in literature which are reviewed in section 2.3. Many steady-state models are available in the open literature but only a few studies deal with the dynamic models. Subsequently, these dynamic models are also reviewed.

The productivity of LDPE using high-pressure technology in industrial tubular reactor is reported to be 30 – 35% per pass which is quite low. Thus, even small improvement in the reactor performance may lead to high-revenue to the poly-olefin industry. Therefore, process industry always aims to maximize the monomer conversion. At the same time, due to complex operating conditions, quality of polymer also deteriorates and pose safety constrains on reactor operation. Thus,

studies comprising of LDPE reactor optimization at steady-state, unsteady-state and for grade transition are reviewed in the last section.

2.2 Reaction Kinetics

A lot of work has been done on the kinetics of free-radical ethylene polymerization due to commercial importance of the high-pressure process (Woodbrey and Ehrlich, 1963; Ehrlich and Mortimer, 1970; Luft et al., 1982 and 1983; Goto et al., 1981; Brandolin et al., 1996). The conventional high-pressure process operates by a free-radical mechanism. Free radicals are generated by decomposition of initiators (organic peroxides, oxygen, azo compounds) employed at different locations of the tubular reactor. The generation of free radicals is called initiation.

Oxygen was used as initiator in the early industrial process due to its ease of feeding into the reactor. However, with the development of high-pressure pumps and compressors and new initiators, new plants employ solutions of liquid catalyst. This is to ensure the precise control of temperature profiles inside the reactor. The mechanism by which oxygen generates the free-radicals is rather complicated and it is not well understood. It can act as inhibitor at lower temperatures. In general, oxygen is believed to react in multi-step manner where oxygen first reacts with monomer to form peroxides. These peroxides then decompose and progressively react with monomer to generate chain radicals which initiate the polymerization. Tatsukami et al. (1980) studied the oxygen initiation of ethylene at high-pressures. They postulated the reactions which account for initiation and inhibition effects of oxygen. In the tubular reactor process, oxygen is still widely used, either alone, or sometimes in combination with liquid initiators. Brandolin et al. (1988) fitted the measured

temperature profile to obtain the kinetic rate parameters. Reaction rate order of 1.1 with respect to oxygen for the initiation reaction involving monomer and oxygen as reactants was obtained in their work. The initiators are selected based on their half lives at the reaction temperature. Their half lives should be in the range of 1 s to get control over the reaction rate. The initiators should be readily soluble in the alkanes and should produce active radicals.

Bubak (1980) demonstrated the thermal initiation of ethylene in the experimental studies carried out at high-pressures up to 2500 atm and temperature between 180 to 250 ºC. The overall order for this reaction was reported to be three. The thermal polymerization is very slow and thought to be very minor for ethylene at certain operating conditions (Brandolin et al., 1988). However, Hollar and Ehrlich (1983) discussed that this reaction might be important at higher temperatures causing run-away conditions in the tubular reactor.

The free radicals react with ethylene to form a primary alkyl radical. These radicals add to ethylene molecules during propagation and increase the chain length. The growing radicals react with each other and form one or two dead polymers due to termination by combination or by disproportionation, respectively. A terminal double bond is formed in the dead chain from the disproportionation reaction. Thermal degradation is another termination reaction in which growing radical dissociates into dead chain and initiation radical.

Active free-radical sites on a live polymer chain can jump to a solvent, monomer, or modifier molecule, or the radical site could break away from the live polymer chain. It can also jump to another site on the same polymer chain or another polymer chain. These chain transfer reactions, which can affect the size, structure, and end groups on the polymer, are described below.

In chain transfer to monomer, transfer of the active radical can occur between a live polymer chain and a monomer molecule (ethylene).

$$\sim CH_2 - \dot{C}H_2 \; + \; C_2H_4 \xrightarrow{k_{trm}} \sim CH_2 - CH_3 \; + \; CH_2 - \dot{C}H$$

A dead polymer chain and a new polymer radical are formed. This reaction occurs through a hydrogen abstraction mechanism and leaves an unsaturated end segment on the dead polymer chain. Chain transfer to monomer is small in case of ethylene. This reaction is quite similar in other monomer systems as well.

Chain transfer agents such as impurities (propane, butane, hexane etc), are added in the reaction mixture to control the chain length of growing molecule or in other words the molecular weight of growing polymer. Reactivity of a growing macromolecule is transferred to the telogen leading to formation of dead polymer and initiation radical, in chain transfer to solvent reaction (Zabisky et al., 1992). Such reactions occur via the same mechanism (hydrogen abstraction) as chain transfer to monomer.

$$\sim CH_2 - \dot{C}H_2 \; + \; R - CH_3 \xrightarrow{k_{trs}} \sim CH_2 - CH_3 \; + \; R - \dot{C}H_2$$

LCBs are produced in LDPE through an intermolecular chain transfer reaction between a polymer radical and a dead polymer chain. The active radical attacks the dead chain at an internal carbon, transferring the radical to the dead chain and terminating itself. The new polymer radical then continues to propagate from the free radical on the internal carbon to form a long chain branch. Pladis and Kiparissides (1998) concluded that chain transfer to polymer is the primary reaction in the formation of LCBs. These branches widen the molecular weight distribution in high pressure PEs. The reactions of termination by disproportionation, β-scission and transfer to monomer produce polymer chains with terminal double bonds. These double bonds might react with radicals and can propagate to form LCBs (Zabisky et

al., 1992). The LCBs can also be obtained using metallocene catalyzed low pressure ethylene polymerization.

$$\sim CH_2 - \dot{C}H_2 \; + \; \sim CH_2 - CH_2 \sim \xrightarrow{k_{trp}} \sim CH_2 - CH_3 \; + \; \sim CH_2 - \dot{C}H$$

The back-biting or intramolecular chain transfer reaction is the major source of SCBs in LDPE. The number of short chain branches found on the backbone polymer chain primarily controls the density of homopolymer LDPE. Chain transfer can also occur within the growing free radical or between the two growing chains. The former is called intra-molecular chain transfer or back-biting reaction, and accounts for the SCBs. The latter reaction, inter-molecular chain transfer, produces LCBs in LDPE. The back-biting reaction, which was proposed by Rodel (1953), occurs with the carbon atom preceded by four carbons back down the chain. Subsequent studies have shown that these branches contain entirely ethyl- and butyl-groups along the chain. These groups are formed due to second back-bite which occurs immediately after the first was done, which was investigated and concluded by Willborn (1959) by infra-red treatment. Experimental evidence has been presented for multiple back-bites also. These short branches account for the lower crystallinity, density, melting point, and other associated physical properties of commercial high-pressure polyethylene.

$$\sim CH_2 - CH_2 - CH_2 - CH_2\cdot \xrightarrow{k_{bb}} \sim CH_2 - \dot{C}H - CH_2 - CH_3$$

Another structural impurity known to exist in polyethylene produced at high pressure is vinyl and vinylidene type unsaturation. The formation of vinyl and vinylidene type unsaturation is closely associated with the SCB mechanism. These unsaturations are due to the scission of secondary and tertiary radicals. The ‘multiple back-biting’ mechanism can lead to tertiary radicals which undergo β-scission to form vinylidene.

$$\sim CH_2 - \dot{C}H - C_4H_9 \xrightarrow{k_{b1}} \sim CH_2 - CH = CH_2 + CH_3CH_2\dot{C}H_2$$

Similarly, the formation of vinylidene groups (> C ═ CH_2) can be explained by the following scission reaction of tertiary radicals:

$$\sim CH_2 - \overset{C_2H_5}{\overset{|}{\dot{C}}} - CH_2 - C_4H_9 \xrightarrow{k_b} \sim CH_2 - \overset{C_2H_5}{\overset{|}{C}} = CHCH_3 + CH_3CH_2\dot{C}H_2$$

The thermal decomposition of monomer and polymer into carbon and a mixture of methane and hydrogen is highly exothermic reaction which may result in reactor run away in the form of huge temperature, and hence the pressure evolution.

2.3 Reactor Modeling and Simulation

Ethylene, along with oxygen, initiators and telogens, is used as main building block to produce LDPE by free radical polymerization in a tubular reactor at very rigorous conditions. An appropriate mathematical model for the process should be able to predict the product properties as close as possible to the real plants. The accuracy of model depends on various assumptions made in the model. Thus, a model builder should keep in mind that one must often compromise model details and complexity with available information and final use of the model. The model alleviates the use of pilot plant and trial-and-error procedures in the industrial plants. Also, it helps in understanding the effects of operating variables on the product properties and estimating the optimal operating conditions to achieve certain performance criteria.

A detailed study has been carried out on modeling of LDPE process (Agrawal and Han, 1976; Chen et al., 1976; Goto et al., 1981; Donati et al., 1982; Zabisky et al., 1992; Kiparissides et al., 1993b; and Brandolin et al., 1996). Agrawal and Han (1975) studied the effects of axial mixing and various operating parameters on the reactor

performance. In tubular reactors, pressure pulse is sent using control valve for a short time which subsequently increase the reaction mixture velocity and strip the deposited polymer in the tubular reactor wall. Some researchers have argued that this pulse valve effect inside the LDPE tubular reactor should be modeled with axial mixing in the plug flow. Chen et al. (1976) showed that axial mixing can be neglected for all practical purposes using the same reactor system of Agrawal and Han (1975). Their observations were based on Peclet number which was quite high due to high Reynolds number (large turbulence). Moreover, Donati et al. (1982) and Yoon and Rhee (1985) also observed that axial mixing has minor effect on the reactor performance and therefore can be neglected under typical industrial operating conditions.

In most of the studies, single phase (homogeneous phase) of ethylene and polyethylene is assumed. This will be a good assumption because the reaction mixture is homogeneous under many industrial operating conditions. Zabisky et al. (1992) showed that polymer-rich phase may exist near the tube wall and reaction rates will be much different there. However, they discussed that a typical characteristic, grainy film appearance, of two-phase resins is not observed in the LDPE produced from high-pressure tubular reactors. Thus, the assumption of single phase was employed in their modeling study. Bubak (1980) showed that the reaction mixture exists as single phase in an extended pressure and temperature region above 1500 bar and 150 ºC, respectively.

Many studies have used constant velocity along the tube length which varies with the reaction mixture density. The density depends on reaction mass temperature, pressure, and composition and therefore it varies along the tubular reactor axis. Thus, variation in velocity should be accounted in a comprehensive model.

A detailed survey of modeling studies on LDPE reactors in the open literature showed significant discrepancies in the kinetic rate parameters from different sources as summarized by Gupta et al. (1985). Therefore, these kinetic data can not be relied on for simulation and optimization. It gave us an impetus to look for the model which used the kinetic data to verify the industrial result. Brandolin et al. (1996) calculated rate parameters and molecular-weight parameters by non-linear regression from measured temperature profile and molecular properties. However, they showed the kinetic rate parameters for initiators and telogen in a range due to confidential reasons. Zabisky et al. (1992) also did not reveal the kinetic rate parameters obtained after validation of model to industrial data due to proprietary reasons. Asteasuain et al. (2001b) gave the design features, steady-state operating conditions, measured temperature profile along the reactor length, monomer conversion and number-average molecular weight at reactor exit. They adopted the simplified model and kinetic parameters from Brandolin et al. (1996) and Asteasuain et al. (2001a). The model selected from Asteasuain et al. (2001b) was modified in our study. Physical properties variations and pressure variation along the axial length are included in the model. Chain transfer to polymer, β-scission of secondary radical and tertiary radicals reactions are involved in reaction kinetic scheme apart from the reactions taken from Asteasuain et al. (2001b). These reactions affect the SCB and LCB. An error function representing the sum of the square of difference between the model predicted and industrial values is employed for getting the best-fit (tuned) values of the parameters in the model. The similar approach has been reported in the literature (Brandolin et al., 1988; Zabisky et al., 1992; Brandolin et al., 1996; and Asteasuain et al., 2001a; in production of LDPE in high-pressure tubular reactor; Bhaskar et al., 2001 on PET and nylon 6 by Wajge et al., 1994) to obtain reactor kinetic parameters. These tuned

parameters predicted the results in good agreement with industrial results (temperature profile, end point monomer conversion and number-average molecular weight reported by Asteasuain et al., 2001b).

Buchelli et al. (2005a) determined the fouling thickness using the heat-transfer model and industrial plant data. They calculated the fouling thickness and fouling deposition rate over time, and concluded, using mass transfer rate and Reynolds analogy, that a small fraction of precipitated polymer gets attached to reactor inner wall to produce fouling. In their subsequent study (Buchelli et al., 2005b), the authors modeled formation of fouling layer by considering two phase behavior of ethylene and polyethylene mixture at the lower temperature near the reactor inner wall using CFD simulation. It was suggested that polymer rich phase and monomer rich phase exist near the boundary layer. It was further suggested that coolant temperature on jacket side should be increased so that reactor wall temperature increases and therefore deposited polymer temperature will be increased, to take away deposited polymer by the ethylene stream. However, prediction of reactor wall inside temperature was opposite to observed temperature in the real plant. The effect of fouling on reactor temperature, polymer properties, fractional conversion, and axial mixing were studied in Buchelli et al. (2005c). The focus of these studies was on modeling the fouling behavior and determination of fouling thickness, and its effect on reactor performance using CFD simulations. Their studies did not carry out any optimization study using the developed model.

The LDPE production using tubular reactor technology at high-pressure is well established in the industry. Many steady-state models are available in the open literature (e.g., Zabisky et al., 1992; Kiparissides et al., 1993b; Brandolin et al., 1996; Agrawal et al., 2006) but only a few studies deal with the dynamic models (e.g.,

Kiparissides et al., 1996; Cervantes et al., 2000; Asteasuain et al., 2001b). These dynamic models are fairly small and simple. Kiparissides et al. (1996) carried out the on-line optimization on a high-pressure tubular reactor. But, they have assumed quasi-steady state and negligible dynamics in the model based on measurements and control. These assumptions are not admissible as discussed by Hafele et al. (2006). Cervantes et al. (2000) minimized the grade transition time between two steady-states corresponding to two polymer grades in a large-scale industrial LDPE plant. Asteasuain et al. (2001b) presented a dynamic model of an LDPE reactor, and then obtained the optimal start-up policies. They maximize the outlet conversion and minimize the time required for the reactor to stabilize, while forcing the polymer properties at some desired values during start-up. Again, these studies did not account for the spatial and time variations in the physico-chemical properties. Also, some reactions are not included in the reaction kinetics, which are important in defining the polymer quality. In this study, a comprehensive dynamic model for the production of LDPE in a tubular reactor is presented and simulation results using this model are discussed in detail. Hafele et al. (2005) simulated an industrial tubular reactor for LDPE production using an adaptive method of lines where adaptation of grid nodes is done dynamically. Hafele et al. (2006) used this dynamic model to study the effects of reactor wall and material recycles on the plant dynamics. However, they did not provide complete details on their approach for proprietary reasons.

2.4 LDPE Tubular Reactor Optimization

Process industries always aim to run at the maximum production capacities due to economic reasons while simultaneously maintaining the polymer quality. Kiparissides et al. (1994) singled out ethylene conversion as the most prominent objective due to

high cost involved in the operation of high-pressure tubular LDPE reactor. However, several end use properties, e.g., strength, impact resistance, etc. are governed by average-molecular weight of the polymer produced and in turn depends on the reactor operating variables. Safety requirement in the reactor and specific polymer grade (determined by M_n and *PDI*) impose multiple constraints to the process. Thus, the design and operation of LDPE polymerization reactor require optimization using multiple objectives and constraints, which are often conflicting in nature as discussed in detail by Lee and Marano (1979). Yoon and Rhee (1984) adopted maximum principle theory to find out the optimum temperature policy which would maximize the exit monomer conversion. But, they did not consider polymer quality specifications in the optimization study. Mavridis and Kiparissides (1985) maximized the productivity of ethylene using a single scalar objective function, which was a weighted average of other two objectives (M_n and *PDI*). Optimal wall temperature and the initiator and chain transfer agent concentrations in a fixed-size tubular reactor were obtained. Kiparissides et al. (1994) employed almost the same objective function in terms of the ethylene conversion and quality (melt index and density) of the final product for on-line optimization of a high-pressure LDPE tubular reactor. The problem was divided in two phases with firstly tuning some key model parameters to eliminate any mismatch in the process and then used this adapted model to optimize the process. Brandolin et al. (1991) maximized the conversion while considering several operational policies relating to polymer properties. Temperature and initiator concentration were considered as optimal control variables. Cervantes et al. (2000) minimized the switching time between two steady states corresponding to two different polymer grades. Optimum butane flow rate was determined by employing dynamic optimization on the whole plant. Asteasuain et al. (2001b) found the optimal

start-up policies for attaining maximum productivity and steady-state operation in minimum time. This was a dynamic optimization problem involving the initiator and telogen concentration as control variables. Finally, Yao et al. (2004) maximized the productivity while considering jacket temperature, as a function of reactor length, as the control variable. Genetic algorithm was utilized for the steady state optimization of LDPE tubular reactor. A direct comparison of their simulation results with experimental data could not be established due to unavailability of these data. Moreover, no product quality specifications were considered in the optimization.

A few optimization studies have also been reported under unsteady (dynamic) operation of LDPE reactors. Asteasuain et al. (2001b) first presented a dynamic model of an LDPE reactor, and then obtained the optimal start-up policies. They maximized the outlet conversion and minimized the time required for it to stabilize, while forcing the properties at some desired values during start-up. The feed flow rates of the two initiators and of telogen were used as decision variables. Cervantes et al. (2000) presented a dynamic model for an entire LDPE plant with a feed mixture of ethylene, methane, butane and impurities. They minimized the switching time between two steady-states corresponding to two different grades of polymer.

Polymer industries are subjected to market fluctuations which necessitate producing as many as 30-40 different grades in a single polyolefin plant (Chatzidoukas et al., 2003). The production of LDPE in tubular reactors is a typical process where unsteady states during plant operation are commonly observed. Also, the stocking costs are huge thus what is required for the market should be produced just in time. So, frequent grade changes are expected in a LDPE plant. In addition, LDPE plants are connected with the upstream and downstream processes which influence the throughput of the plant directly (Hafele et al., 2006). Therefore, grade

transition of polymers with high quality in a polymer plant becomes an essential and important issue. During grade change, off-specification product is produced which incurs loss of revenue to the polymer industry. Thus, change in the polymer grade should be made with minimum polymer off-specification and grade change over time.

The polymer grades are typically characterized by the various attributes such as average molecular weight, density, melt-index, and other physical properties. The different grades of LDPE of desired specifications are obtained by switching between appropriate steady-states (Cerventes et al., 2000). The grade transition coupled with control strategies in any polyolefin industry can be carried out in two steps. First, the optimal grade transition recipes are identified offline for manipulated and controlled variables in the presence of constraints on process input, output and state variables using a dynamic model. Next, these optimal trajectories are implemented after selecting the feedforward and feedback controllers and their parameters (Chatzidoukas et al., 2003). This study focuses on the first aspect where optimal grade transition trajectories are obtained using offline optimization.

In all the studies involving more than one objective, a weighted sum of the multiple objectives is used as a single, *scalar* objective function. This allows the use of simpler optimization algorithms, but the solution depends on the values selected for the weighting factors, and so there is some degree of arbitrariness involved. A more important disadvantage of the combining the several objectives into a scalar quantity ('scalarization') is that the algorithm may miss some optimal solutions (Haimes, 1977). In recent years, several multi-objective adaptations of GA that can solve such problems have become available. These have been used in the present study to obtain solutions of a few meaningful MOO problems for an industrial LDPE reactor.

2.5 Summary

This chapter presented detailed information available in literature for reaction mechanism scheme in free-radical polymerization of ethylene. Various research groups used different set of reactions in narrating the polymer properties and process behavior. Thereafter, various steady-state mathematical models are reviewed for their merits and limitations. These models are then used in optimizing LDPE reactor operation. A thorough review of optimization studies of LDPE tubular reactor showed that most of the articles combine multiple objectives into single objective by assigning arbitrary weights to individual objective and solve the resulting problem using single objective optimization algorithms.

Chapter 3

Genetic Algorithms and Constraint-handling Techniques for MOO

3.1 Introduction

The chapter starts with an overview of genetic algorithms (GAs) used for solving multi-objective optimization (MOO) problems. These are classified into non-elitist and elitist algorithms based on elite-preserving mechanism. Then, an elitist non-dominated sorting GA (NSGA-II) and its jumping gene (JG) adaptations are described. All these algorithms are discussed for unconstrained MOO problems. But, real-world problems without constraints are very rare. Hence, a popular and easy-to-apply approach, penalty function method, for solving constrained MOO problems is presented and its merits and limitations are outlined. Penalty function approach is susceptible to the penalty parameter value; therefore, a systematic approach, constrained-dominance principle, is suggested in the literature which is illustrated in this chapter. This approach is implemented in NSGA-II-JG and NSGA-II-aJG for the first time for solving the constrained MOO problems. These algorithms are tested on constrained problems and the results are compared to those using the real-coded NSGA-II.

3.2 Genetic Algorithms for Multi-objective Optimization

GA (Goldberg, 1989) is a robust and popular technique for global optimization; it mimics natural genetics, using operators like reproduction, crossover and mutation to guide the search in the feasible domain. It requires only the values of the objectives and does not require any initial guesses and derivatives of functions involved. Most real-world problems require the simultaneous optimization of several objectives

(MOO) which are often conflicting in nature. Also, some objectives are non-commensurate and these can not be combined into single and meaningful scalar objective function. In several, earlier studies, these objectives were combined into single scalar objective function, using arbitrary weighting factors and the resulting problem was solved by single objective optimization algorithms. But, this approach suffers from assigning a-priori basis weighting factors and losing some optimal solutions (Chankong and Haimes, 1983; Haimes, 1977).

Instead of pre-fixing a weighting factor and finding the corresponding Pareto-optimal solution, multi-objective evolutionary algorithms (MOEAs) were suggested to find multiple trade-off solutions in one single run. The first real MOEA was suggested by Schaffer (1984) with the name of vector evaluated genetic algorithm (VEGA). This was the first multi-objective genetic algorithm (MOGA) used to find a set of non-dominated solutions, which are equally good (i.e., none of them is better than the others with respect to all objectives). The non-dominated solutions are also called Pareto-optimal solutions or set in the context of MOO. The curve formed by joining these solutions is called Pareto-optimal front. In VEGA, each objective was treated as an element of an objective vector (instead of scalar objective function) and represented truly the MOO. Though, the population members had tendency to crowd near an individual optimal solution due to lack of explicit diversity-preserving mechanism. This problem was later eliminated by careful implementation of the non-domination concept and explicit diversity-preserving operator. The three implementations – multi-objective GA (called MOGA; Fonseca and Fleming, 1993), niched-Pareto GA (NPGA; Horn et al., 1994), and non-dominated sorting genetic algorithm (NSGA; Srinivas and Deb, 1994) – used the suggestions of Goldberg (1989) and found well-converged and well-distributed sets of non-dominated

solutions in both test and application problems. The common aspect of these algorithms is that none of them has used elite-preserving operator. NSGA has been applied successfully to optimize several industrially important systems (Bhaskar et al., 2000).

Elite-preserving operator favors the elites of a population by giving them an opportunity to be part of the next generation. The elitism can be introduced either locally or globally in MOO. For local elitism, consider two off-springs generated from two parents after crossover and mutation operations; out of these four solutions, the best two solutions are selected for the next generation. Thus, the two elite parents are given opportunity for their survival for next generations. Similarly, in global elitism, the parent population (N) and off-spring population (N) are combined, and the N better solutions from these $2N$ members are selected for the next generation. The use of elitism makes sure that the fitness of the best solution in the population does not deteriorate. In fact, Rudolph (1996) has proved that GAs converge to the global optimal solution of some functions in the presence of elitism. Rudolph (2001) used elitism in multi-objective evolutionary algorithms but this algorithm lacked diversity preservation mechanism. Thereafter, Deb et al. (2002) suggested an elitist non-dominated sorting GA (NSGA-II) which contains both elite-preservation strategy and diversity-preserving mechanism. A detailed account of various adaptations of GAs proposed by researchers for generating Pareto-optimal solutions can be found in the recent textbooks (Deb, 2001; Coello et al., 2002).

The performance of NSGA-II has been further enhanced by incorporating one of several jumping gene (JG) adaptations (Simoes et al., 1999; Kasat and Gupta, 2003; Man et al., 2004; Guria et al., 2005). Kasat and Gupta (2003) observed that JG concept borrowed from nature provides the genetic diversity in the pool thus

counteracting the negative effect of elitism; overall, it decreases computational time (number of generations) required for solving the multi-objective problem. The existence of JG, a DNA, is predicted in 1940s by McKClintock (1987) which could come in and out of the chromosome. But, it was believed that DNA is stable and invariable until 1960s when JG could be isolated in E. Coli. And these are named as transposons. Later, the role of transposons was understood in transferring bacterial resistance to antibodies and genetic diversity in natural populations. There are various kind of transposons. Of these, two types of transposons are taken into consideration by Kasat and Gupta (2003), and applied them in NSGA-II algorithm.

3.3 NSGA-II and its JG Variants

The binary-coded elitist NSGA-II is a population-based search technique. It starts with mapping the decision variable vector on to their binary equivalents (l_{substr}: number of binaries representing a decision variable), via linear mapping formula (Deb, 2001). The mapped binary variables are placed side by side so as to form an individual, called a chromosome. Now, the parent population (say set PP), comprising a set of such chromosomes (N_{pop}), is created using a sequence of random numbers (generated using the random seed parameter, S_r). Each of these chromosomes is decoded into real values of the decision variables to calculate the objective function values. The available NSGA-II code maximizes all the objective functions. Hence, a problem involving the minimization of a function, J, is converted to a maximization problem by using the transformation: $I = 1/(1+J)$. These objective function values are called fitness values, which are the indices of the merit of an individual. The parent population is then distributed to various fronts based on the non-domination criteria. Also the crowding distance for each chromosome in each front is calculated. The

crowding distance of a solution is a measure of the search space around it not occupied by any other solution in the population.

Now, the better parents (say, set BP) are selected, based on their ranking and crowding distance, from the parent population. The daughter population is obtained after performing crossover and mutation (using crossover (p_c) and mutation (p_m) probabilities, respectively) on the better parents. At this stage, JG/aJG operation is checked (whether needed or not) on each chromosome (say, 1001|10011|0) sequentially based on the specified jumping gene probability (p_{JG}) and a random number. If JG/aJG is needed, another random number is generated between 0 and 1, and then multiplied by l_{chrom}, the total number of binaries in the chromosome. The resulting number is rounded off to convert into an integer. It defines the position of the beginning of a transposon or jumping gene (for instance, at the end of the fourth binary in the above chromosome). Similarly, the second location is identified by generating another random number (say, after 9^{th} binary in the chromosome). While, in aJG operation, this second location is found out by using the specified string length, l_{aJG} (for example, l_{aJG} = 5; so a bar is placed after the 4 + 5 = 9^{th} binary), of the jumping gene (Guria et al., 2005). Then, the set of binaries between these two locations are replaced by a new set of randomly generated binaries of the same size. The individuals after crossover, mutation and jumping gene operations on the set BP, form another population set (say, set DP). Objective function at each of these individuals is calculated. The set DP is then added to better parent population (set BP). After reclassifying the combined BP and DP sets into fronts, the better individuals (sat set EP) are selected as the population for the next generation. This completes one generation and the process is carried on until the stopping criterion

($N_{gen,max}$: maximum number of generations) is met. The working principle of NSGA-II and its JG adaptations is also shown in Figure 3.1.

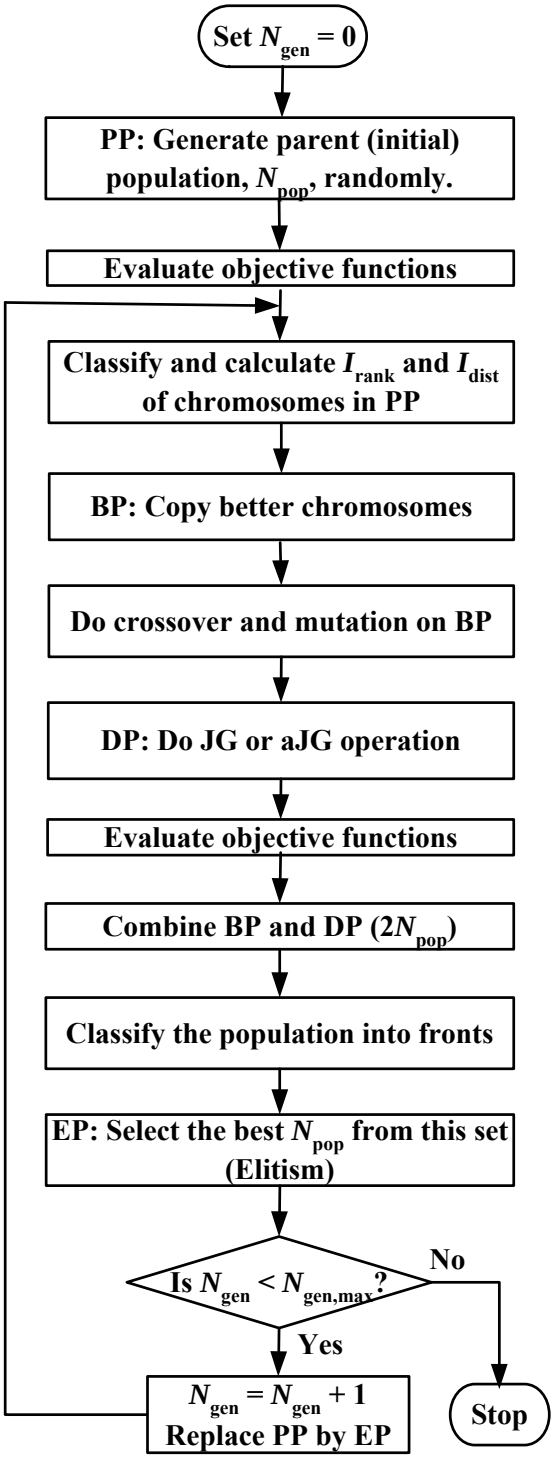

Figure 3.1 Flow chart of NSGA-II and its JG adaptations

3.4 Penalty Function Method

The constraints are quite common in real-world optimization problems. They might be equality and/or inequality constraints, and divide the search space into feasible and infeasible regions. And, similar to single objective optimization (SOO), Pareto-optimal solutions (for MOO) should be feasible. Coello and Christiansen (1999) suggested that any solution which violates any of the constraints should be ignored. But, it becomes quite difficult to find feasible solutions (each of which satisfies all the assigned constraints) in most real-world problems. So, Deb (2000) suggested that infeasible solutions should be evaluated and compared among themselves and with feasible solutions. Also, the measure of overall constraint violation of an infeasible solution is suggested in SOO. In this way, GAs can be guided into feasible region by emphasizing the solutions with less overall constraint violation.

In trying to solve constrained optimization problems using GAs or classical optimization methods, penalty function methods have been the most popular approach, because of their simplicity and ease of implementation (Deb, 2000). For each solution/chromosome, constraint violation of each constraint is calculated. And, all these violations are summed up together to calculate the overall constraint violation. This violation is then multiplied with the penalty parameter, R, and the product is subtracted from each of the objective function values (for a problem of maximization of objective functions). This parameter for each objective function may be different such that the constraint violation is comparable to the objective function value. The overall constraint violation becomes zero if a solution is feasible else it penalizes the original objective function. Once the penalized function is formed, then any unconstrained MOO methods discussed earlier can be used.

In single objective GA literature (e.g., Michalewicz, 1992; Homaifair et al., 1994), a number of static and dynamic strategies are given to update the penalty parameter. The dependency of GA's performance on the penalty parameter has led researchers to devise sophisticated penalty function approaches such as multi-level penalty functions (Homaifair et al., 1994), dynamic penalty functions (Joines and Houck, 1994), and penalty functions involving temperature-based evolution of penalty parameters with repair operators (Michalewicz and Attia, 1994). All these approaches require extensive experimentation for setting up appropriate parameters needed to define the penalty function. Michalewicz and Schoenauer (1996) concluded that static penalty function method is more robust than any sophisticated method (dynamic strategies). It is because each sophisticated method is problem-dependent; it may work well on one problem but may not work so well on other problems, as discussed by Deb (2000).

Deb (2001) has presented the working methodology of penalty function approach and illustrated its application to MOO of a test problem. NSGA is applied to obtain the Pareto-optimal solutions. The effects of choosing various penalty parameters were also studied. It was noted that if an adequate penalty parameter is not chosen, then infeasible Pareto-optimal set is obtained. However, when an appropriate parameter is chosen (by slowly increasing the parameter value) the resulting Pareto-optimal front was feasible and close to the true Pareto-optimal set. Interestingly, a large value of penalty parameter over-emphasized the constraints in initial generations and NSGA converged near to a portion of the Pareto-optimal set.

3.5 Constrained-Dominance Principle for Handling Constraints

Several constraint-handling techniques have been used with evolutionary algorithms, and a bibliography of articles on this topic is available in Coello and

Coello (1999) (this is a technical report and it is available on http://www.cs.cinvestav.mx/~constraint). Deb (2001) illustrated the application of penalty function approach, a popular constraint handling strategy, in NSGA-II on a test problem for handling the constraints. He observed that, when the chosen penalty parameter is small, the penalty effect is less and therefore the resulting optimal solutions are infeasible. On the other hand, a large value of penalty parameter over-emphasizes the constraints in the initial populations, which results in poor distribution of solutions in the Pareto-optimal front. Thus, multi-objective evolutionary algorithms work well if an appropriate penalty parameter is chosen; else, a set of infeasible solutions or a poor distribution of solutions is likely.

Therefore, a systematic approach of constrained-dominance principle for handling the constraints in MOO was proposed by Deb et al. (2002). Motivated by these, constrained-dominance principle is successfully implemented in the binary-coded NSGA-II-aJG and NSGA-II-JG for handling the constraints for the first time and its effectiveness is evaluated for the test problems.

3.5.1 Implementation and Testing

Deb et al. (2002) proposed a more systematic and parameter-less constraint-handling approach for solving constrained MOO problems. This approach is referred as constrained-dominance principle, which is used in selecting the better one of the two solutions chosen in the binary tournament selection. In the presence of constraints, there exist three possible scenarios: (1) both the solutions are feasible, (2) one solution is feasible and other is infeasible, and (3) both solutions are infeasible. For SOO, Deb (2000) proposed the efficient and simple strategy of selecting the

solution with better function value in case of 1, feasible solution in case of 2 and the solution with less overall constraint violation in case of 3.

Later, Deb et al. (2002) incorporated this strategy in MOO by modifying the definition of domination between two solutions, *i* and *j*, as follows.

Definition: A solution *i* is constraint-dominating solution *j*, if any of the following conditions is true.

(1) Solution *i* is feasible and solution *j* is infeasible.

(2) Both solutions are infeasible but solution *i* has a smaller overall constraint violation.

(3) Solutions *i* and *j* are feasible and solution *i* dominates solution *j* in the usual manner.

The detailed description of this method can be found in Deb et al. (2002). We implemented it in the binary-coded NSGA-II-aJG and the results of testing it on four constrained problems (Table 3.1) are discussed in this section. The same implementation can be used with NSGA-II and NSGA-II-JG. The test problems are defined in Deb et al. (2002), where they used them to compare constrained-dominance principle approach in the real-coded NSGA-II (NSGA-II-RC) with other constraint-handling methods. The available NSGA-II-aJG code maximizes the objective functions; hence a problem involving the minimization of a function, *J*, is converted to a maximization problem by using the transformation, $G = 1/(1 + J)$.

The design of an industrial LDPE tubular reactor (Agrawal et al., 2007) is optimized for two objectives using NSGA-II and its JG variants with constrained-dominance principle to handle the constraints. The results obtained are compared with those obtained with the penalty function method for constraint-handling in NSGA-II-aJG. These results are discussed later on in Chapter 5.

Table 3.1 Constrained test problems used in this study (Deb et al., 2002)

Problem	Variable bounds	Objective functions	Constraints
CONSTR	$0.1 \le x_1 \le 1.0$ $0 \le x_2 \le 5.0$	$f_1(\boldsymbol{x}) = x_1$ $f_2(\boldsymbol{x}) = (1 + x_2)/x_1$	$g_1(\boldsymbol{x}) = 9x_1 + x_2 \ge 6$ $g_2(\boldsymbol{x}) = 9x_1 - x_2 \ge 1$
SRN	$-20 \le x_1 \le 20$ $-20 \le x_2 \le 20$	$f_1(\boldsymbol{x}) = (x_1 - 2)^2 + (x_2 - 1)^2 + 2$ $f_2(\boldsymbol{x}) = 9x_1 - (x_2 - 1)^2$	$g_1(\boldsymbol{x}) = x_1^2 + x_2^2 \le 225$ $g_2(\boldsymbol{x}) = x_1 - 3x_2 \le -10$
TNK	$0 \le x_1 \le \pi$ $0 \le x_2 \le \pi$	$f_1(\boldsymbol{x}) = x_1$ $f_2(\boldsymbol{x}) = x_2$	$g_1(\boldsymbol{x}) = -x_1^2 - x_2^2 + 1 + 0.1cos(16arctan(x_1/x_2)) \le 0$ $g_2(\boldsymbol{x}) = (x_1 - 0.5)^2 + (x_2 - 0.5)^2 \le 0.5$
WATER	$0.01 \le x_1 \le 0.45$ $0.01 \le x_2 \le 0.1$ $0.01 \le x_3 \le 0.1$	$f_1(\boldsymbol{x}) = 106780.37(x_2 + x_3) + 61704.67$ $f_2(\boldsymbol{x}) = 3000x_1$ $f_3(\boldsymbol{x}) = (305700)2289x_2/[(0.06)2289]^{0.65}$ $f_4(\boldsymbol{x}) = (250)2289exp(-39.75x_2 + 9.9x_3 + 2.74)$ $f_5(\boldsymbol{x}) = 25(1.39/(x_1x_2) + 4940x_3 - 80)$	$g_1(\boldsymbol{x}) = 0.00139/(x_1x_2) + 4.94\,x_3 - 0.08 \le 1.00$ $g_2(\boldsymbol{x}) = 0.000306/(x_1x_2) + 1.082x_3 - 0.0986 \le 1.00$ $g_3(\boldsymbol{x}) = 12.307/(x_1x_2) + 49408.24x_3 + 4051.02 \le 50000.00$ $g_4(\boldsymbol{x}) = 2.098/(x_1x_2) + 8046.33x_3 - 696.71 \le 16000.00$ $g_5(\boldsymbol{x}) = 2.138/(x_1x_2) + 7883.39x_3 - 705.04 \le 10000.00$ $g_6(\boldsymbol{x}) = 0.417/(x_1x_2) + 1721.26x_3 - 136.54 \le 2000.00$ $g_7(\boldsymbol{x}) = 0.164/(x_1x_2) + 631.13x_3 - 54.48 \le 550.00$

Note: All objective functions are of minimization type.

3.5.2 Results and Discussion

The values of the computational parameters in NSGA-II-RC are taken from Deb et al. (2002). We have not attempted to get the best values of computational parameters for the three test problems (CONSTR, SRN, and TNK) for NSGA-II-aJG but with a few exceptions for WATER problem as discussed below. The results of the first three test problems were practically in-variant to the computational parameters.

Each test problem is solved by an algorithm using 500 generations with a population of 100 so that the results by NSGA-II-RC and NSGA-II-aJG could be compared for the same number of generations and population size. Figure 3.2 shows that NSGA-II-RC and NSGA-II-aJG produced the same Pareto-optimal set for the CONSTR problem. The second problem, SRN, was originally described in Srinivas and Deb (1995). Here, the constrained Pareto-optimal set is a subset of the unconstrained Pareto-optimal set. Both objective functions, f_1 and f_2, in the SRN minimization problem were maximized using the transformation $G = 1/(1000 + J)$ to avoid division by zero. NSGA-II-aJG produced non-dominated solutions which are the same as those obtained by NSGA-II-RC, as shown in Figure 3.3.

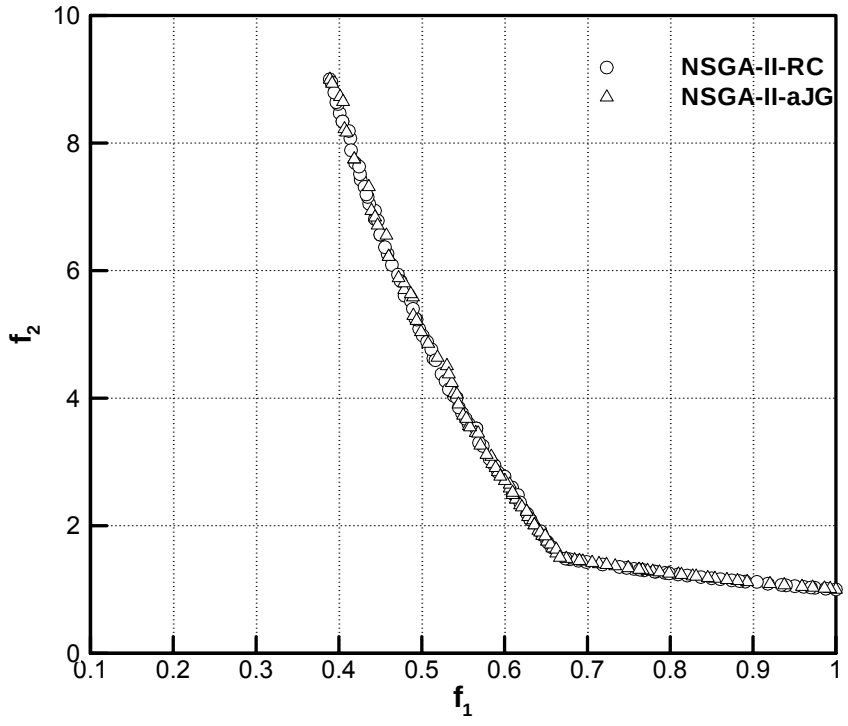

Figure 3.2 Pareto-optimal sets by NSGA-II-RC (○) and NSGA-II-aJG (Δ) for the CONSTR problem.

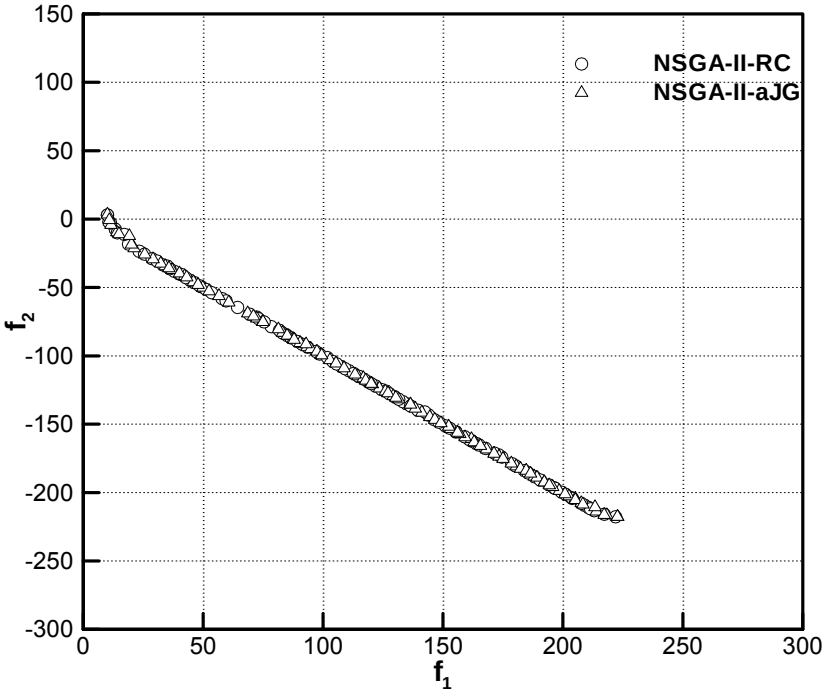

Figure 3.3 Pareto-optimal sets by NSGA-II-RC (○) and NSGA-II-aJG (Δ) for the SRN problem.

The third problem TNK was suggested by Tanaka et al. (1995), and has a discontinuous Pareto-optimal region, falling entirely on the first constraint boundary. In the Figure 3.4 shows the 100 non-dominated points obtained using NSGA-II-aJG for the TNK problem. The Pareto-optimal front is very close to that obtained by NSGA-II-RC. Here, the Pareto-optimal region is discontinuous but both these algorithms could easily find it without difficulty. The last problem, WATER, involves five objective functions, seven constraints, and three decision variables. This problem is for optimal planning for a storm drainage system in an urban area. It was described originally in Musselman and Talavage (1980), and subsequently studied by Cheng and Li (1999), Ray et al. (2001) and Deb et al. (2002). The variables are: x_1 = local detention storage capacity, x_2 = maximum treatment rate and x_3 = the maximum

allowable overflow rate. The objective functions to be minimized are: f_1 =drainage network cost, f_2 = storage facility cost, f_3 = treatment facility cost, f_4 = expected flood damage cost, and f_5 = expected economic loss due to flood. The detailed description of the problem and constraints can be obtained from Musselman and Talavage (1980).

The objectives are normalized via f_1/80000, f_2/1500, f_3/3000000, f_4/6000000 and f_5/8000, as was done in Deb et al. (2002). The Pareto-optimal solutions are shown in Figure 3.5 in terms of some pair-wise interactions among normalized objective functions; other pair-wise interactions were quite scattered and not plotted here but can be provided if needed. It can be seen from Figure 3.5 that NSGA-II-aJG performed reasonably well on the WATER problem compared to NSGA-II-RC. Both these algorithms produced scattered solutions unless the *best* values of computational parameters are used. The best set for NSGA-II-aJG includes – S_r = 0.2, p_{JG} = 0.8, p_m = 0.001, p_c = 0.8 and l_{aJG} = 15. Deb et al. (2002) did not provide the seed parameter, S_r, and therefore different values for it were tried; NSGA-II-RC gave scattered solutions for all seed values tried except for S_r = 0.45. The results for NSGA-II-RC shown in Figure 3.5 are obtained using this particular seed value.

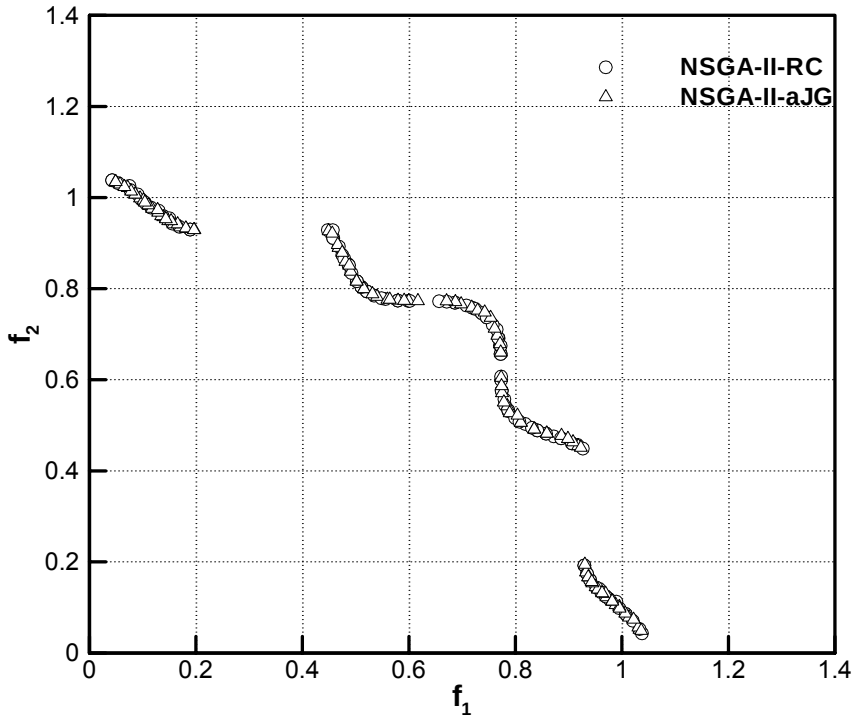

Figure 3.4 Pareto-optimal sets by NSGA-II-RC (○) and NSGA-II-aJG (Δ) for the TNK problem.

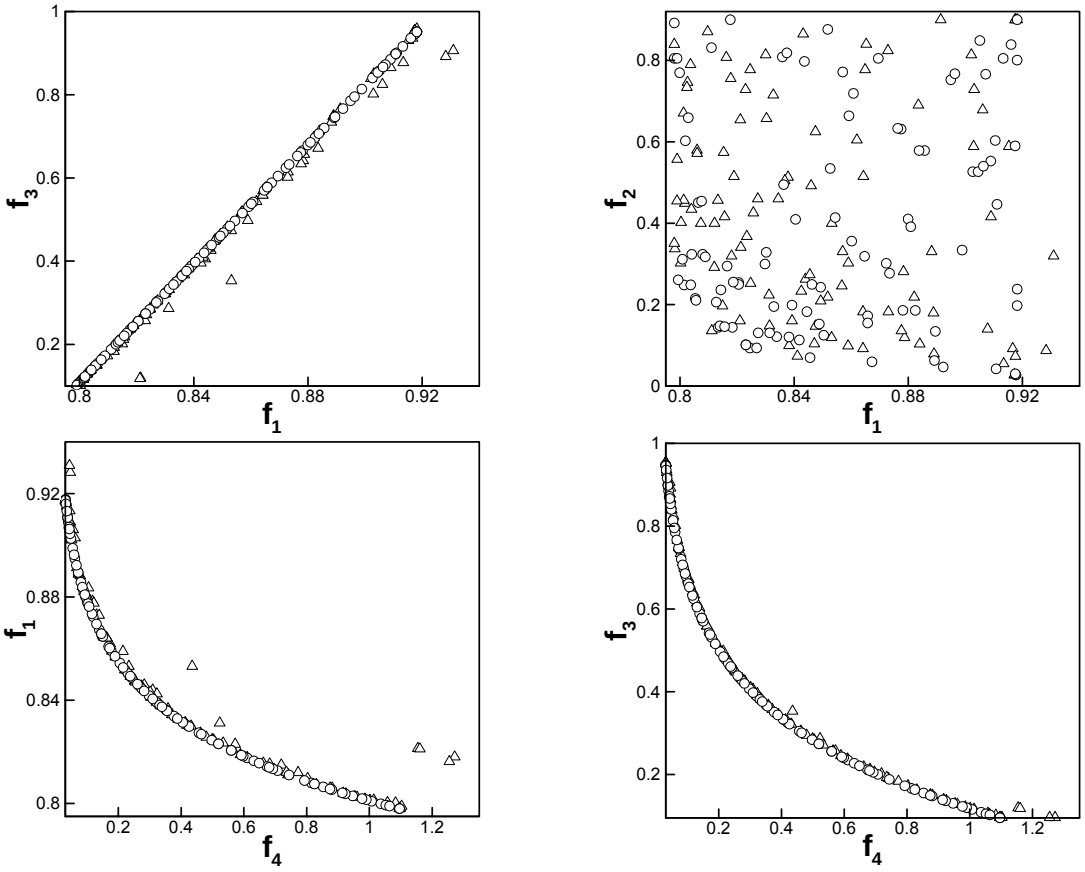

Figure 3.5 Pareto-optimal sets by NSGA-II-RC (○) and NSGA-II-aJG (Δ) for the WATER problem.

3.6 Conclusions

In this chapter, the basic understanding of non-elitist and elitist GA for MOO is presented. These algorithms simultaneously optimize multiple objectives in a single run and do not require pre-fixed weighting factors to produce the Pareto-optimal solutions. NSGA-II incorporates diversity preserving mechanism and elite-preservation strategy. The working methodology of binary-coded NSGA-II and its JG adaptations is presented. For handling the constraints in MOO, a popular approach, namely, penalty function method is discussed. However, the difficult aspect of the penalty function approach is to find appropriate penalty parameters needed to guide the search towards the constrained optimum. Therefore, a systematic approach of

constrained-dominance principle for handling the constraints is implemented and tested in the binary-coded NSGA-II-JG and NSGA-II-aJG, for the first time. NSGA-II-aJG performed equally well as NSGA-II-RC did for three of the four test problems. However, for a difficult problem, WATER, NSGA-II-aJG performed reasonably as compared to NSGA-II-RC for handling the constraints.

Chapter 4

Reactor Modeling, Simulation and Optimization

4.1 Introduction

Ethylene, along with initiators and telogens, is used for producing LDPE by free radical polymerization in a tubular reactor at extreme conditions, namely, 150 – 250 MPa and 325 – 625 K. A typical commercial reactor has several reactions, heating and cooling zones, with intermediate addition of initiators, monomer and solvent, so that the conditions of polymerization differ significantly in each zone. The single-pass conversion of ethylene in this reactor is reported to be about 20 – 35 %. The LDPE produced in these reactors contains several short-chain branches (mainly ethyl- and butyl-groups), which are responsible for (Luft et al., 1982) its lower crystallinity, density, melting point, tensile strength, etc. The minimization of these groups would improve the quality and strength of the polymer. Some vinyl and vinylidene groups (unsaturated) are also present on the polymer chains. These are undesirable, since they make the final product susceptible to cracking due to oxide formation. Optimum operation of reactors should attempt to minimize these side products too. Yet another important requirement for optimal reactor operation is the maximization of the production (maximization of the monomer conversion for a given feed flow rate), while producing a product having a desired value of the number (or weight) average molecular weight, M_n (or M_w), so that the product has the desired physical properties.

Several detailed studies have been reported on the modeling of LDPE reactors in the literature. Agrawal and Han (1975) studied the effects of various operating parameters on the performance of the reactor. They incorporated axial mixing to simulate the effect of pressure pulsing. However, Chen et al. (1976) showed that axial

mixing can be neglected because the Peclet number is quite high due to turbulence. Donati et al. (1981) and Yoon and Rhee (1985) also observed that axial dispersion has negligible effect on the reactor performance. Hence, an ideal plug flow model can be used to describe LDPE reactors. A pressure drop (Brandolin et al., 1996) of 10 – 30% along the reactor length is observed in industrial practice. This also affects the molecular weight of the polymer since the propagation rate constant is dependent on the pressure (Anspon, 1964). In fact, the molecular weight distribution of the product is broader because of this. Some workers (Agrawal and Han, 1975; Yoon and Rhee, 1985; Goto et al., 1981; Gupta et al., 1985; Kiparissides et al., 1993b; Mavridis and Kiparissides, 1985; Zabisky et al., 1992) used the quasi steady state approximation to avoid integrating stiff ordinary differential equations (ODEs). This need not be assumed these days due to the availability of powerful algorithms and computers. The most interesting observation that can be made from a survey of these modeling studies is the significant discrepancies in the values of the rate constants. These have been alluded to by Gupta et al. (1985). In more recent studies, (Brandolin et al., 1996; Zabisky et al., 1992) the rate constants were estimated using industrial data. For example, Brandolin et al. (1996) simulated an industrial LDPE reactor and calculate the kinetic parameters using the temperature profiles and the properties of the product. Since industrial data were involved, these workers did not provide complete information due to proprietary reasons. The same is true for the study of Zabisky et al. (1992) who also did not provide exact values of their tuned kinetic parameters. Asteasuain et al. (2001b) provided the design features, steady-state operating conditions, measured temperature profiles, and the monomer conversions and number-average molecular weights at the reactor exit for yet another industrial reactor. Again, a few important details are not provided.

The dynamic model of Asteasuain et al. (2001b) has been modified to the steady-state model for use in this study. The model incorporates the axial variation of physical properties and pressure in addition to temperature and concentration as well as several main and side reactions, e.g., intramolecular chain transfer, chain transfer to polymer, β-scission of secondary and tertiary radicals, etc. (the latter give the extent of long- and short-chain branching and the amount of unsaturation). We assume (and provide) reasonable values for all the missing information. Our model description is therefore, quite complete and useful for researchers. Best-fit values of several model parameters are obtained using the reported industrial data (Asteasuain et al., 2001b). A similar approach has been used earlier for LDPE (Brandolin et al., 1996; Zabisky et al., 1992; Asteasuain et al., 2001a; Brandolin et al., 1988), PET (Bhaskar et al., 2001), and nylon 6 (Wajge et al., 1994). This model is then used to optimize the LDPE reactor operation.

Several studies on the optimization of LDPE reactors have been reported. A variety of objective functions, decision variables and constraints have been used (Lee and Marano, 1979). Yoon and Rhee (1985) used the maximum principle to obtain the optimum temperature policy required to maximize the monomer conversion at the exit. Polymer quality (through M_n, M_w, or the side products) is not a concern in this study. Brandolin et al. (1991) obtained the optimal temperature and initiator concentration profiles that maximize the monomer conversion, while using several constraints on the polymer properties [through M_n, *PDI*, etc.]. Mavridis and Kiparissides (1985) maximized the productivity of ethylene while controlling M_n and *PDI* in the product, using reactor wall temperature and the concentrations of the initiator and the chain transfer agent as decision variables. Kiparissides et al. (1994) tuned an industrial reactor and use almost the same objective function for on-line

optimization of an LDPE tubular reactor. Yao et al. (2004) used genetic algorithm (GA) to obtain the optimal jacket temperature profile required to maximize the polymer production. No requirements on the product properties were considered.

A few optimization studies have also been reported under unsteady (dynamic) operation of LDPE reactors. Asteasuain et al. (2001b) first presented a dynamic model of an LDPE reactor, and then obtained the optimal start-up policies. They maximized the outlet conversion and minimized the time required for it to stabilize, while forcing the properties at some desired values during start-up. The feed flow rates of the two initiators and of telogen were used as decision variables. Cervantes et al. (2000) presented a dynamic model for an entire LDPE plant with a feed mixture of ethylene, methane, butane and impurities. They minimized the switching time between two steady-states corresponding to two different grades of polymer.

In all the studies involving more than one objective, a weighted sum of the multiple objectives is used as a single, *scalar* objective function. This allows the use of simpler optimization algorithms, but the solution depends on the values selected for the weighting factors, and so there is some degree of arbitrariness involved. A more important disadvantage of the combining the several objectives into a scalar quantity ('scalarization') is that the algorithm may miss some optimal solutions (Haimes, 1977). In recent years, several multi-objective adaptations of GA that can solve such problems have become available. These have been used in the present study to obtain solutions of a few meaningful multi-objective optimization problems for an industrial LDPE reactor.

GA (Holland, 1975; Goldberg, 1989; Deb, 2001) is an extremely robust technique that mimics natural genetics using operators like reproduction, crossover and mutation to guide the search in the feasible domain. It requires only the values of objectives and

does not require any initial guesses. One of its recent adaptations, the elitist non-dominated sorting genetic algorithm (NSGA-II; Deb, 2001) can be used to solve multi-objective optimization (MOO) problems. This algorithm and its earlier versions (NSGA/NSGA-I) have been applied successfully to optimize several industrially important systems (Bhaskar et al., 2000). The performance of GA including NSGA-II has been further enhanced by incorporating one of several jumping gene (JG) adaptations (Kasat and Gupta, 2003; Simoes et al., 1999; Guria et al., 2005). Very recently, multi-objective differential evolution was applied to optimizing an adiabatic styrene reactor (Babu et al., 2005) that was solved earlier (Yee et al., 2003) by NSGA for multiple objectives.

In this study the *operation* of an industrial LDPE tubular reactor is optimized using two objectives: maximization of the monomer conversion and minimization of the (weighted average value of the) concentration of the undesirable side products (methyl, vinyl, and vinylidene groups). The binary-coded NSGA-II (Deb, 2001) and its JG adaptations, NSGA-II-JG (Kasat and Gupta, 2003) and NSGA-II-aJG (Guria et al., 2005) are used. Pareto-optimal solutions (sets of non-dominated or equally good solutions, in which, on moving from any one point to any other, one objective function improves while the other worsens) are obtained. A decision maker can be provided these and he/she can use his/her industrial intuition to select any one of these points as the 'preferred' solution. To the best of our knowledge, this is the first study using multiple objectives (without scalarization) for an industrial LDPE reactor.

4.2 Reactor Modeling and Simulation

4.2.1 Formulation

Figure 4.1 shows the industrial LDPE tubular reactor (Asteasuain et al., 2001b) simulated and optimized in this study. It is typical of several industrial reactors. Equations T1-1 – T1-10 in Table 4.1 give the fairly general kinetic scheme which captures all molecular developments in LDPE product. All the reactions are considered to be elementary except reaction 1, which is of order 1.1 with respect to oxygen (Brandolin et al., 1988). The elementary reaction mechanism includes initiation, propagation, termination by combination, thermal degradation, transfer to polymer, transfer to solvent, β-scission of secondary and tertiary radicals, and intramolecular chain transfer. The reactor model includes mass, energy, and momentum balances for a tubular reactor. Ideal plug flow conditions are assumed in the reactor and jacket sides, i.e., there are no radial temperature or concentration gradients in the tubular reactor and jackets, and no axial mixing. These underlying assumptions are valid for high Reynolds numbers (Chen et al., 1976) and very high L_t/D_{int} ratio (Zabisky et al., 1992). The reaction mixture is assumed to be homogeneous (single phase), i.e., ethylene-polyethylene mixture behaves as a supercritical fluid in the range of the given operating conditions. The polymer condensation, either due to large temperature difference or higher conversion, near the reactor wall implies the presence of two-phase reaction mixture (polymer rich and monomer rich) in these reactors. The reaction rates will be very different there. However, the grainy film appearance of polymer, a typical characteristic of two-phase reaction for polymers obtained in autoclave reactors, is not observed in the polymer product obtained from tubular reactors (Zabisky et al., 1992). Assumption of constant initiator efficiency provided the good agreement of model prediction to the industrial

data in the mathematical model of Brandolin et al. (1996). Asteasuain et al. (2001b) simplified this model considering reduced reaction mechanism, constant initiator efficiency, constant jacket fluid temperatures, and constant physical properties throughout the reactor. Thereafter, this model was used in the optimization framework to obtain the optimal start-up policies using gPROMS. Since the model developed in our study is based on these two models, constant initiation efficiency was retained in our study also. The model is written using axial length, z, as the independent variable, and the differential equations are integrated along the reactor length. Equations T1-11 – T1-19 constitute mass balance on each species in the reactor, and heat transfer (Equation T1-20) from the reaction-mixture to the coolant through jacket walls followed by momentum balance (Equation T1-21). The characteristic equations (Equations T1-24 and T1-25) describe the growing and dead polymer concentrations in terms of bivariate moments (Equations T1-22 and T1-23) of orders n and p. The complete set of model equations (Equations T1-11 – T1-25; Brandolin et al., 1996; Katz and Saidel, 1967) for steady state operation is similar to those presented by Brandolin et al. (1996). Moment closure equations relating the third order moments to the lower ones, based on the log-normal distribution (Zabisky et al., 1992), are also included in this table (Equations T1-26 and T1-27). The physical properties of the reaction mixture such as the density (ρ), viscosity (μ), and the thermal conductivity (K), vary along the axial location (Equations T2-1, T2-5, and T2-7 respectively). Linear additivity (Gupta et al., 1985) is assumed for these. Table 4.2 (Gupta et al., 1985; Mavridis and Kiparissides, 1985; Zabisky et al., 1992; Asteasuain et al., 2001b; Micheles and Geldermans, 1942; Parks and Richards, 1948; Poling et al., 2001; Kiparissides et al., 1993b; Lacunza et al., 1998; Coulson et al., 1996) gives the correlations used.

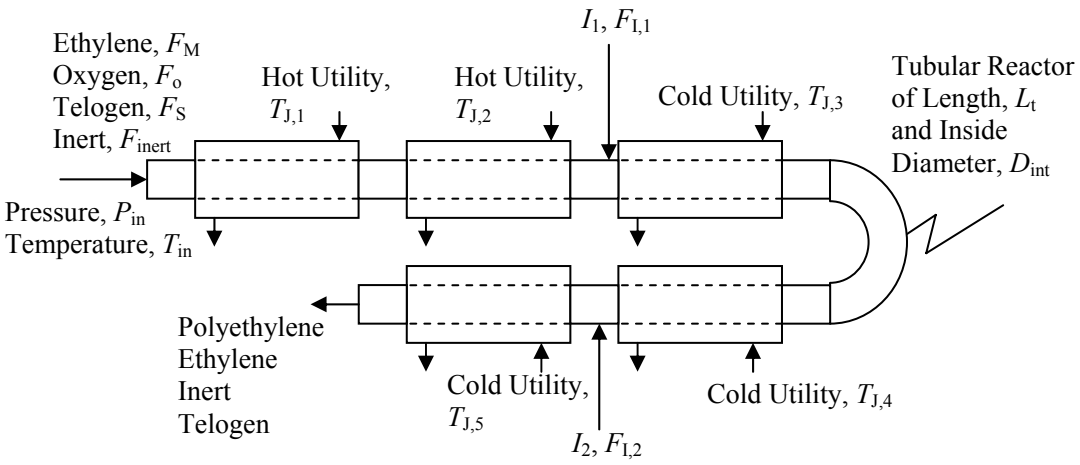

Figure 4.1 Schematic diagram of an industrial LDPE reactor (Asteasuain et al., 2001b)

Table 4.1 Kinetic Scheme and Model Equations for the LDPE Reactor (Brandolin et al., 1996)

KINETIC SCHEME ($x, y = 0, 1, 2, \ldots$; $i, j = 1, 2, \ldots$)

Oxygen initiation

$$O_2 + M \xrightarrow{k_o} 2R_1(0) \qquad \text{(T1-1)}$$

Peroxide initiation

$$I_m \xrightarrow{f_m k_{dm}} 2R_1(0);\ m = 1, 2 \qquad \text{(T1-2)}$$

Propagation

$$R_i(x) + M \xrightarrow{k_p} R_i(x+1) \qquad \text{(T1-3)}$$

Termination by combination

$$R_i(x) + R_j(y) \xrightarrow{k_{tc}} P_{i+j-1}(x+y) \qquad \text{(T1-4)}$$

Thermal degradation

$$R_i(x+1) \xrightarrow{k_{tdt}} P_i(x) + R_1(0) \qquad \text{(T1-5)}$$

Chain transfer to telogen or solvent

$$R_i(x) + S \xrightarrow{k_{trs}} P_i(x) + R_1(0) \qquad \text{(T1-6)}$$

Chain transfer to polymer

$$R_i(x) + P_j(y) \xrightarrow{k_{trp}} P_i(x) + R_{j+1}(y) \qquad \text{(T1-7)}$$

Intramolecular chain transfer (short-chain branching)

$$R_i(x) \xrightarrow{k_{bb}} R_i(x) \qquad \text{(T1-8)}$$

β-Scission of secondary radical (vinyl group formation)

$$R_i(x+1) \xrightarrow{k_{b1}} P_i(x) + R_1(0) \qquad \text{(T1-9)}$$

β-Scission of tertiary radical (vinylidene group formation)

$$R_i(x+1) \xrightarrow{k_b} P_i(x) + R_1(0) \qquad \text{(T1-10)}$$

MODEL EQUATIONS:

$$\frac{dv}{dz} = -\frac{v}{\rho}\left(\frac{d\rho}{dz}\right) \qquad \text{(T1-11)}$$

$$v\frac{dC_{I_m}}{dz} = \left(-k_{dm}C_{I_m} - C_{I_m}\frac{dv}{dz}\right);\ m = 1, 2 \qquad \text{(T1-12)}$$

$$v\frac{dC_{O_2}}{dz} = \left(-k_o C_M C_{O_2}^{1.1} - C_{O_2}\frac{dv}{dz}\right) \qquad \text{(T1-13)}$$

$$v\frac{dC_S}{dz} = \left(-k_{trs}C_S\lambda_{00} - C_S\frac{dv}{dz}\right) \qquad \text{(T1-14)}$$

$$v\frac{dC_M}{dz} = \left(-k_o C_M C_{O_2}^{1.1} - k_p C_M\lambda_{00} - C_M\frac{dv}{dz}\right) \qquad \text{(T1-15)}$$

$$v\frac{dC_{M_e}}{dz} = \left(k_{bb}\lambda_{00} - C_{M_e}\frac{dv}{dz}\right) \qquad \text{(T1-16)}$$

Table 4.1 …. continued…b

$$v\frac{\mathrm{d}C_{\mathrm{V_i}}}{\mathrm{d}z}=\left\{k_{\mathrm{b1}}\left(\lambda_{00}-C_{\mathrm{R_1(0)}}\right)-C_{\mathrm{V_i}}\frac{\mathrm{d}v}{\mathrm{d}z}\right\} \tag{T1-17}$$

$$v\frac{\mathrm{d}C_{\mathrm{V_{id}}}}{dz}=\left\{k_{\mathrm{b}}\left(\lambda_{00}-C_{\mathrm{R_1(0)}}\right)-C_{\mathrm{V_{id}}}\frac{\mathrm{d}v}{\mathrm{d}z}\right\} \tag{T1-18}$$

$$v\frac{\mathrm{d}C_{\mathrm{R_1(0)}}}{\mathrm{d}z}=\left\{\begin{array}{l}2k_{\mathrm{o}}C_{\mathrm{M}}C_{\mathrm{O_2}}^{1.1}+2\sum_{j=1}^{2}f_j k_{\mathrm{d}j}C_{\mathrm{I}_j}-k_{\mathrm{p}}C_{\mathrm{M}}C_{\mathrm{R_1(0)}}-k_{\mathrm{tc}}\lambda_{00}C_{\mathrm{R_1(0)}}\\+k_{\mathrm{tdt}}(\lambda_{00}-C_{\mathrm{R_1(0)}})+k_{\mathrm{trs}}C_{\mathrm{S}}\left(\lambda_{00}-C_{\mathrm{R_1(0)}}\right)-C_{\mathrm{R_1(0)}}\frac{\mathrm{d}v}{\mathrm{d}z}\end{array}\right\} \tag{T1-19}$$

$$\rho C_{\mathrm{P}}v\frac{\mathrm{d}T}{\mathrm{d}z}=-\left\{\frac{4U\left(T-T_{\mathrm{J}}\right)}{1000D_{\mathrm{int}}}+k_{\mathrm{p}}C_{\mathrm{M}}\lambda_{00}(\Delta H)\right\}\ \text{(Asteasuain et al., 2001b)} \tag{T1-20}$$

$$\frac{\mathrm{d}P}{\mathrm{d}z}=-10^{-6}\left(\frac{2f_{\mathrm{r}}\rho v^2}{D_{\mathrm{int}}}+\rho v\frac{\mathrm{d}v}{\mathrm{d}z}\right) \tag{T1-21}$$

Moment Equations:

$$\lambda_{np}=\sum_{i=1}^{\infty}\sum_{x=0}^{\infty}i^n x^p C_{\mathrm{R}_i(x)}\ ;\ n=0,\ 1,\ \ldots\ ;\ p=0,\ 1,\ 2,\ \ldots\ \text{(Katz and Saidel, 1967)} \tag{T1-22}$$

$$\mu_{np}=\sum_{i=1}^{\infty}\sum_{x=0}^{\infty}i^n x^p C_{\mathrm{P}_i(x)}\ ;\ n=0,\ 1,\ \ldots\ ;\ p=0,\ 1,\ 2,\ \ldots\ \text{(Katz and Saidel, 1967)} \tag{T1-23}$$

$$v\frac{\mathrm{d}\lambda_{np}}{\mathrm{d}z}=\left\{\begin{array}{l}2k_{\mathrm{o}}C_{\mathrm{M}}C_{\mathrm{O_2}}^{1.1}\delta_{p0}+2\sum_{j=1}^{2}f_j k_{\mathrm{d}j}C_{\mathrm{I}_j}\delta_{p0}+pk_p C_{\mathrm{M}}\lambda_{n,p-1}-k_{\mathrm{tc}}\lambda_{00}\lambda_{np}\\+k_{\mathrm{tdt}}\left(\lambda_{00}\delta_{p0}-\lambda_{np}\right)+k_{\mathrm{trs}}C_{\mathrm{S}}\left(\lambda_{00}\delta_{p0}-\lambda_{np}\right)\\+k_{\mathrm{trp}}\left(\lambda_{00}\sum_{j=0}^{n}({}^nC_j)\mu_{j,p+1}-\lambda_{np}\mu_{01}\right)-\lambda_{np}\frac{\mathrm{d}v}{\mathrm{d}z}\end{array}\right\} \tag{T1-24}$$

$n = 0, 1, \ldots ; p = 0, 1, 2, .$

. .

$$v\frac{\mathrm{d}\mu_{np}}{\mathrm{d}z}=\left\{\begin{array}{l}\frac{k_{\mathrm{tc}}}{2}\sum_{j=0}^{n}\sum_{k=0}^{j}\sum_{i=0}^{p}({}^nC_j)({}^jC_k)({}^pC_i)(-1)^{n-j}\lambda_{ki}\lambda_{j-k,p-i}+k_{\mathrm{tdt}}\lambda_{np}\\+k_{\mathrm{trs}}C_{\mathrm{S}}\lambda_{np}+k_{\mathrm{trp}}\left(\lambda_{np}\mu_{01}-\lambda_{00}\mu_{n,p+1}\right)-\mu_{np}\frac{\mathrm{d}v}{\mathrm{d}z}\end{array}\right\} \tag{T1-25}$$

$n = 0, 1, \ldots ; p = 0, 1, 2, \ldots$

Moment Closures:

$$\mu_{03}=\mu_{00}\left(\frac{\mu_{02}}{\mu_{01}}\right)^3 \tag{T1-26}$$

$$\mu_{13}=\mu_{10}\left(\frac{\mu_{12}}{\mu_{11}}\right)^3 \tag{T1-27}$$

Table 4.1 …. continued…c

Definitions:

$$X_{\mathrm{M}} = 1 - \frac{v}{v_{\mathrm{in}}}\left(\frac{C_{\mathrm{M}}}{C_{\mathrm{M_{in}}}}\right) \quad \text{(T1-28)}$$

$$M_{\mathrm{n}} = 28\left(\frac{\mu_{01} + \lambda_{01}}{\mu_{00} + \lambda_{00}}\right) \quad \text{(T1-29)}$$

$$M_{\mathrm{w}} = 28\left(\frac{\mu_{02} + \lambda_{02}}{\mu_{01} + \lambda_{01}}\right) \quad \text{(T1-30)}$$

$$PDI = \frac{M_{\mathrm{w}}}{M_{\mathrm{n}}} \quad \text{(T1-31)}$$

$$\mathrm{SCB}/1000\ \mathrm{CH_2} = \left(\frac{500 C_{\mathrm{M_e}}}{\mu_{01} + \lambda_{01}}\right) \quad \text{(T1-32)}$$

$$\mathrm{Vinyl}/1000\ \mathrm{CH_2} = \left(\frac{500 C_{\mathrm{V}_i}}{\mu_{01} + \lambda_{01}}\right) \quad \text{(T1-33)}$$

$$\mathrm{Vinylidene}/1000\ \mathrm{CH_2} = \left(\frac{500 C_{\mathrm{V_{id}}}}{\mu_{01} + \lambda_{01}}\right) \quad \text{(T1-34)}$$

Table 4.2 Property Correlations

$\Delta H(\text{kJ/kmol}) = -21500 \times 4.1868$; (Asteasuain et al., 2001b)

$$\rho(\text{kg/m}^3) = \frac{\left\{1 + 28C_{\text{M}}\left(V_{\text{p}} - V_{\text{M}}\right)\right\}}{V_{\text{p}}} \text{ ; (Gupta et al., 1985)} \quad \text{(T2-1)}$$

$$\rho_{\text{M}}(\text{kg/m}^3) = 745.18 - 0.51T \text{ ; } (T \text{ in K; Micheles and Geldermans, 1942}) \quad \text{(T2-2)}$$

$$V_{\text{p}}(\text{m}^3/\text{kg}) = -6.793\times10^{-3} + 1.558\times10^{-5}T - 4.828\times10^{-8}T^2 + 5.118\times10^{-11}T^3 \text{ ; } T \le 426 \text{ K}$$

$$V_{\text{p}}(\text{m}^3/\text{kg}) = 9.135\times10^{-4} + 5.731\times10^{-7}T \text{ ; } T > 426 \text{ K;}$$

(T in K; Parks and Richards, 1948) (T2-3)

$$W_{\text{M}} = \frac{28C_{\text{M}}}{\rho} \quad \text{(T2-4)}$$

$$K(\text{W/m - K}) = 418.68\left(5.0\times10^{-4}W_{\text{M}} + 3.5\times10^{-4}W_{\text{p}}\right) \text{ ; (Zabisky et al., 1992)} \quad \text{(T2-5)}$$

$$\left[\left(\eta - \eta^{\text{o}}\right)\xi + 1\right]^{0.25} = 1.023 + 0.23364\rho_{\text{r}} + 0.58533\rho_{\text{r}}^2 - 0.40758\rho_{\text{r}}^3 + 0.09332\rho_{\text{r}}^4 \quad \text{(a)}$$

$$\xi = 10^7\left(\frac{T_{\text{c}}}{M'^3\left(9.869P_{\text{c}}\right)^4}\right)^{\frac{1}{6}} \quad \text{(b)}$$

$$\eta^{\text{o}}\xi = 4.61T_{\text{r}}^{0.618} - 2.04e^{-0.449T_{\text{r}}} + 1.94e^{-4.058T_{\text{r}}} + 0.1 \text{ ; } 0.1 < \rho_{\text{r}} < 3$$

all viscosities in Pa-s (Poling et al., 2001) (c)

(T2-6)

$$\eta_{\text{s}} = \eta\exp\left[2.00 + 0.001\times a_{\text{v}}\left(\frac{\mu_{01}}{\mu_{00}}\right)^{0.556}\mu_{01} + \frac{E_{\text{v}}}{\text{R}}\left(\frac{1}{T} - \frac{1}{423}\right)\right] \text{ ;}$$

all viscosities in Pa-s (Kiparissides et al., 1993a) (a)

$$E_{\text{v}}(\text{kJ/kmol}) = -4.1868(500 - 560\mu_{01}) \quad \text{(b)}$$

(T2-7)

h_{w} (W/m^2-K)= 0.03 × 41868 ; (Mavridis and Kiparissides, 1985) (T2-8)

$$h_{\text{i}}(\text{W/m}^2\text{ - K}) = \frac{K(\text{Nu})}{D_{\text{int}}} \quad \text{(T2-9)}$$

$$\text{Nu} = 0.166\left(\text{Re}^{2/3} - 125\right)\text{Pr}^{0.33}\left(1 + \left(D_{\text{in}}/L\right)^{2/3}\right) \text{ ; } 1398 < \text{Re} < 10{,}000$$

$$\text{Nu} = 0.026\,\text{Re}^{0.8}\,\text{Pr}^{0.33} \text{ ; Re} > 10{,}000\text{; (Zabisky et al., 1992)} \quad \text{(T2-10)}$$

h_{o} (W/m^2-K) = 10,000 ; m = 1; (Coulson et al., 1996) (T2-11)

$$h_{\text{o}}(\text{W/m}^2\text{ - K}) = \frac{K_{\text{J}m}\left(0.026\,\text{Re}_{\text{J}m}^{0.8}\,\text{Pr}_{\text{J}m}^{0.33}\right)}{D_{\text{e}}} \text{ ; } m = 2, \ldots, 5\text{; (Lacunza et al., 1998)}$$

(T2-12)

$$\text{Re}_{\text{J}m} = \frac{D_{\text{e}}\rho_{\text{J}m}v_{\text{J}m}}{\mu_{\text{J}m}} \text{ ; } m = 2, \ldots, 5 \quad \text{(T2-13)}$$

$$D_{\text{e}}(\text{m}) = \frac{\left(D_{\text{Ji}}^2 - D_{\text{o}}^2\right)}{D_{\text{o}}} \quad \text{(T2-14)}$$

$$\frac{1}{U} = \left\{ \frac{1}{h_i} + \frac{1}{h_w} + \frac{D_{int}}{D_o h_o} \right\} \qquad \text{(T2-15)}$$

An average constant temperature of jacket fluid in each zone is assumed in this study. The jacket fluid normally flows counter-currently in industrial LDPE reactors. The 'correct' modeling of such systems requires the solution of the coupled set of several ODEs for the inner (reacting) fluid and the energy balance of the outer (counter-currently flowing) fluid. This needs iterative solutions (Asteasuain et al., 2001b) and is prohibitively time consuming, and unsuited for optimization studies (where the model has to be solved several times over for each chromosome in each generation). The assumption of a constant (average) temperature of the coolant, though not exact, goes around this problem. And, since data are being 'tuned', errors associated with this assumption will be taken care of by tuning.

The coupled non-linear ODEs describing the reactor are integrated using the D02EJF subroutine in the NAG library. This subroutine uses Gear's technique (Ray and Gupta, 2001) to integrate the stiff equations. A tolerance (TOL) of 10^{-5} is used. A decrease in the value of this parameter to 10^{-8} changes the results only in the fourth decimal place. Oxygen is used as the initiator and n-butane (Brandolin et al., 1988) as the inert solvent in the feed stream, while initiator, I_1 (tert-butyl peroxypivalate; Goto et al., 1981), and initiator I_2 (tert-butyl 3,5,5 trimethyl-peroxyhexaonate; Kiparissides et al., 1993b) are used as intermediate feeds, as shown in Figure 4.1. Details of the industrial system (Asteasuain et al., 2001b) are given in Table 4.3. This table also includes reasonable values (assumed for this study) of the missing details (Asteasuain et al., 2001b) of the reactor. The rate constants (Brandolin et al., 1996) are provided in Table 4.4. On integration, the model gives the profiles of several molecular properties of LDPE [M_n, M_w, *PDI*, SCB), and the vinyl and vinylidene group concentrations, as

defined in Equations T1-29 – T1-34 in Table 4.1], the temperature, pressure and concentrations of the monomer, telogen, and initiators, as a function of the axial position, z.

Table 4.3 Details of the Industrial LDPE Tubular Reactor Studied (Asteasuain et al., 2001b)

Quantities	Numerical values
Total reactor length (L_t)	1390 m
Inside diameter of reactor (D_{int})	0.05 m
*Wall thickness of reactor (t)	0.0254 m
Number of zones (N_z)	5
*Inner diameter of outer (jacket) wall (D_{Ji})	0.2032 m
Axial lengths of zones (L_{zm}, m = 1, . . . , 5)	60, 100, 180, 510, 540 m
Flow rate of monomer (F_M)	11 kg/s
Flow rate of oxygen (F_o)	6.8×10^{-5} kg/s
Flow rate of telogen (F_S)	7.4×10^{-2} kg/s
Flow rate of inert (F_{inert})	0.22 kg/s
Flow rate of initiator-1 ($F_{I,1}$)	1.0×10^{-3} kg/s
Flow rate of initiator-2 ($F_{I,2}$)	1.6×10^{-4} kg/s
*Flow rates of jacket fluids (V_{Jm}, m = 2, . . . , 5)	4.03×10^{-3}, 3.94×10^{-3}, 3.32×10^{-3}, 0.26×10^{-3} m^3/s
Inlet temperature (T_{in})	349.15 K
Inlet pressure (P_{in})	227.98 MPa
Mean jacket temperatures ($T_{J,m}$, m = 1, . . . , 5)	441.15, 498.15, 498.15, 441.15, 441.15 K
Specific heat of reaction mixture (C_{Pm}, m = 1, . . . , 5)	2.42834, 2.42834, 3.1401, 3.1401, 4.01933 kJ/kg-K
Initial conditions for moments (λ_{np}, μ_{np}; n = 0, 1; p = 0, 1, 2)	0.0 kmol/m^3

* Values of the parameters assumed in this study

The model parameters are tuned using three sets of industrial data (Asteasuain et al., 2001b): the temperature, $T^{ind}(z_j)$, read from the plot (Asteasuain et al., 2001b), with an accuracy of ± 2 K at several discrete points, z_j; j = 1, 2, . . . , 33 (with z_j = 0, 23, 51, 56, 79, 107, 135, 166, 180, 205, 266, 308, 350, 387, 429, 467, 509, 546, 597, 635, 677, 714, 751, 803, 855, 898, 929, 971, 1022, 1101, 1162, 1241, 1321 m for the five zones: $0 \le z \le 60$ m, $60 \le z \le 160$ m, $160 \le z \le 340$ m, $340 \le z \le 850$ m, and 850

$\leq z \leq$ 1390 m), and the values of the monomer conversion, the number-average molecular weight and the side-product concentrations in the final product. The sum-of-squares of the normalized error, I, between the model-predicted and the industrial values:

$$I(\boldsymbol{u}) = \sum_{i,j} \left(1 - \frac{S_i^{\text{ind}}(z_j)}{S_i^{\text{m}}(z_j)} \right)^2 \tag{4.1}$$

is minimized. In Equation (4.1), S_i is the value of the i^{th} property, and superscripts m and ind represent the values predicted by the model and the industrial values, respectively. $\boldsymbol{u}$ represents the vector of parameters that are tuned. Binary-coded NSGA-II (Deb, 2001) is used to minimize I.

4.2.2 Estimation of Model Parameters

The rate constants in Table 4.4 are taken mostly from Brandolin et al. (1996) except the parameters, A_{trs}, E_{trs}, and ΔV_{trs}, characterizing chain transfer to the telogen. These are taken from Asteasuain et al. (2001a). The kinetic parameters, A_{d1}, $E_{\text{d1,}}$ $\Delta V_{\text{d1,}}$ A_{d2}, $E_{\text{d2,}}$ and ΔV_{d2}, for the two initiators are given (Brandolin et al., 1996) as ranges due to proprietary reasons. The activation energies of the two initiators (E_{d1} and E_{d2}) need to be tuned using the industrial data. While average values (of the ranges given by Brandolin et al., 1996) of A_{d1}, $\Delta V_{\text{d1,}}$ A_{d2}, and ΔV_{d2} are used in the model. Similar tuning (Brandolin et al., 1996; Zabisky et al., 1992; Asteasuain et al., 2001a; Brandolin et al., 1988) of kinetic parameters has been used earlier, too, to obtain the rate constants for ethylene polymerization. The first four industrial values (j = 1 – 4) of the temperatures, $T^{\text{ind}}(z_j)$, are not used for tuning since no reaction is taking place in this zone, and the reactor is only acting as a heat exchanger. It is found that the model tuned with only these two parameters underestimates the values of the monomer

conversion, $X_{M,f}$, and the number-average molecular weight, $M_{n,f}$, of the product. Moreover, the temperature peak in the first zone is overestimated while the peak in the second zone is underestimated. This suggests that we use additional parameters for accurate prediction of industrial data.

Table 4.4 Rate Constants (Brandolin et al., 1996; Asteasuain et al., 2001a)

$$k = Ae^{-\left(\frac{E+10^3 P\Delta V}{RT}\right)}$$

A: (1/s; m^3/kmol-s; $m^{3.3}$/$kmol^{1.1}$-s); E: kJ/kmol; P: MPa; ΔV: m^3/kmol; T: K; R = 8.314 kJ/kmol-K

Rate constant	A	E	ΔV
k_o	$^{+}1.6 \times 10^{11}$	*132168	-12.1×10^{-3}
k_{d1}	$^{o}1.0 \times 10^{14}$	*119929	$^{o}14.0 \times 10^{-3}$
k_{d2}	$^{o}1.0 \times 10^{12}$	*123117	$^{o}11.6 \times 10^{-3}$
k_p	4.0×10^{5}	*17431	-16.8×10^{-3}
k_{tc}	8.7×10^{8}	15282	9.2×10^{-3}
k_{tdt}	7.7×10^{9}	79968	-10.0×10^{-3}
$^{\dagger}k_{trs}$	7.0×10^{4}	*18406	0.0
k_{trp}	5.2×10^{4}	36844	-19.0×10^{-3}
k_{bb}	1.2×10^{10}	*60537	0.0
k_{b1}	1.4×10^{9}	*84747	-9.90×10^{-3}
k_b	4.4×10^{9}	*70205	-9.90×10^{-3}

* Values of the parameters obtained in the present study. These differ from those of Brandolin et al. (1996) and Asteasuain et al. (2001a).

$^{+}$ $m^{3.3}$/$kmol^{1.1}$-s

† Asteasuain et al. (2001a).

^{o} Average values of the parameters based on the ranges reported by Brandolin et al. (1996).

Note: Efficiencies, f_1 and f_2, of the two initiators are 0.98 (fitted in the range of 0.75 – 1.00; Brandolin et al., 1996), and 1.00 (Brandolin et al., 1996), respectively. The efficiency of oxygen is assumed to be 1.00.

Several simulations were made to study the effect of the individual parameters on the results. The set of tuning parameters used is expanded in stages till satisfactory agreement is attained. The activation energy, E_o, characterizing initiation by oxygen, and the activation energy, E_p, describing the propagation reaction are incorporated in the earlier set (to give a total of four parameters). The former should help in

improving the agreement of the temperature peak in the first zone (since oxygen affects the exothermic polymerization in this zone), while the latter affects the polymerization in the entire reactor, and should help to improve the agreement of the results elsewhere. Unfortunately, this does not help too, since the temperature peak in the second zone is still underestimated. The parameters influencing the rates of heat transfer are then incorporated. Since steam is used for heating the reaction mixture in the first zone, use of the high value of h_o (10,000 W/m^2-K; Coulson et al., 1996) for condensing steam would not help. Hence, the four volumetric flow rates, $V_{J2} - V_{J5}$, of the jacket fluid (that influence h_o in those zones) are added on to the set of parameters used for tuning. Kiparissides et al. (1993b) cited the value of a_v (Equation 53) in their work) as 0.0225. However, the same group of workers (Kiparissides et al., 1993a) used a different value of 0.017 (Equation 68) in another paper. This suggests that this parameter, which influences the viscosity of the reaction mass and hence the value of h_i, also needs to be included in the set of tuning parameters. The tuning with two parameters in the first stage also led to the underestimation of $M_{n,f}$. Since the solvent (chain transfer) controls the molecular weight of the product without affecting the temperature of the reaction mass much, the corresponding rate parameter, E_{trs}, is also included for tuning purposes.

Asteasuain et al. (2001b) do not provide the concentrations of the side products, methyl, vinyl and vinylidene groups, in the final polymer. The tuned model predicts results for these that agree *qualitatively* with those reported by Brandolin et al. (1996). However, *quantitative* agreement is necessary for a good model. Most workers (Brandolin et al., 1996; Anspon, 1964; Goto et al., 1981; Gupta et al., 1985; Kiparissides et al., 1993b; Gaylord and Mark, 1959; Kalyon et al., 1994; Woodbrey and Enrlich, 1963) report methyl (M_e), vinyl (V_i) and vinylidene (V_{id}) contents in the

product as 25 – 30, 0.08 – 0.13, and 0.4 – 0.8, respectively, per 1000 CH_2. Values ($[M_e]_f$, $[V_i]_f$, and $[V_{id}]_f$) of SCB/1000 CH_2 of 30, vinyl/1000 CH_2 as 0.1, and vinylidene/1000 CH_2 of 0.7 (Goto et al., 1981; Gupta et al., 1985) are used as 'industrial' values for tuning the model. The parameters, E_{bb}, E_{b1}, and E_b, associated with the corresponding reactions, also need to be used for tuning. The complete set of 13 model parameters used finally for tuning all the available results are: $\boldsymbol{u} \equiv [E_o, E_{d1}, E_{d2}, E_p, E_{trs}, E_{bb}, E_{b1}, E_b, V_{J2}, V_{J3}, V_{J4}, V_{J5}, a_v]$. The exact objective function to be minimized, is given by

$$I(\boldsymbol{u}) = \sum_{j=5}^{33} W_{T,j}\left(1-\frac{T^{ind}(z_j)}{T^{m}(z_j)}\right)^2 + W_{M_n}\left(1-\frac{21900}{M_{n,f}^{m}}\right)^2 + W_{X_M}\left(1-\frac{0.30}{X_{M,f}^{m}}\right)^2 + W_{M_e}\left(1-\frac{30}{[M_e]_f^{m}}\right)^2 + W_{V_i}\left(1-\frac{0.10}{[V_i]_f^{m}}\right)^2 + W_{V_{id}}\left(1-\frac{0.70}{[V_{id}]_f^{m}}\right)^2 \tag{4.2}$$

In Equation (4.2), W_j is the weighting factor associated with the normalized square error of the j^{th} quantity. The values of these weighting factors are set to one except for W_{M_n} [= 15] and W_{X_M} [= 5] to give more emphasis for better prediction of $M_{n,f}$ and $X_{M,f}$. The lower and upper bounds and the final tuned values of these parameters are shown in Table 4.5. The values used for the computational parameters (best values) in the binary-coded NSGA-II are given in Table 4.6. Figure 4.2 shows that the agreement between the model predictions (for the temperature profile, the monomer conversion and the number-average molecular weight at the end, and estimates of the several side products (Goto et al., 1981; Gupta et al., 1985; Asteasuain et al., 2001b) and the industrial results is quite good. Table 4.7 shows a comparison of these quantities at the end of the reactor.

Table 4.5 Bounds, Final Tuned Values, and Reported Values of the Parameters

Bounds	Final tuned values	Reported values (Brandolin et al., 1996)
$125604 < E_o < 138164$	132168	135945
$117230 < E_{d1} < 136071$	119929	94621 – 133140
$117230 < E_{d2} < 133977$	123117	94621 – 132721
$14653 < E_p < 18003$	17431	17626
$14653 < E_{trs} < 20934$	18406	$^{+}$17253
$56521 < E_{bb} < 66988$	60537	61964
$71175 < E_{b1} < 87922$	84747	79967
$62802 < E_b < 87922$	70205	79967
$0.5 \times 10^{-3} < {}^{*}V_{J2} < 7.0 \times 10^{-3}$	4.03×10^{-3}	$^{o}1.2 \times 10^{-3}$
$0.5 \times 10^{-3} < {}^{*}V_{J3} < 7.0 \times 10^{-3}$	3.94×10^{-3}	$^{o}1.2 \times 10^{-3}$
$0.5 \times 10^{-3} < {}^{*}V_{J4} < 5.0 \times 10^{-3}$	3.32×10^{-3}	$^{o}1.2 \times 10^{-3}$
$0.1 \times 10^{-3} < {}^{*}V_{J5} < 5.0 \times 10^{-3}$	0.22×10^{-3}	$^{o}1.2 \times 10^{-3}$
$0.009 < a_v < 0.0185$	0.018	$^{\Delta}$0.017

* Values of parameters in m^3/s

$^{+}$ Asteasuain et al. (2001a).

^{o} Yao et al. (2004).

$^{\Delta}$ Kiparissides et al. (1993a).

Table 4.6 Values of the (*best*) Computational Parameters Used in Binary-coded NSGA-II, NSGA-II-JG, and NSGA-II-aJG

Parameter	NSGA-II (for parameter estimation)	NSGA-II (for optimization)	NSGA-II-JG	NSGA-II-aJG (for 2- and 4-obj optimization)
N_{gen}	100	*600	*900	*700
N_{pop}	100	200	200	200
l_{substr}	30	30	30	30
l_{chrom}	390	330	330	330
l_{aJG}	---	---	---	70
p_c	0.8	0.95	0.9	0.8
p_m	0.01	0.015	0.005	0.01
p_{JG}	---	---	0.8	0.8
S_r	0.9	0.95	0.9	0.6

* Generations required for convergence of the Pareto-optimal set for $M_{n,f} = 21900 \pm 200$ kg/kmol

Table 4.7 Comparison of the Model-Predicted Values to the Industrial Data (Goto et al., 1981; Gupta et al., 1985; Asteasuain et al., 2001b)

Quantity at the reactor exit	Industrial data	Model prediction
Monomer conversion (Asteasuain et al., 2001b)	0.30	0.2971
Number-average molecular weight (kg/kmol; Asteasuain et al., 2001b)	21900	21901
CH_3 groups (SCB) per 1000 CH_2 (Gupta et al., 1985)	30	30.13
Vinyl groups per 1000 CH_2 (Goto et al., 1981)	0.1	0.1
Vinylidene groups per 1000 CH_2 (Gupta et al., 1985)	0.7	0.7
Weight-average molecular weight (kg/kmol)	-	145380

The temperature profile in Figure 4.2a shows that the first two zones are acting as preheating zones to heat the reaction mixture. Reaction is not occurring in these two zones. The free radical population is generated in the third zone after feeding in the first initiator, and these radicals react with monomer molecules to form polymer via polymerization reaction. A sharp temperature peak is observed in this zone due to the exothermic nature of polymerization reaction. Monomer conversion (X_M) also shows sudden jump corresponding to this temperature peak and almost all initiator is exhausted at this point. After that, X_M remains practically constant until another initiator is added in the fifth zone. Second initiator is added in the fifth zone to boost the monomer conversion as shown in Figure 4.2b. This initiator is also depleted soon after its introduction into the reactor. Note that the reaction mixture is cooled in the fourth zone to the optimal level for half-life of second initiator which governs the maximum efficiency of initiator.

Number-average molecular weight (M_n) profile shows that it suddenly drops in the third zone and becomes steady as the reaction mixture enters the cooling zone (Figure 4.2c). This decrease in molecular weight corresponds to the increase in the reaction temperature. Initiator decomposition is more temperature dependent than chain

growth, while chain termination is hardly affected (Luft et al., 1983). Thus free radical population is increased and they react with monomer molecules to form polymer chains, but these chains tend to be smaller. Hence average molecular weight is reduced. However, the change in M_n at the beginning of the fifth zone is less abrupt than the one observed in the third zone which might be due to the presence of already formed polymer in the reaction mixture (Brandolin et al., 1996). Figure 4.2d shows that SCB in LDPE is observed once polymer is formed in the third zone and it remains almost constant till the second peroxide is injected in the fifth zone. The less abrupt change in methyl group concentration again accounts for already formed polymer change. The trends for vinyl and vinylidene concentrations can similarly be explained (Figures 4.2e and f).

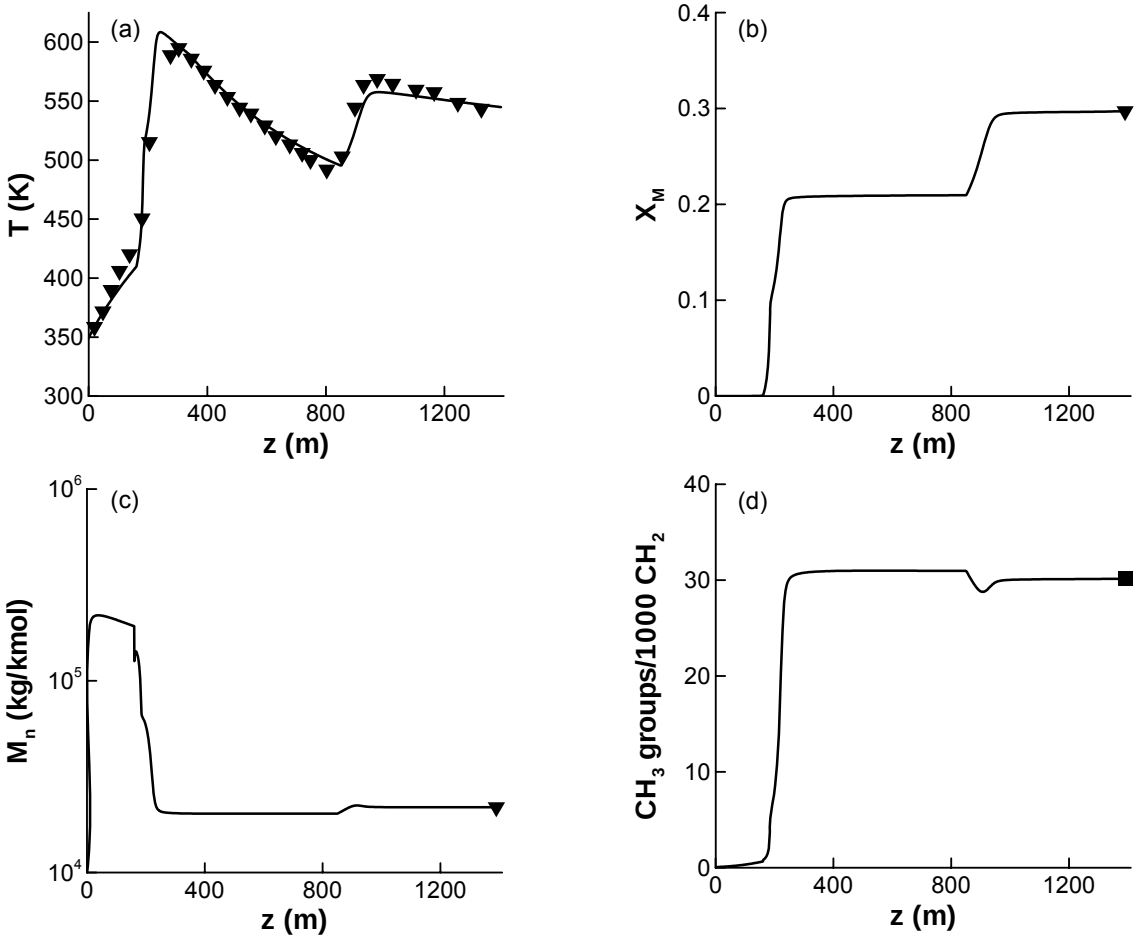

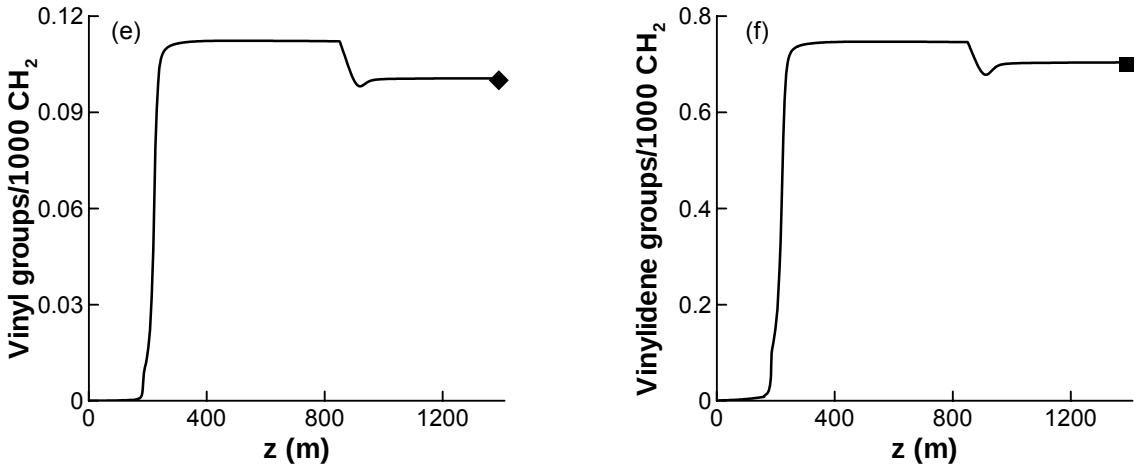

Figure 4.2 Model predictions; (▼): industrial data (Asteasuain et al., 2001b)**; (♦): industrial estimate** (Goto et al., 1981) **and (■): industrial estimates** (Gupta et al., 1985) **for the LDPE reactor of Figure 4.1.**

Note that the tuning of the model parameters is performed using a single set of operating conditions even though several sets of operating conditions should be used for reliable modeling. Jacket fluid flow rates are included in the set of tuned model parameters which should have been part of the operating data used in the model parameter estimation. Both these could have been avoided if more data were available (Asteasuain et al., 2001b) or we had industrial data of our own. We did not provide the statistical inferences (confidence intervals and correlation structure) on the parameter estimates due to high complexity of the problem and limited industrial data. However, over-parameterization of the problem is avoided by addition of extra parameters only after careful examination. We started with tuning only 2 parameters and progressively added more parameters to improve the predictions. In fact, the model was tuned with 26 parameters (pre-exponential factors and activation volumes along with activation energies for the respective rate parameters), but later we found that almost the same results could be obtained with only 13 model parameters.

4.3 Multi-Objective Optimization of LDPE Tubular Reactor

4.3.1 Formulation

MOO of the industrial LDPE reactor described above is now carried out using the model developed. The two objective functions used are: maximization of the monomer conversion, $X_{M,f}$, and minimization of the (weighted average value of the) undesirable side product contents ($[M_e]_f$, $[V_i]_f$, and $[V_{id}]_f$). In industry, number-average molecular weight of the product is normally fixed depending on the required polymer grade but it can vary within an acceptable range about this fixed value. On the other hand, undesired side products should be minimized to improve the polymer quality and strength although some may place them appropriately in constraints. Although thermodynamics and safety considerations govern conversion, other factors such as economics can lead to an optimal conversion. Also, multi-objective optimization provides the opportunity to consider more objectives. Hence, we choose conversion and side products as objectives. Solution of this problem provides a range of solutions to the decision maker, who can choose one of them depending on other considerations such as safety, ease of operability, market demand, economics etc. The binary-coded NSGA-II (Deb, 2001), as well as its two JG adaptations, NSGA-II-JG (Kasat and Gupta, 2003) and NSGA-II-aJG (Guria et al., 2005) (both binary-coded) are used. In this study, the optimization assumes that the reactor geometry (reactor length (L_t), inside diameter (D_{int}) and jacket diameter (D_{Ji}), monomer feed rate (F_M), and flow rates of the jacket fluid are fixed and only the 'operating' variables are used as the decision variables for the optimization, which are the inlet temperature, T_{in}, the feed flow rates, F_o, F_S, $F_{I,1}$, and $F_{I,2}$, of oxygen, solvent and the two additional initiators added in-between, the five average temperatures, $T_{J,1} - T_{J,5}$, of the jacket fluids and the inlet pressure, P_{in}. In total, there are 11 decision variables. The temperature of the

reaction mass along the axial length at one meter interval is stored and then the maximum temperature in the reactor, $T_{max}(z)$, is found. A local constraint, $T_{max}(z) \leq T_{max,d}$ (= 610.15 K), is imposed on the temperature to ensure safety, while the number average molecular weight, $M_{n,f}$, of the product is constrained to lie (exactly) at a desired value of $M_{n,d}$ of 21,900 kg/kmol (Asteasuain et al., 2001b). These two constraints are handled by incorporating them as penalty functions (Deb, 2001; Edgar et al., 2001) with weighting factors, $w_1 = 10^9$ and $w_2 = 10^{10}$, respectively, in both the objective functions. Both these constraints are used in the normalized forms. It should be noted that the constraint on temperature is an inequality constraint while that on M_n is an equality constraint. The bracketed inequality constraint (Deb, 2001) is used in the penalty term for the former. Lower and upper bounds are placed on each of the decision variables. The above problem is written mathematically as:

$$\text{Max } G_1 \equiv X_{M,f} - w_1\left(1-\frac{M_{n,f}}{M_{n,d}}\right)^2 - w_1\left\langle 1-\frac{T_{max}(z)}{T_{max,d}}\right\rangle^2 \tag{4.3a}$$

$$\text{Max } G_2 \equiv \frac{1}{1+\left(\frac{[M_e]_f}{30}+\frac{[V_i]_f}{0.1}+\frac{[V_{id}]_f}{0.7}\right)} - w_2\left(1-\frac{M_{n,f}}{M_{n,d}}\right)^2 - w_2\left\langle 1-\frac{T_{max}(z)}{T_{max,d}}\right\rangle^2 \tag{4.3b}$$

Subject to

Bounds:

$323.15 \leq T_{in} \leq 403.15$ K (Brandolin et al., 1988) (4.3c)

$5 \times 10^{-5} \leq F_o \leq 10 \times 10^{-5}$ kg/s (Brandolin et al., 1988) (4.3d)

$5 \times 10^{-5} \leq F_S \leq 0.5$ kg/s (Asteasuain et al., 2001b) (4.3e)

$5 \times 10^{-5} \leq F_{I,1} \leq 5 \times 10^{-3}$ kg/s (Asteasuain et al., 2001b) (4.3f)

$5 \times 10^{-5} \leq F_{I,2} \leq 5 \times 10^{-3}$ kg/s (Asteasuain et al., 2001b) (4.3g)

$383.15 \leq T_{J,m} \leq 543.15$ K ; $m = 1, \ldots, 5$ (4.3h)

$192.52 \leq P_{in} \leq 253.31$ MPa (Brandolin et al., 1988) (4.3i)

Local constraints:

Model equations (4.3j)

The bracket operator, $<\alpha>$, denotes the absolute value of the operand (α), if the operand is negative. Otherwise, it returns a value of zero if α is non-negative. The bounds (Equations 4.3c – 4.3g); Equation 4.3i) for most of the decision variables have been chosen based on information in the literature (Asteasuain et al., 2001b; Brandolin et al., 1988). The bounds (Equation 4.3h) for the five average jacket temperatures have been selected so as to give a range around the values reported by Asteasuain et al. (2001b). The available NSGA-II codes maximize all the objective functions. Hence, a problem involving the minimization of a function, J, is converted to a maximization problem by using the transformation, $G = 1/(1 + J)$ [see the first term on the right hand side in Equation 4.3b].

While solving Equation (4.3), it was observed that the simulation was taking an excessive amount of CPU time for *some* chromosomes. These chromosomes were then studied in detail, individually. It was found that this occurred only when F_S was selected below a certain value. Under these conditions, the balance equations became extremely stiff in certain ranges of z, as reflected by the very high number of function evaluations called by the NAG library subroutine, D02EJF. Hence, the lower bound of F_S was increased. Since F_S also affects the other decision variables, the bounds of these, too, were changed from those selected initially (Equation 4.3). Rajesh et al. (2000) had encountered a similar problem in the MOO of steam reformers. One of the decision variables, $(H/C)_{in}$, had to be constrained to lie within a certain range of values selected by GA for two other decision variables, viz., the inlet temperature and

$(S/C)_{in}$ to avoid getting negative values of the intra-pellet mole fractions (chromosome-specific bounds). The modified bounds for the decision variables used in place of those in Equation (4.3) are given below:

$323.15 \leq T_{in} \leq 403.15$ K (4.4a)

$5 \times 10^{-5} \leq F_o \leq 10 \times 10^{-5}$ kg/s (4.4b)

$2 \times 10^{-2} \leq F_S \leq 0.5$ kg/s (4.4c)

$5 \times 10^{-5} \leq F_{I,1} \leq 5 \times 10^{-3}$ kg/s (4.4d)

$5 \times 10^{-5} \leq F_{I,2} \leq 5 \times 10^{-3}$ kg/s (4.4e)

$413.15 \leq T_{J,1} \leq 543.15$ K (4.4f)

$473.15 \leq T_{J,2} \leq 543.15$ K (4.4g)

$473.15 \leq T_{J,3} \leq 543.15$ K (4.4h)

$413.15 \leq T_{J,4} \leq 543.15$ K (4.4i)

$413.15 \leq T_{J,5} \leq 543.15$ K (4.4j)

$182.39 \leq P_{in} \leq 248.25$ MPa (4.4k)

The solution of Equation (4.3) with these bounds overcomes the problem of excessive CPU time.

4.3.2 Results and Discussion

The solution of the MOO problem is obtained using an empirically determined best set of values of the several computational parameters. These are given in Table 4.6. The CPU time for a typical (reference) run of 700 generations on a P4 computer (3.0 GHz, 1 GB RAM) is 7 hours and 5 minutes. This computer system can do 220 MFlops (million floating point operations per second) according to the LINPACK benchmark program available at http://www.netlib.org for a matrix of order 500. Some solutions, perhaps local optimal (see Figure 4.3), are obtained with NSGA-II

for $M_{n,f} = M_{n,d} \pm 0$ kg/kmol (a 'hard' constraint) rather than a Pareto-optimal set of solutions. We then relax ('soften') the end-point constraint and allow $M_{n,f}$ to lie within a *small* range of $M_{n,d}$ (well within the experimental error of ± 10 % for molecular weights), in particular, $M_{n,f} = M_{n,d} \pm 200$ kg/kmol, $M_{n,f} = M_{n,d} \pm 20$ kg/kmol, and $M_{n,f} = M_{n,d} \pm 2$ kg/kmol. Interestingly, Pareto sets of optimal points are obtained with excellent spreads (see Figure 4.3a). The Pareto sets for the first two problems superpose, giving confidence on the solutions. Since it is difficult to distinguish the overlapping points, these results are re-plotted in Figure 4.3b using vertical displacements of 0.2. It is observed from Figure 4.3a that the results for the $M_{n,f} = M_{n,d} \pm 0$ kg/kmol case are quite far from those for the other two cases. This gives rise to a suspicion that the algorithm may be converging to local optima. The results obtained with a smaller range of $M_{n,f}$ (= $M_{n,d} \pm 2$ kg/kmol) do not converge to the common Pareto set even for a very large number of generations (it seems to converge to the same Pareto set, however, in 10,000 generations when different algorithms, NSGA-II-JG and NSGA-II-aJG are used; this is discussed later). These possibly reflect the failure of the binary-coded NSGA-II to converge to the global optimal solution when one attempts to satisfy the constraint on $M_{n,f}$ exactly (hard constraint).

We attempt to improve the solutions by using NSGA-II-JG and NSGA-II-aJG. Best values of the computational parameters are again obtained empirically for *each* of the JG adaptations. These values are also listed in Table 4.6. Figure 4.4 shows the converged Pareto sets generated using the three techniques, NSGA-II, NSGA-II-JG, and NSGA-II-aJG, for the case when $M_{n,f} = M_{n,d} \pm 200$ kg/kmol. Hereafter, the problem with $M_{n,f} = M_{n,d} \pm 200$ kg/kmol using NSGA-II-aJG is referred to as the reference case. It is clear that all the three techniques give almost similar Pareto sets, with a larger range, a good distribution of points (good spread) though NSGA-II

converges to the Pareto-optimal set in the lowest number of generations (600), as compared to NSGA-II-aJG (700 generations) or NSGA-II-JG (900 generations).

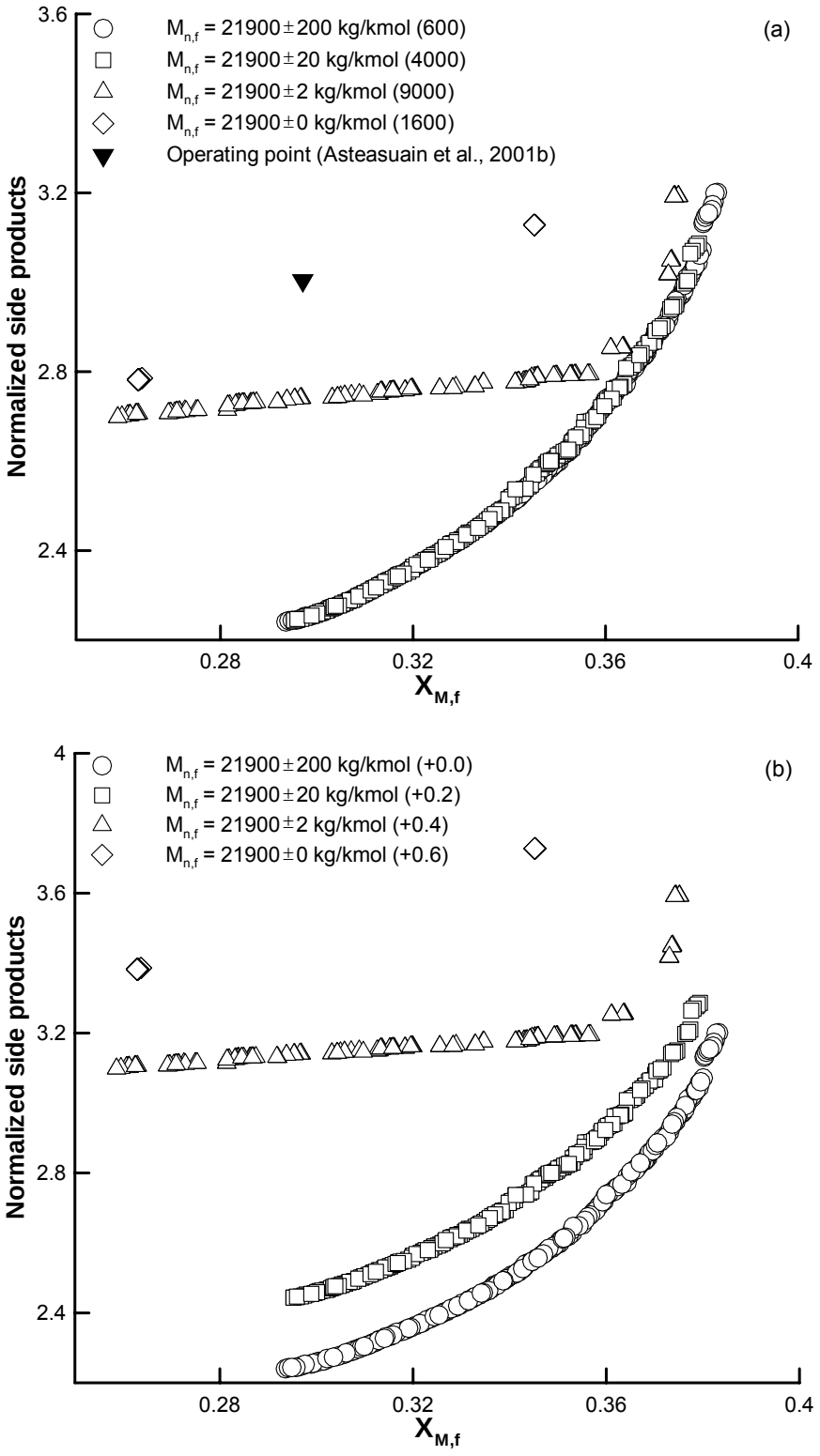

Figure 4.3 (a) Converged solutions for several end-point constraints on $M_{n,f}$ using NSGA-II. Numbers in parenthesis refer to the number of generations. (b) The results of Figure 4.3a are re-plotted with vertical shifts of 0.2 (i.e., the values of the ordinate for $M_{n,f}$ = 21900 ± 20 kg/kmol are displaced vertically upwards by 0.2, etc.)

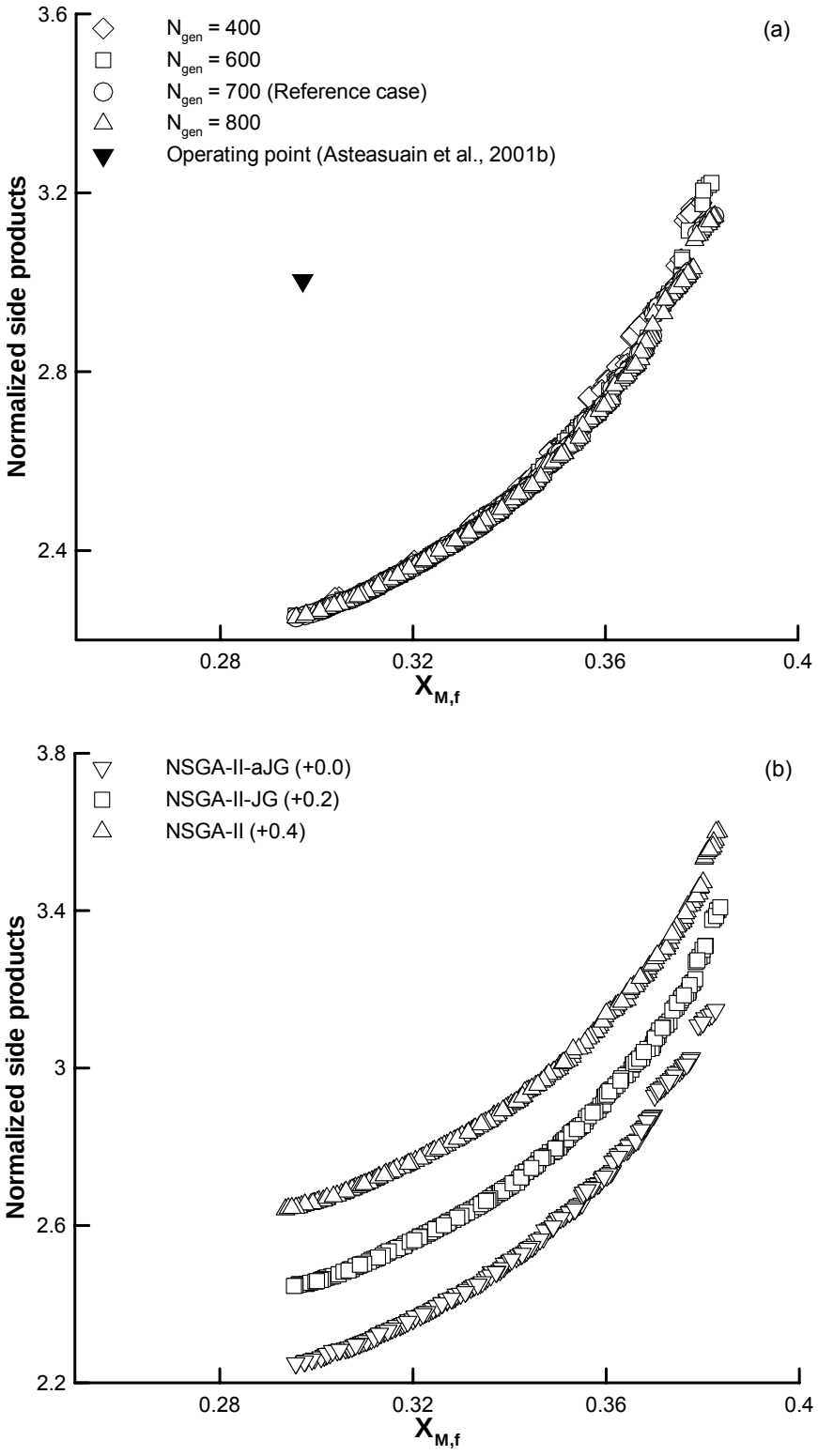

Figure 4.4 (a) Converged Pareto-optimal sets for $M_{n,f}$ = 21900 ± 200 kg/kmol using NSGA-II and its JG adaptations. Numbers in parenthesis indicate the number of generations. (b) Results of Figure 4.4a re-plotted with vertical shifts of 0.2, as in Figure 4.3b.

Figure 4.5 shows how the solutions converge for the reference case with NSGA-II-aJG. It is clear that the solutions at the 700th generation can be considered to be acceptable (converged). In contrast, Figure 4.6 shows that when the MOO problem is solved using $M_{n,f} = M_{n,d} \pm 20$ kg/kmol, the convergence is extremely slow, and the same Pareto set is obtained only after about 6000 generations. The solutions for several cases (± 1100, ± 20, ± 2 kg/kmol) by both NSGA-II-JG and NSGA-II-aJG converged to the reference Pareto (in Figure 4.6). (The results for NSGA-II-JG are not shown in Figure 4.6 for clarity, but can be provided on request.). Since NSGA-II did not converge for the $M_{n,f} = M_{n,d} \pm 2$ kg/kmol case (Figure 4.3) while NSGA-II-aJG did (Figure 4.6, as did NSGA-II-JG), this indicates better performance of the latter technique(s) than NSGA-II when (near) hard end-point constraints are used. NSGA-II uses the concept of elitism, borrowed from nature, in which better chromosomes are copied to the next generation. But, diversity decreases due to elitism. To avoid this, Kasat and Gupta (2003) introduced jumping genes (JG) into NSGA-II. It seems that the relatively poor performance of NSGA-II for problems with (near) hard end-point constraints is due to the loss in diversity of chromosomes while NSGA-II-JG and NSGA-II-aJG introduce higher exploratory capability into the algorithm. Thus, they perform better than NSGA-II to solve difficult problems similar to the one studied herein. In fact, Kasat and Gupta (2003) too observed that NSGA-II could not converge to the global Pareto-optimal set for ZDT4 (Zitzler et al., 2000) problem but NSGA-II-JG did, indeed, converge. We could not converge to the reference Pareto set for the $M_{n,f} = M_{n,d} \pm 0$ kg/kmol case by all the three techniques, NSGA-II, NSGA-II-JG and NSGA-II-aJG. This is shown in Figure 4.7.

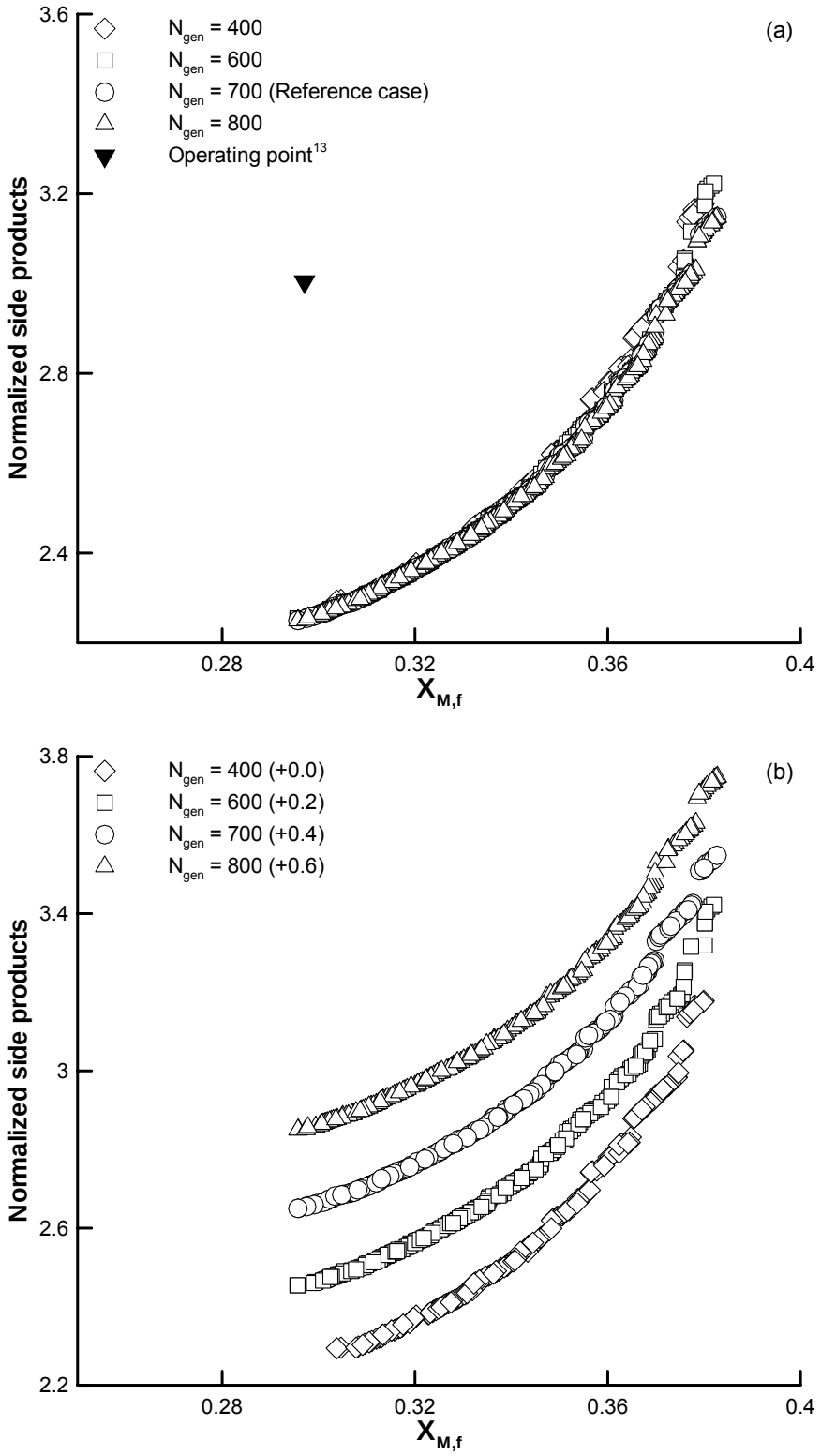

Figure 4.5 (a) Pareto-optimal sets for $M_{n,f}$ = 21900 ± 200 kg/kmol (reference case) using NSGA-II-aJG for different number of generations (indicated in parenthesis). (b) Results of Figure 4.5a re-plotted with vertical shifts of 0.2, as in Figure 4.3b.

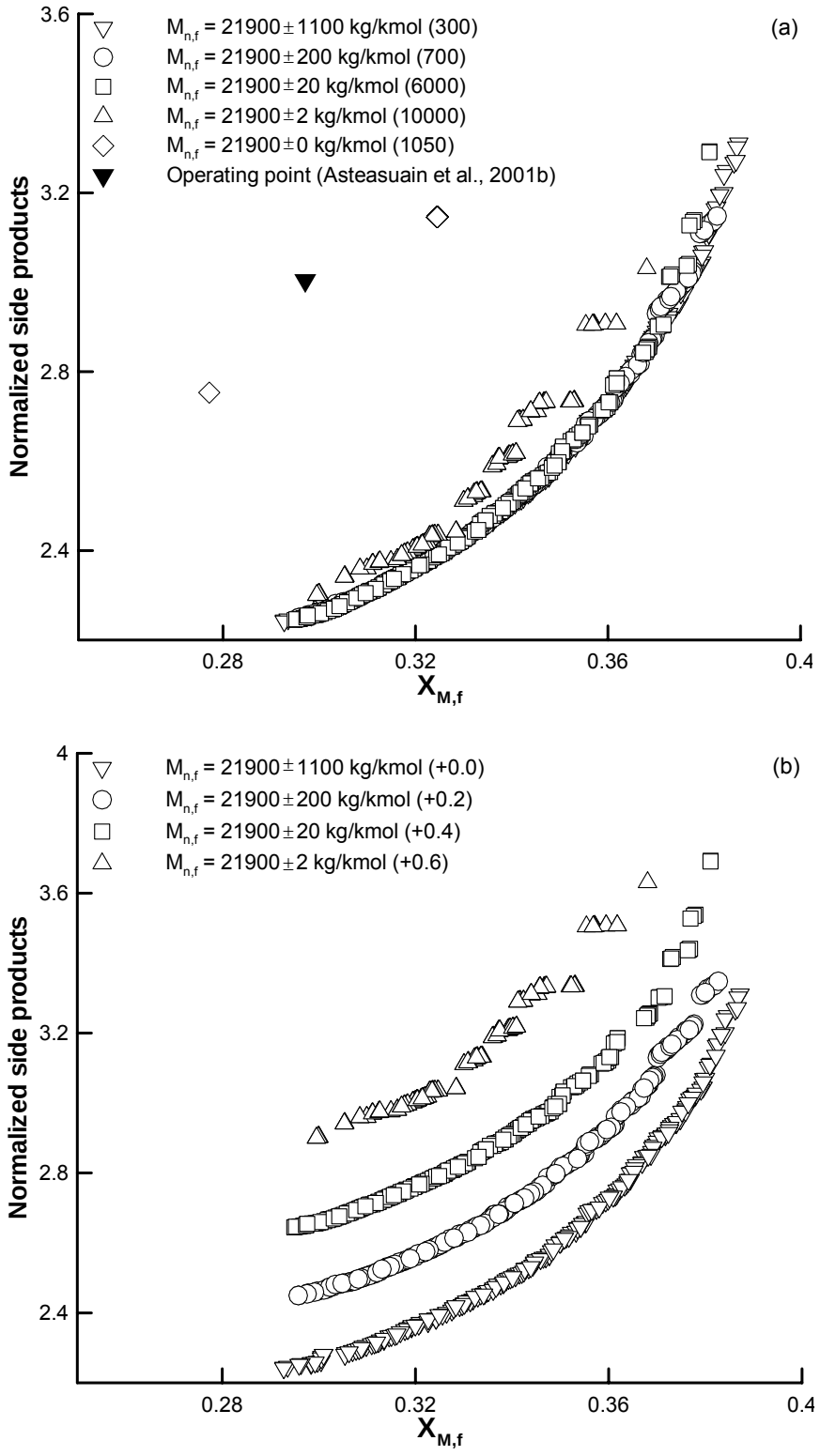

Figure 4.6 (a) Converged Pareto sets for problems having different end-point constraints on $M_{n,f}$ using NSGA-II-aJG. Numbers in parenthesis indicate the generation numbers. (b) Vertically shifted converged Pareto sets of Figure 4.6a (as in Figure 4.3b)

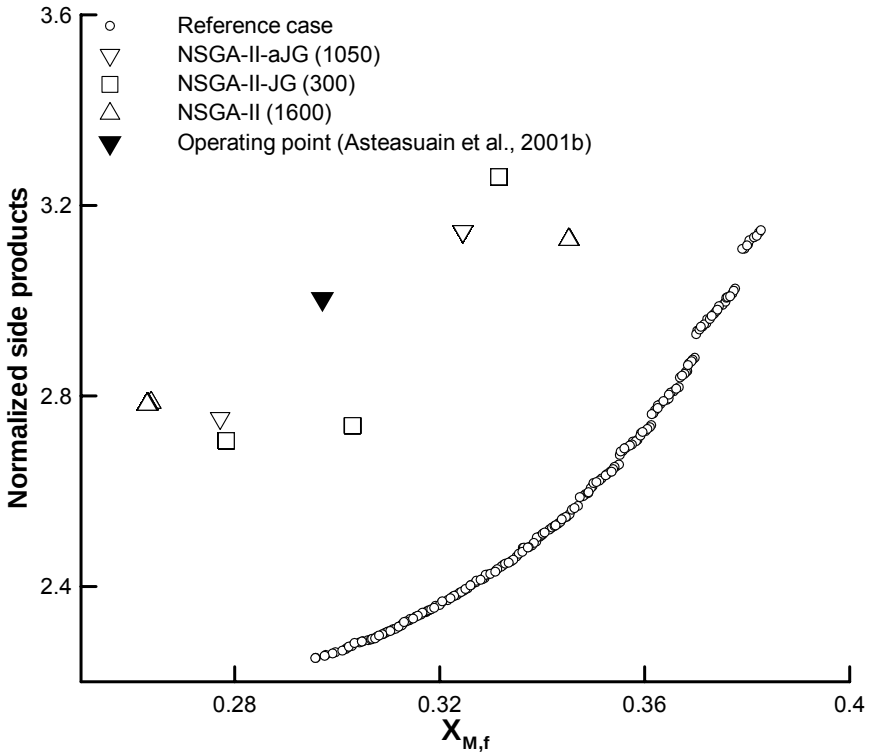

Figure 4.7 Solutions for $M_{n,f}$ = 21900 ± 0 kg/kmol using NSGA-II and its JG adaptations. Numbers in parenthesis indicate the generation number. Results for NSGA-II-aJG (1050) and NSGA-II (1600) are the same as those in Figures 4.6 and 4.3, respectively.

Our attempts on using different computational parameters to improve these results, failed. All these indicate that the solutions (in Figures 4.3, 4.6 and 4.7) of the $M_{n,f} = M_{n,d} \pm 0$ kg/kmol case are local optima or that the methods have failed. NSGA-II could have failed due to the loss in diversity of the chromosomes in this particular problem. However, jumping genes (JG) are supposed to counteract this problem but they also failed to create diversified pool for chromosomes. In general, optimization methods are guaranteed to converge only when the underlying assumptions (such as continuity and convexity) are satisfied. Further, stochastic methods including NSGA-II do not have guarantee that they will converge in a limited number of generations/iterations. Convergence to the global optimum is even more difficult for complex problems with equality constraints.

An interesting observation was made by *identifying* solutions having $M_{n,f} = M_{n,d} \pm 0.1$ kg/kmol (the range of values *actually* present in the solutions for the $M_{n,f} = M_{n,d} \pm 0$ kg/kmol case) in the several Pareto sets of Figure 4.6. These are shown in Figure 4.8. In the Pareto set corresponding to $M_{n,f} = 21900 \pm 20$ kg/kmol, two chromosomes ($X_{M,f} = 0.3003$; normalized side products = 2.2597 and $X_{M,f} = 0.3401$; normalized side products = 2.5106) are found having $M_{n,f}$ = 21900.04 kg/kmol and 21899.98, respectively. Six solutions (shown by triangles; two are very close) having $M_{n,f} = 21900 \pm 0.1$ kg/kmol are identified in the near-converged Pareto set for $M_{n,f} = 21900 \pm 2$ kg/kmol. No such solutions are found in the Pareto sets for $M_{n,f} = 21900 \pm 1100$ kg/kmol and $M_{n,f} = 21900 \pm 200$ kg/kmol. The existence of such solutions, lying on the converged Pareto set and satisfying the end-point constraint of $M_{n,f} = 21900 \pm 0.1$ kg/kmol, and their not being 'caught' by the algorithms when used with $M_{n,f} = 21900 \pm 0$ kg/kmol, confirms the failure of the binary-coded NSGA-II and its JG variants for problems in which the end-point constraint on $M_{n,f}$ is forced exactly. We suggest that solutions of such problems should be *assembled* by screening the solutions of several MOO problems with softer constraints of the type $M_{n,f} = M_{n,d} \pm \mu$ kg/kmol, where μ is an arbitrary number. Our earlier study (Bhaskar et al., 2001) on the MOO of the third-stage wiped-film PET reactor also involved similar hard end-point constraints on the molecular weight, and unique solutions were obtained. However, the MOO code was run using different values of the random seed, a computational parameter, and Pareto sets were then assembled. One must be extremely careful while solving MOO problems involving hard end-point constraints on the molecular weight (and, possibly, other properties) before inferring that the solution is unique rather than a Pareto set. Indeed, it may be worthwhile to re-visit some of the earlier studies

involving hard end-point constraints and explore if the correct solutions are, indeed, Pareto sets.

Figure 4.9 shows the Pareto-optimal set for the reference case as well as plots of the decision variables and constraints corresponding to the several points in the Pareto set. Plots of the methyl, vinyl, and vinylidene contents are also shown. It is observed from the Pareto set that higher monomer conversions can be achieved only with higher side products. The actual operating point (shown by filled delta) for the industrial reactor gives much higher concentrations of the side products (for the same conversion), and so this type of study offers scope of considerable improvement of industrial LDPE reactors. The plots of the decision variables reveal that the optimal solution depends, to a large extent, on four decision variables, F_S, $F_{I,1}$, $F_{I,2}$ and P_{in}. When the flow rates, $F_{I,1}$ and $F_{I,2}$, of the two initiators are increased, higher conversions (at the cost of higher side products) are obtained, as expected. The effect of increasing these two flow rates need to be counteracted by a decrease in F_S (to maintain the molecular weight). Other decision variables are almost constant with some amount of scatter.

Ehrlich and Mortimer (1970) mention that an increase in pressure helps lower the SCB, vinyl and vinylidene contents significantly. Figure 4.9 shows that higher inlet pressures (and therefore, higher pressures in the entire reactor) are indicated at higher monomer conversions so as to keep the side product concentrations in check. The decrease of the concentration of the methyl group as the pressure goes up (till it attains its upper bound; see Figures 4.9(l) and 4.9o) is attributed to the fact that the pressure dependence of the propagation rate constant is more significant than that of the branching reactions, as shown by Machi et al. (1966; 1968).

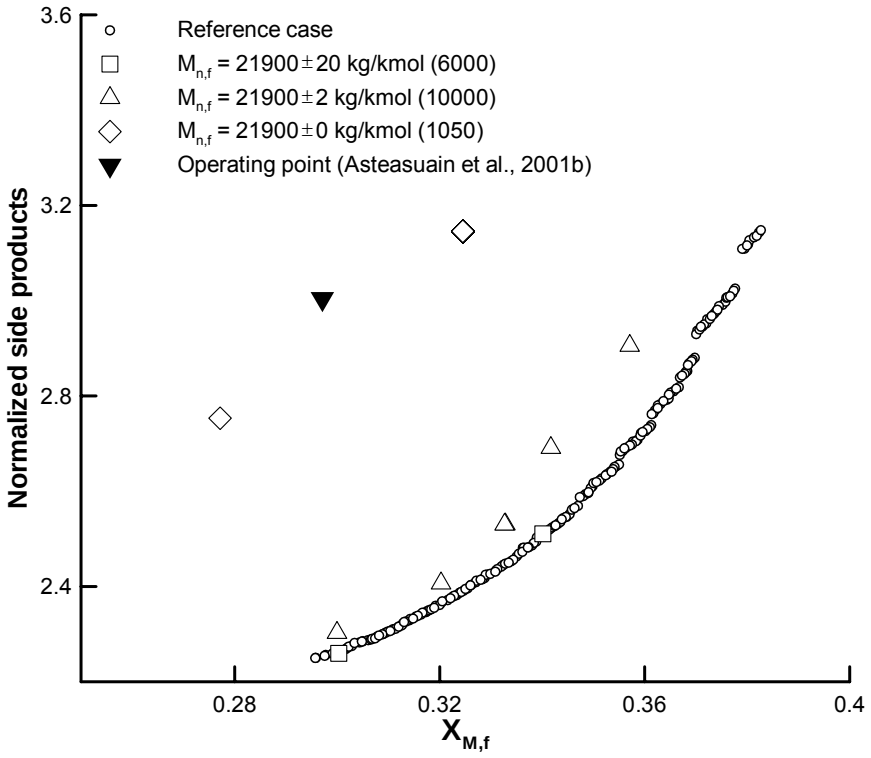

Figure 4.8 Points having $M_{n,f}$ = 21900 ± 0.1 kg/kmol from among the Pareto sets of Figure 4.6a. These points are compared to the reference case.

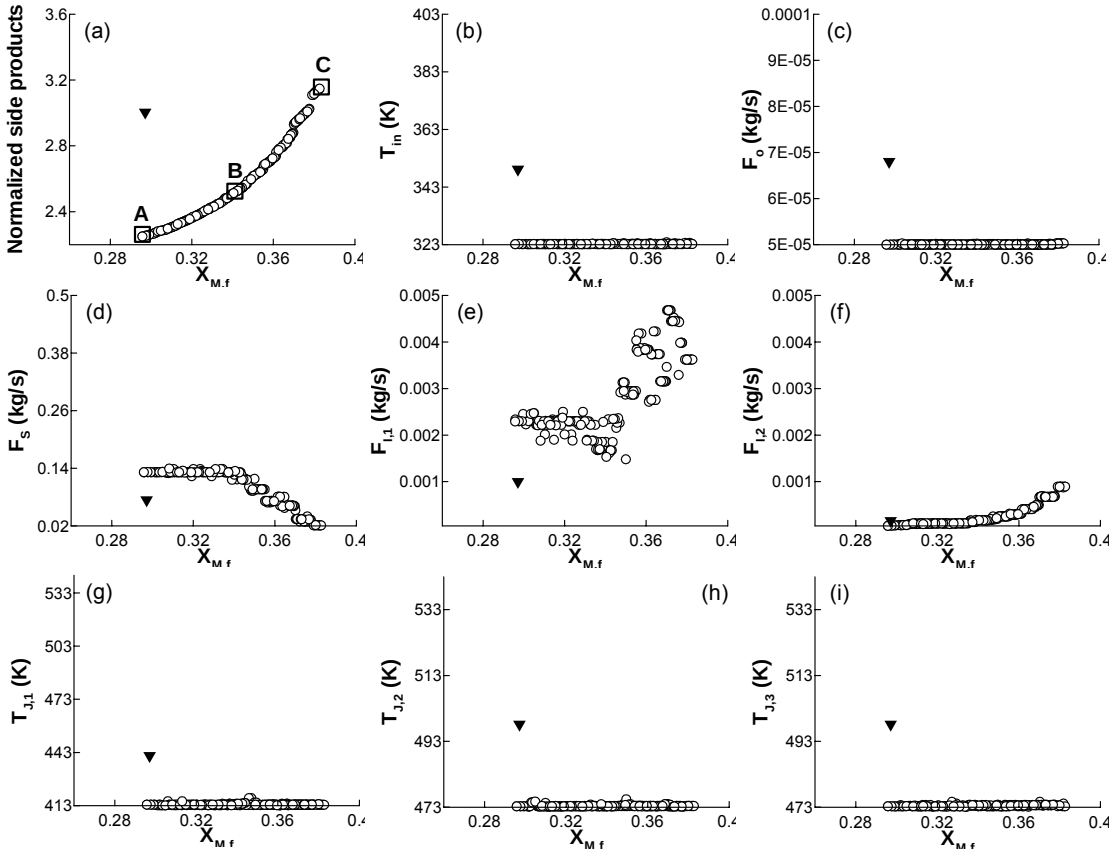

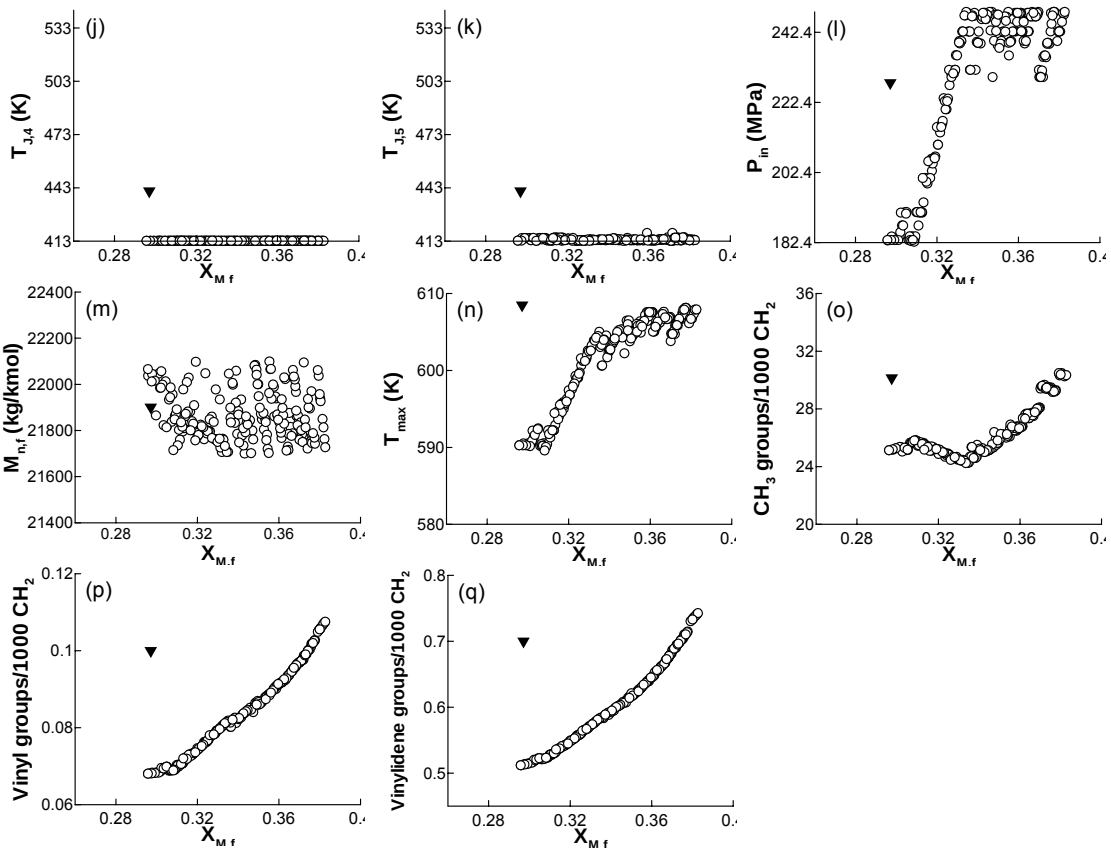

Figure 4.9 Pareto-optimal points and the corresponding decision variables and constraints for the reference case ($M_{n,f}$ = 21900 ± 200 kg/kmol; NSGA-II-aJG). Industrial data (▼) are shown.

Validity of whole range of optimization variables with the industrial data is shown by generating temperature, monomer conversion, and number-average molecular weight profiles for chromosomes A, B, and C chosen from the Pareto-optimal set (Figure 4.9a). These chromosomes cover the complete range of non-dominated solutions in the Pareto-optimal set. The profiles in Figure 4.10 for these three chromosomes are comparable to those in Figure 4.2 for the industrial operation. Temperature profile for chromosome A in Figure 4.10a shows that the initial rate of polymerization in 5th reactor zone decreases due to low initiator flow rate ($F_{I,2}$). It reflects lower monomer conversion as against the chromosome C shown in Figure 4.10b. This is obvious as higher initiator concentration increases the concentration of free radicals, and subsequently the conversion of the monomer molecules (Yao et al.,

2004). At this point, butane flow rate (F_S) is reaching to the lower bound and thus making the chain transfer reaction less significant (Cervantes et al., 2000); consequently the product molecular weight (M_n) increases. These molecular weight profiles for the chromosomes are shown in Figure 4.10c.

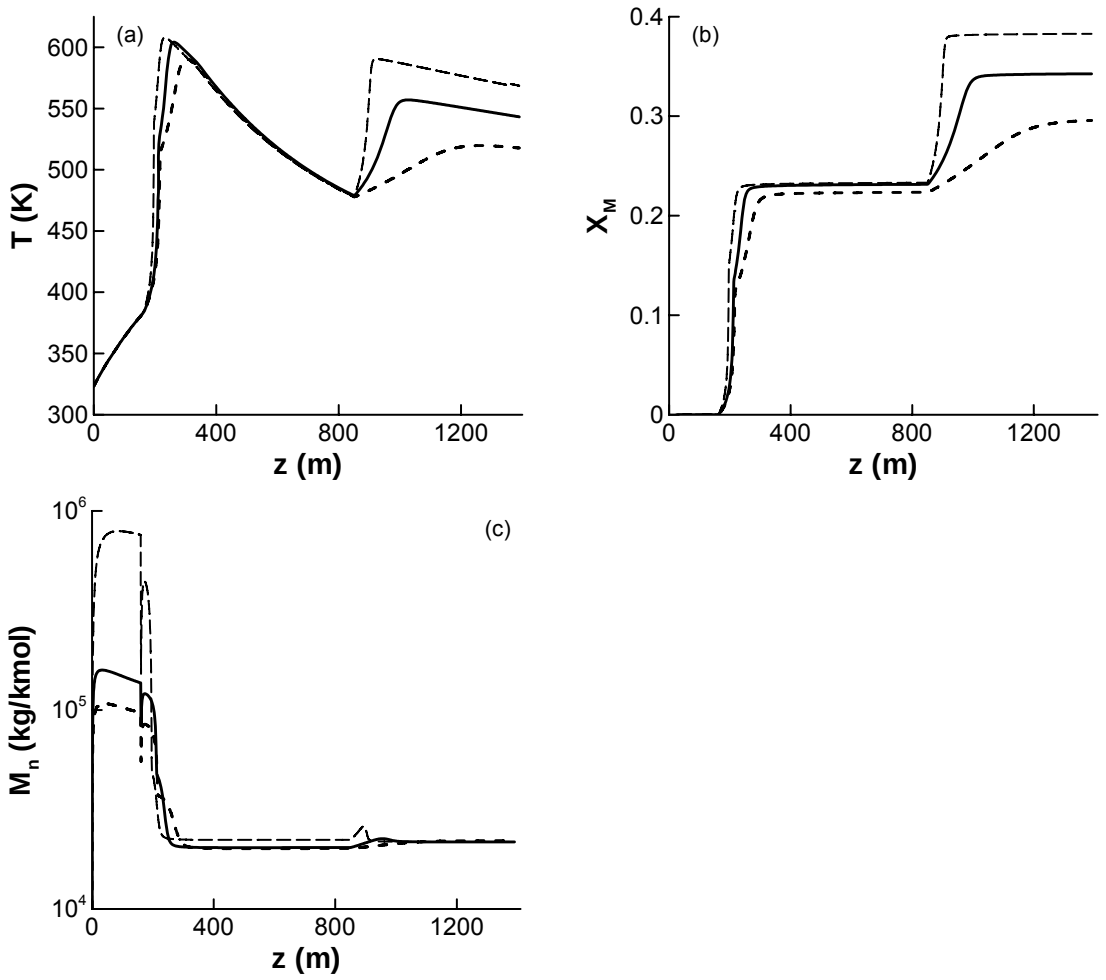

Figure 4.10 Temperature, monomer conversion and number-average molecular weight profiles for chromosomes A (---), B (—) and C (− − −) shown in Figure 4.9a

In the Pareto-optimal set, there exist some points for which monomer conversion reach values of about 38% (Figure 4.9a). These values are higher than the usual reported values (20 - 35%) in the industrial reactors and there might be some problems of high viscosities, reactor fouling and even clogging at that level of

conversion. In fact, this is the advantage with multiple non-dominated solutions (equally good points) in the Pareto-optimal set; the decision maker can choose a point (based on his/her industrial experience and intuition) which has an acceptable/lower monomer conversion (around 35%) for operating the plant. In general, 'higher level qualitative considerations' are required to decide upon the preferred solution as suggested by Deb (2001). We also studied the effect of monomer flow rate, F_M, on the Pareto-optimal set. As expected, Figure 4.11 shows that monomer conversion can be reduced with higher amount of monomer fed to the tubular reactor. These results provide more options to the decision maker to choose from.

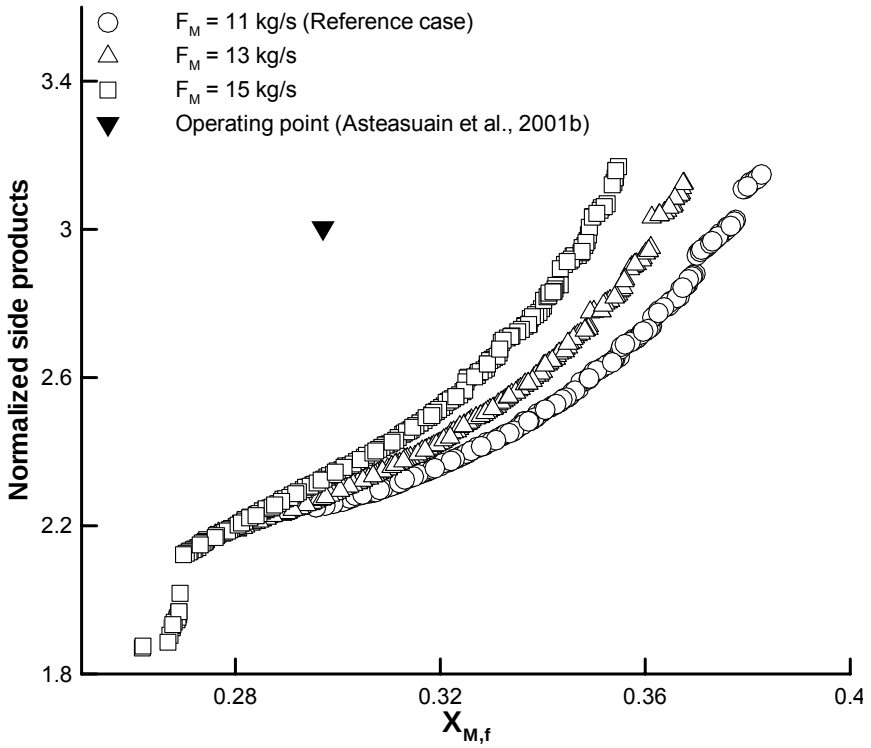

Figure 4.11 Effect of F_M on the Pareto-optimal set (reference case)

4.3.3 Four-objective Optimization

A 4-objective optimization problem is now studied in which each of the side products is taken as an independent objective function, i.e., there are four objective functions: maximization of the monomer conversion, $X_{M,f}$, minimization of methyl ($[M_e]_f$), vinyl ($[V_i]_f$) and vinylidene ($[V_{id}]_f$) contents in the product, respectively, per 1000 CH_2. This problem is formulated to study the formation of each side product individually instead of the weighted average of the side-products, which was done in the 2-objective problem. These results will identify the need and potential for selectively reducing a particular side product. Binary-coded NSGA-II-aJG is used for MOO of reference case, i.e., $M_{n,f}$ = 21900 ± 200 kg/kmol. Decision variable set and local constraint on reactor temperature are the same as described those in formulation of 2-objective optimization problem. Again, the constraints are handled by the penalty function method with weighting factors, $w_1 = 10^9$ and $w_2 = w_3 = w_4 = 10^{10}$, respectively, in all the objective functions. The mathematical formulation of above problem is written as follows:

$$\text{Max } G_1 \equiv X_{M,f} \tag{4.5a}$$

$$\text{Max } G_2 \equiv \frac{1}{1+\left(\frac{[M_e]_f}{30}\right)} \tag{4.5b}$$

$$\text{Max } G_3 \equiv \frac{1}{1+\left(\frac{[V_i]_f}{0.1}\right)} \tag{4.5c}$$

$$\text{Max } G_4 \equiv \frac{1}{1+\left(\frac{[V_{id}]_f}{0.7}\right)} \tag{4.5d}$$

Subject to

Bounds:

Equation (4.4) (4.5e)

Constraints:

$M_{n,f} = 21{,}900 \pm 200$ kg/kmol (reference) (4.5f)

$T_{max}(z) \leq 610.15$ K (4.5g)

Model equations (4.5h)

Figure 4.12 shows solution of the optimization problem. The best set of computational parameters is given in Table 4.6. Since it is not possible to plot these results as a 4-dimensional Pareto set, the four objective functions are plotted as a function of the chromosome number (after rearranging the results so that the conversion increases continuously with the chromosome number). Much more scatter is observed for the methyl group concentrations in this 4-objective problem than was observed for the earlier 2-objective problem. This scatter could not be reduced by a change of the computational parameters. However, vinyl and vinylidene group concentrations are showing the increasing trends with monomer conversion (Figures 4.12c and 4.12d). Similar trends were also observed in 2-objective problem. The optimal values of the individual (normalized) side product concentrations have been summed up and plotted as a function of the monomer concentration in Figure 4.12f. The two objective references Pareto sets (in Figure 4.5a) are also plotted. The results for the two and four objective optimization problems are comparable. This suggests that one can easily combine the three side products into a single objective for *this* problem, and it is not necessary to solve a four objective optimization problem. Nevertheless, the Pareto-optimal set for the 2-objective problem is superior to the Pareto-optimal solutions obtained from the 4-objective problems. The optimal solutions for the 4-objetive problem show some scatter but with somewhat increased range of solutions.

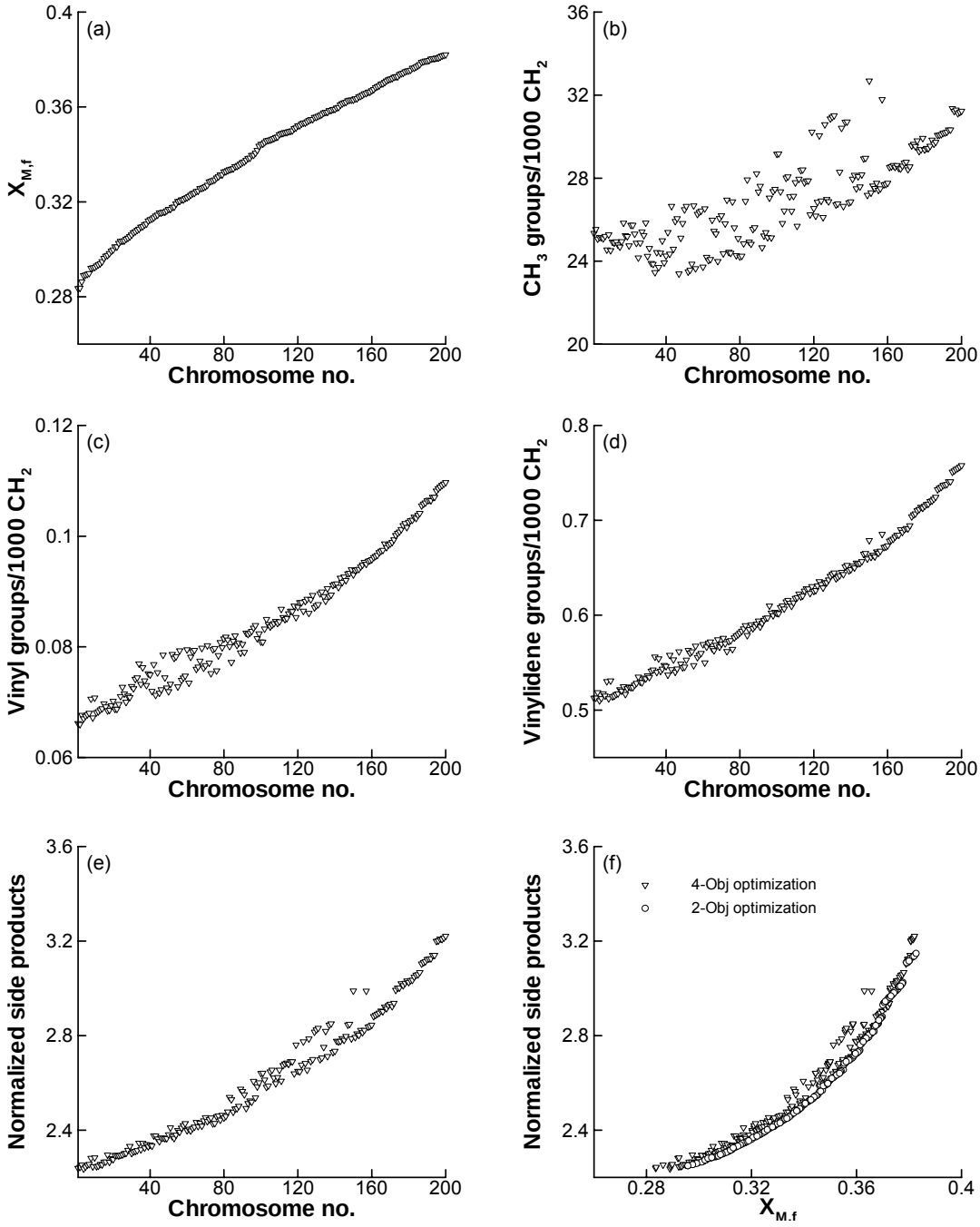

Figure 4.12 Results for the 4-objective optimization problem in Equation (4.5) (NSGA-II-aJG)

The computational parameters were varied, in the range of ±10 % of the best values in Table 4.6, one by one to see their effect on the results. It was observed that the Pareto-optimal set is not too sensitive to these variations in the range. These results are, therefore, not provided here (but can be supplied on request).

4.4 Conclusions

A comprehensive mathematical model for the production of LDPE in high-pressure tubular reactors is developed. Complete details are provided. Tuned values of the several model parameters are obtained so as to get good agreement of model predictions with industrial data on the temperature profile, the monomer conversion and the number-average molecular weight of the product, as well as estimates of the concentrations of the several side products. Thereafter, a two objective optimization study of the operating reactor (with constraints on the molecular weight and the temperature of the reaction mass) is carried out. Considerable improvement in the reactor performance is indicated. Pareto-optimal solutions are obtained. The present study suggests that solutions of problems involving hard (equality) end-point constraints should be assembled by obtaining solutions of several MOO problems with softer constraints, rather than by solving the problem only once, lest erroneous results are obtained. Furthermore, the binary-coded NSGA-II-aJG and NSGA-II-JG perform better than NSGA-II near the hard end-point constraints. The results of a four objective problem (with each of the three normalized side product concentrations taken individually as objective functions) are found to be comparable to that of a two objective problem in which these three are added together and taken as a single objective function.

Chapter 5

Design Stage Optimization

5.1 Introduction

LDPE is one of the most widely used polymers in the world. Nearly one quarter of its annual production of 84 million tones worldwide, is produced by high-pressure technology (Kondratiev and Ivanchev, 2005). Therefore, even small improvement in polymer production and/or properties can generate large revenue for the poly-olefins industry. The end properties of polymer, viz., tensile strength, stiffness, tenacity etc. are related to molecular parameters, which include average molecular weight, polydispersity index, SCB and LCB, and distribution of functional groups etc. The operating and design variables often influence the molecular parameters in non-commensurable ways. Therefore, these applications are perfect scenarios for MOO. This article presents enhancement in the production, quality and strength of LDPE, simultaneously, by MOO of an industrial high-pressure tubular reactor for ethylene polymerization at *design* stage. The non-dominated sorting genetic algorithm (NSGA-II; Deb, 2001) and its JG adaptations (Simoes et al., 1999; Kasat and Gupta, 2003; Man et al., 2004; Guria et al., 2005) are used to optimize the reactor performance. NSGA-II-JG introduces a new JG operator along with the usual operators of NSGA-II; it probabilistically selects two sites in the chromosome string and replaces the in-between portion with a new, same-sized, randomly generated binary string (Kasat and Gupta, 2003). Where as, in binary-coded NSGA-II-aJG, the second site in the chromosome is selected by the pre-defined string length of jumping genes, as described by Guria et al. (2005). The working methodology of these three algorithms is described in Kasat and Gupta (2003) and Agrawal et al. (2006).

Many studies on the modeling and simulation of high-pressure tubular reactor to produce LDPE have been reported in the literature, which were reviewed by Zabisky et al. (1992) and Kiparissides et al. (1993a). In contrast, only some studies (Yoon and Rhee, 1985; Mavridis and Kiparissides, 1985; Brandolin et al., 1991; Kiparissides et al., 1994; Cervantes et al., 2000; Asteasuain et al., 2001b; Yao et al., 2004) have appeared on the optimization of LDPE tubular reactor in the open literature. But, interestingly, all the studies on modeling used different kinetic parameters to simulate the reactor. Zabisky et al. (1992), Kalyon et al. (1994), and Brandolin et al. (1996) used industrial data and tuned the kinetic parameters but they did not provide the complete details of either tuned kinetic parameters or the reactor data due to proprietary reasons. In our earlier study (Agrawal et al., 2006), we modified the model of Asteasuain et al. (2001b), simulated an *industrial* high-pressure tubular reactor and tuned the model parameters using reported industrial data (Asteasuain et al., 2001b). Complete details of the model including parameter values are available in Agrawal et al. (2006), and are not reported here for brevity.

Agrawal et al. (2006) used the developed model for MOO of the industrial LDPE tubular reactor at *operation* stage. The two important objectives considered for optimization were maximization of X_M and minimization of normalized side products (short chain branches, vinyl, and vinylidene groups), both at the reactor exit. The LDPE, which is produced in the tubular reactor at high-pressure conditions, consists of several short chain branches, primarily, ethyl and butyl groups. These branches deteriorate quality and strength of the polymer by lowering crystallinity, density, melting point, tensile strength, etc. (Luft et al., 1982). Therefore, these groups should be minimized to enhance quality and strength of the product. Also, some unsaturated groups (vinyl and vinylidene) are present in the LDPE chains, which make the

product susceptible to cracking due to oxide formation. Hence, the minimization of these groups enhances strength of the polymer product. Another important objective is to maximize the monomer conversion per pass for the constant monomer feed to the reactor. Various polymer grades are required in the industry for different applications. These grades are defined by the number-average molecular weight, $M_{n,f}$, of the polymer product. Therefore, an end-point equality constraint on the $M_{n,f}$ is imposed to meet the market requirements. Indeed, a polymer is characterized by its several physical attributes such as density, melt flow index, degradation by sunlight, optical clarity, etc. These are related (often in an imprecise manner) to several molecular parameters, e.g., the entire molecular weight distribution (MWD, which could possibly be inferred through the number- and weight-average molecular weights), SCB, LCB, concentration of double bonds, etc. One has to select only a few of these molecular properties to get results that can be computed, as well as can be interpreted meaningfully. Since the MWD of the LDPE produced in high pressure reactors is 'normal' (unlike for polypropylene, using the Zeigler-Natta system), M_w and M_n are related. Also, Asteasuain et al. (2006) and Padhiyar et al. (2006) have used M_n as the variable describing quality of the polymer, when minimizing the amount of off-specification polymer for a grade change-over problem. In addition, Mavridis and Kiparissides (1985) and Asteasuain et al. (2001b) have used M_n as the single molecular property to represent the grade of the polymer. Brandolin et al. (1991) have optimized LDPE reactors using several *single* objective functions (the weighted sum of the final values of X_M, M_n, and the weight-average number of branch points). Moreover, reaction mixture temperature may shoot up to a very high value due to exothermic polymerization reactions. Polyethylene molecule starts decomposing at about 350°C, which creates the run-away condition in the reactor and may blow up

the reactor, if the pressure valve is not relieved. Therefore, safe operation of the reactor is ensured by incorporating an inequality constraint on reactor temperature, locally, to avoid this condition.

In the earlier study (Agrawal et al., 2006), eleven decision variables were used to optimize the *operation* of the high-pressure tubular reactor for LDPE production. The focus of the present study is the optimization of this tubular reactor at *design* stage for multiple objectives, which involves more decision variables and hence is more challenging. As in our previous study (Agrawal et al., 2006), binary-coded NSGA-II and its JG adaptations failed to converge to the Pareto-optimal set when an hard equality constraint on $M_{n,f}$ is imposed; however, correct global Pareto-optimal points are obtained by running several problems involving softer constraints of the type: $M_{n,f} = M_{n,d} \pm$ an arbitrary number. These interesting results are discussed in detail.

Deb (2001) showed that the penalty parameter for handling constraints by penalty function approach plays an important role in multi-objective evolutionary algorithms. If the parameter is not chosen properly, then it may create a set of infeasible solutions or a poor distribution of solutions. Therefore, a systematic approach of *constrained-dominance principle* for handling the constraints was proposed by Deb (2001). Motivated by these, *constrained-dominance principle* is successfully implemented in the binary-coded NSGA-II-aJG and NSGA-II-JG for handling the constraints for the *first* time and its effectiveness is evaluated for the design stage optimization of the industrial LDPE reactor.

5.2 Modeling and Simulation of LDPE Tubular Reactor

Commercially, LDPE is produced in tubular reactors, which consist of several tubes connected together with 180° bends. This is a well-established technology for

producing LDPE worldwide. The tubular reactor (Asteasuain et al., 2001b; Figure 4.1) used in our study, is 1390 m long and 0.05 m in diameter. The tubular reactor is divided into five zones, which are decided due to change in jacket fluid temperature and/or introduction of initiators. The monomer (ethylene), solvent (n-butane), and oxygen (an initiator) are fed into the reactor at 2250 atm and 76°C. The reaction mixture is preheated in the first two zones and then initiator, I_1, is injected in the third zone to start the polymerization reaction. The reaction mixture reaches 325–335°C due to large heat of reaction. Therefore, to avoid run-away condition, the reactant–product mixture is cooled in the third and fourth zones using cooling water flowing counter-currently in the jackets. In order to further increase the monomer conversion, initiator, I_2, is fed into the fifth zone. Later part of this zone acts as a cooler to reduce the mixture temperature to ease separation in downstream operations. The monomer conversion per pass is about 30% at the reactor exit. Solvent is used to control the molecular weight of polyethylene by the process of chain transfer to the solvent. The number-average molecular weight of the polymer at the reactor exit is reported to be 21900 kg/kmol.

For simulating the industrial LDPE reactor, the dynamic model of Asteasuain et al. (2001b) is modified to the steady-state model (Agrawal et al., 2006). In brief, the model is based on plug flow assumption, and incorporates axial variation of concentration, temperature, pressure and hence physical properties, and also several main (Asteasuain et al., 2001b) and side reactions, e.g., intra-molecular chain transfer, chain transfer to polymer, β-scission of secondary and tertiary radicals etc. (the latter give the extent of long- and short-chain branching and the amount of unsaturation). The detailed kinetic scheme is given in Agrawal et al. (2006). The model equations can be described in the following form:

$$\frac{d\boldsymbol{x}}{dz} = f(\boldsymbol{x}, \boldsymbol{u}); \boldsymbol{x}(z=0) = \boldsymbol{x_0} \tag{5.1}$$

Where $\boldsymbol{x}$ represents the vector of state (dependent) variables and $\boldsymbol{u}$ is the control (independent) variables.

$$\boldsymbol{x} = [v, \rho, C_{I,1}, C_{I,2}, C_{O_2}, C_S, C_M, C_{M_e}, C_{V_i}, C_{V_{id}}, T, P, \lambda_{np}, \mu_{np}]^T;$$

$$n = 0, 1; p = 0, 1, 2 \tag{5.2}$$

In Equation (5.1), z denotes the axial distance in the tubular reactor. The model equations are simultaneous, stiff ordinary differential equations which are integrated using D02EJF subroutine (based on Gear's method) in the NAG library. The numerical solution provides profiles of temperature (T), pressure (P), and concentrations of initiators ($C_{I,1}$, $C_{I,2}$, and C_{O_2}), solvent (C_S), and monomer (C_M) along the reactor length. The variation in several molecular properties [M_n, M_w, short-chain branching (SCB), and the vinyl and vinylidene group concentrations] as a function of z, is also calculated.

Complete details (for instance, some of the kinetic rate parameters) of the industrial tubular reactor were not provided by Brandolin et al. (1996) and Asteasuain et al. (2001a) due to proprietary reasons. Therefore, the model parameters were tuned using the industrial data on reactor temperature at several discrete points along the reactor axis, and the values of X_M, M_n, and the side-product concentrations in the final product (Goto et al., 1981; Gupta et al., 1985; Asteasuain et al., 2001b). Binary-coded NSGA-II was used to minimize the sum-of-squares of the normalized error between the model-predicted and the industrial values. The model predicted values (the temperature profile, $X_{M,f}$ and $M_{n,f}$, and estimates of the several side products) were found to be in good agreement with the industrial data. Details of all the model

equations, parameter values, and model validation are reported elsewhere (Agrawal et al., 2006).

5.3 Multi-Objective Optimization

5.3.1 Formulation

For the design stage MOO study of the industrial LDPE tubular reactor, twenty-two decision variables are used: the inlet temperature (T_{in}), the feed flow rates of oxygen (F_o), solvent (F_S) and the two additional initiators ($F_{I,1}$, and $F_{I,2}$) added in-between, the five average jacket fluid temperatures ($T_{J,1} - T_{J,5}$), the inlet pressure (P_{in}), the axial lengths of five zones ($L_{z1} - L_{z5}$), inside diameter (D_{int}), jacket diameter (D_{Jacket}), and flow rates of the jacket fluid ($V_{J,2} - V_{J,5}$). Note that D_{int} and D_{Jacket} are constant for all zones. Saturated steam is used to preheat the reaction mixture in the first zone and therefore jacket fluid flow rate for zone one ($V_{J,1}$) is not included as a decision variable. The monomer feed rate (F_M) to the reactor is kept constant in this study. The details of the MOO problem for simultaneous maximization of conversion and minimization of normalized side products at the reactor exit are given in Table 5.1. The variables: $L_{z1} - L_{z5}$, D_{int} and D_{Jacket} are allowed to vary within ± 20% of their reference values (mostly industrial values). The bounds for the decision variables: T_{in}, F_o, F_S, $F_{I,1}$, $F_{I,2}$, P_{in}, $T_{J,1} - T_{J,5}$ have been chosen based on information in the open literature (Asteasuain et al., 2001b; Brandolin et al., 1988). The bounds for $V_{J,2} - V_{J,5}$ are chosen based on industrial practice (Kalyon et al., 1994). Lower limit of F_S is changed to 5×10^{-2} kg/s (it was 2×10^{-2} kg/s in operation stage optimization) because simulation was found taking an excessive CPU time for *some* chromosomes. Bounds on other decision variables are same as in our previous study (Agrawal et al., 2006).

Both the equality and inequality constraints are incorporated in the objective functions in the form of penalty functions with weighting factors of $w_1 = 10^9$ and $w_2 = 10^{10}$, respectively. This is not required if constraints are handled directly through the *constrained-dominance principle* (Chapter 3).

$$\text{Max } G_1 \equiv X_{\text{M,f}} - w_1\left(1-\frac{M_{\text{n,f}}}{M_{\text{n,d}}}\right)^2 - w_1\left\langle 1-\frac{T_{\max}(z)}{T_{\max,\text{d}}}\right\rangle^2 \tag{5.3a}$$

$$\text{Max } G_2 \equiv \frac{1}{1+\left(\frac{[M_{\text{e}}]_{\text{f}}}{30}+\frac{[V_{\text{i}}]_{\text{f}}}{0.1}+\frac{[V_{\text{id}}]_{\text{f}}}{0.7}\right)} - w_2\left(1-\frac{M_{\text{n,f}}}{M_{\text{n,d}}}\right)^2 - w_2\left\langle 1-\frac{T_{\max}(z)}{T_{\max,\text{d}}}\right\rangle^2 \tag{5.3b}$$

The bracket operator, <α>, used for handling the inequality constraint on temperature, returns the absolute value of operand α if the operand is negative otherwise gives a value of zero. The objective functions, G_1 and G_2, are thus penalized by a large value if either of the two constraints is violated. Therefore, the infeasible chromosomes are killed in the subsequent generations, even if these are produced in the initial population in the optimization by NSGA-II and its JG adaptations.

Preliminary optimization results showed that the jacket fluid velocities in the second and third zones were becoming quite low and consequently resulting in large temperature change in the jacket fluid. Therefore, constraints on jacket fluid velocities were added in the mathematical formulation as depicted in Table 5.1. These bounds on the jacket fluid velocities are based on the typical range reported in the literature (Sinnott, 1999).

Table 5.1 Objectives, constraints and decision variables in the MOO

Objective functions	Constraints	Decision variables
Case 1: Max $J_1 \equiv X_{\mathrm{M,f}}$ Min $J_2 \equiv \left(\frac{[M_\mathrm{e}]_\mathrm{f}}{30} + \frac{[V_\mathrm{i}]_\mathrm{f}}{0.1} + \frac{[V_\mathrm{id}]_\mathrm{f}}{0.7} \right)$	$M_{\mathrm{n,f}} = M_{\mathrm{n,d}} \pm \Delta M_\mathrm{n}$ $M_{\mathrm{n,d}} = 21{,}900$ kg/kmol $\Delta M_\mathrm{n} = 0$, 2, 20, or 200 $T_{\max}(z) \le 610.15$ K $0.3 \le v_{\mathrm{J},m} \le 1.0$ m/s; $m = 2, \ldots, 5$ $\frac{\mathrm{d}\boldsymbol{x}}{\mathrm{d}z} = f(\boldsymbol{x}, \boldsymbol{u})$	$5 \times 10^{-5} \le F_\mathrm{o} \le 10 \times 10^{-5}$ kg/s $2 \times 10^{-2} \le F_\mathrm{S} \le 0.5$ kg/s $5 \times 10^{-5} \le F_{\mathrm{I},1} \le 5 \times 10^{-3}$ kg/s $5 \times 10^{-5} \le F_{\mathrm{I},2} \le 5 \times 10^{-3}$ kg/s $413.15 \le T_{\mathrm{J},m} \le 543.15$ K ; $m = 1, 4, 5$ $473.15 \le T_{\mathrm{J},n} \le 543.15$ K ; $n = 2, 3$ $182.39 \le P_\mathrm{in} \le 248.25$ MPa $50 \le L_{\mathrm{z}1} \le 70$ m $80 \le L_{\mathrm{z}2} \le 120$ m $140 \le L_{\mathrm{z}3} \le 220$ m $400 \le L_{\mathrm{z}4} \le 600$ m $430 \le L_{\mathrm{z}5} \le 650$ m $0.04 \le D_\mathrm{int} \le 0.06$ m $0.1778 \le D_\mathrm{Jacket} \le 0.2286$ m $0.5 \times 10^{-3} \le V_{\mathrm{J},m} \le 25 \times 10^{-3}$ m^3/s ; $m = 2, 3, 4$ $0.1 \times 10^{-3} \le V_{\mathrm{J},5} \le 25 \times 10^{-3}$ m^3/s
Case 2: Same as Case 1 plus Min $J_3 \equiv \frac{F_\mathrm{M}\left(233.8 P_\mathrm{in}^{0.23} + 649.8 X_{\mathrm{M,f}} - 986.8\right)}{6468}$	Same as Case 1 except $\Delta M_\mathrm{n} = 200$ kg/kmol	Same as Case 1

5.3.2 Results and Discussion

The MOO problem was solved using NSGA-II and its JG adaptations. Initially, penalty function approach was employed for handling constraints. The best values of the computational parameters in the NSGA-II algorithms for generating solutions of the design problem are provided in Table 5.2. These values for NSGA-II are same as those used in the operation stage MOO as reported in Agrawal et al. (2006). The computer code was run on a HP workstation (3.60 GHz and 3.25GB RAM). The CPU time on this machine was nearly 8 hours for a typical optimization run for 1000 generations involving 200 chromosomes. This machine can perform 325 MFlops

according to the LINPACK program (available at http://www.netlib.org) for a matrix of the order of 500.

First, the design problem with the equality constraint on $M_{n,f}$ was solved using NSGA-II. It was observed that some non-dominated solutions were obtained rather than the Pareto-optimal solutions (Figure 5.1), which are perhaps the local optimal solutions. NSGA-II took a large number (12000) of generations to give the converged solutions for this case. Now, the end-point constraint on $M_{n,f}$ was relaxed to lie within ±1% (which is well within the experimental error) of the desired molecular weight ($M_{n,d}$), in particular, $M_{n,f}$ = 21900 ± 200 kg/kmol, $M_{n,f}$ = 21900 ± 20 kg/kmol, and $M_{n,f}$ = 21900 ± 2 kg/kmol. For the first problem of $M_{n,f}$ = 21900 ± 200 kg/kmol, the Pareto-optimal set was obtained using NSGA-II with good distribution (spread) of points as shown in Figure 5.1 Hereafter, the Pareto-optimal set obtained for $M_{n,f}$ = 21900 ± 200 kg/kmol case is referred as the reference Pareto-optimal set.

The solutions of the second problem ($M_{n,f}$ = 21900 ± 20 kg/kmol) superimposed on the Pareto-optimal set of the first problem (Figure 5.1), giving confidence on the solutions obtained. However, the solutions of $M_{n,f}$ = 21900 ± 0 kg/kmol, are quite far away from the reference Pareto-optimal set. The solutions of $M_{n,f}$ = 21900 ± 2 kg/kmol, which has a small variability in $M_{n,f}$, did not converge to the reference Pareto-optimal set, even after 18000 generations (Figure 5.1). (NSGA-II-aJG and NSGA-II-JG seems to be converging to the same Pareto set in 19500 and 18000 generations, respectively; this is discussed later.) This shows that NSGA-II is converging to the local or sub-optimal solutions when the MOO problem includes the equality constraint on molecular weight.

Table 5.2 Values of the computational parameters used in the binary-coded NSGA-II, NSGA-II-JG, and NSGA-II-aJG for two-objective design optimization

	Penalty function approach			Constrained-dominance principle		
Parameter	NSGA-II	NSGA-II-JG	NSGA-II-aJG	NSGA-II	NSGA-II-JG	NSGA-II-aJG
N_{gen}*	3000	3300	2500	4500	3200	3000
N_{pop}	200	200	200	200	200	200
l_{substr}	30	30	30	30	30	30
l_{chrom}	660	660	660	660	660	660
l_{JG}	---	---	70	---	---	70
p_c	0.95	0.9	0.8	0.95	0.9	0.8
p_m	0.015	0.005	0.01	0.015	0.005	0.01
p_{JG}	---	0.8	0.8	---	0.6	0.3
S_r	0.95	0.9	0.6	0.95	0.3	0.1

***** Number of generations required for convergence for the case of $M_{n,f} = 21900 \pm 200$

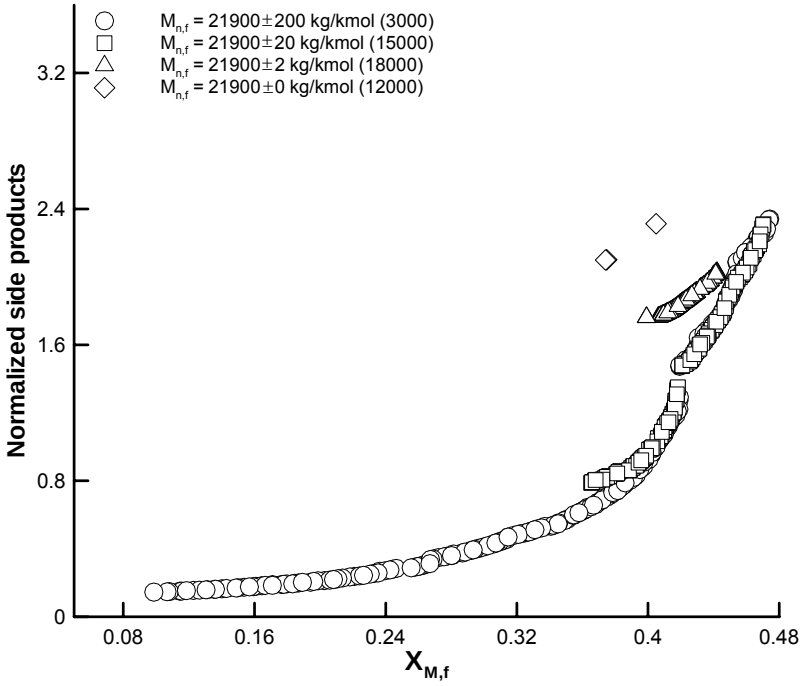

Figure 5.1 Converged solutions for several end-point constraints on $M_{n,f}$ using NSGA-II. Numbers in parenthesis refer to the number of generations.

In order to improve upon the optimization results, NSGA-II-aJG and NSGA-II-JG were endeavored. The best values of computational parameters in both these algorithms are also reported in Table 5.2, which are same as in Agrawal et al. (2006). For the $M_{n,f}$ = 21900 ± 200 kg/kmol case, the converged Pareto-optimal sets by NSGA-II, NSGA-II-JG, and NSGA-II-aJG are shown in Figure 5.2a. To distinguish

the converged Pareto-optimal sets in Figure 2a due to overlapping points, these results are re-plotted with vertical displacements of 0.2 as shown in Figure 2b. NSGA-II-aJG and NSGA-II produced the best Pareto-optimal set in terms of convergence and distribution of points followed by NSGA-II-JG. In addition, NSGA-II-aJG took the least number of generations (2500) in converging to Pareto-optimal solutions in comparison to NSGA-II-JG (3300) and NSGA-II (3000). Guria et al. (2005) also observed that NSGA-II-aJG with the best set of computational parameters is the most rapidly converging technique for the MOO of reverse osmosis desalination units.

The converged Pareto-optimal sets are shown in Figure 5.3 for various end-point constraints on $M_{n,f}$ (± 200 kg/kmol, ± 20 kg/kmol, and ± 2 kg/kmol) using NSGA-II-aJG. $M_{n,f}$ = 21900 ± 20 kg/kmol showed slow convergence and took 9000 generations to converge to the reference Pareto-optimal set of $M_{n,f}$ = 21900 ± 200 kg/kmol, whereas $M_{n,f}$ = 21900 ± 2 kg/kmol required 19500 generations to nearly converge to the same. Similarly, NSGA-II-JG converged to the reference Pareto set for $M_{n,f}$ = 21900 ± 20 kg/kmol in 14000 generations, whereas $M_{n,f}$ = 21900 ± 2 kg/kmol took 18000 generations to nearly converge to the reference Pareto (Figure 5.4). Figure 5.5 shows the converged Pareto-optimal sets for the $M_{n,f}$ = 21900 ± 2 kg/kmol case using NSGA-II and its JG variants. It is clear from the figure that Pareto-optimal sets using NSGA-II and NSGA-II-aJG were closer to the reference Pareto set than that using NSGA-II-JG for $M_{n,f}$ = 21900 ± 2 kg/kmol case. However, neither NSGA-II, NSGA-II-JG nor NSGA-II-aJG could converge to the reference (for $M_{n,f}$ = 21900 ± 200 kg/kmol) Pareto set for $M_{n,f}$ = 21900 ± 0 kg/kmol case (Figure 5.6). Similar results were obtained in our earlier study on the MOO of the LDPE tubular reactor at operation stage (Agrawal et al., 2006). Therefore, all these results indicate that either

the solutions for equality constraint on $M_{n,f}$ are local optimal solutions or NSGA algorithms have failed.

The non-dominated solutions satisfying $M_{n,f}$ = 21900 ± 2 kg/kmol were collected from the Pareto-optimal sets of $M_{n,f}$ = 21900 ± 200 kg/kmol and $M_{n,f}$ = 21900 ± 20 kg/kmol cases using NSGA-II-aJG, and are shown in Figure 5.7; three (shown by open squares) and eight (shown by open triangles) solutions were collected, respectively, from these cases. These solutions were found to be covering the whole range of the reference Pareto set whereas single run of 21900 ± 2 kg/kmol case distributes the non-dominated solutions in the higher conversion side (Figure 5.3). High-conversion solutions are undesirable since the decision maker might be interested in operating the plant at low conversion to produce higher product quality and strength (low side product concentration). Also, $M_{n,f}$ = 21900 ± 2 kg/kmol required almost 18000 generations to converge; therefore, it involves enormous amount of CPU time. In the same CPU time, one could run four optimization cases of $M_{n,f}$ = 21900 ± 200 kg/kmol (with different seeds or by different algorithms) or two cases of $M_{n,f}$ = 21900 ± 20 kg/kmol. Therefore, we suggest to obtain *diversified* solutions near to hard equality constraints on $M_{n,f}$ by identifying the points from among the Pareto-optimal sets of various softer constraints of the type: $M_{n,f} = M_{n,d}$ ± arbitrary number.

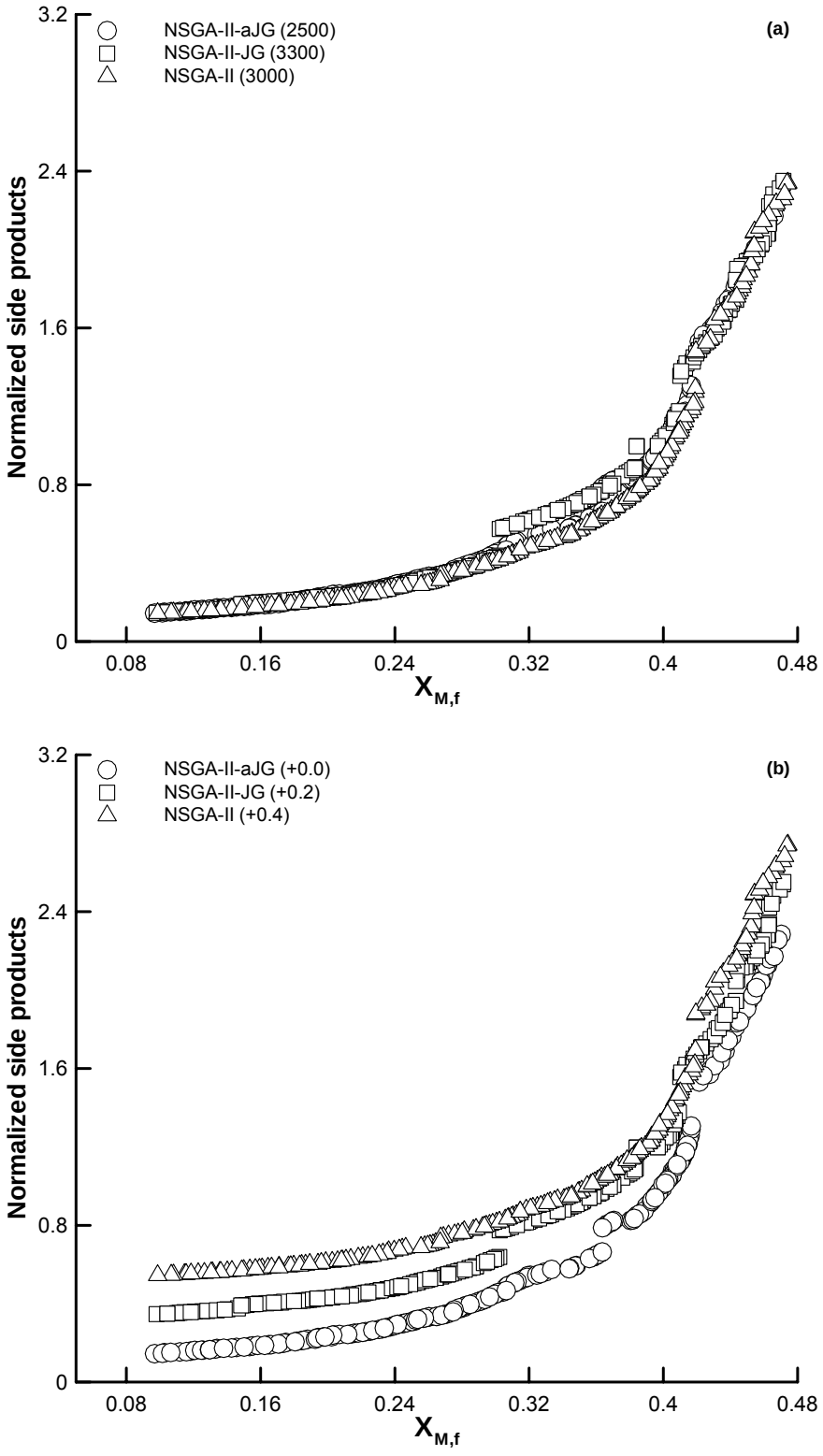

Figure 5.2 (a) Converged Pareto-optimal sets for $M_{n,f}$ = 21900 ± 200 kg/kmol using NSGA-II and its JG adaptations. Numbers in parenthesis indicate the number of generations. (b) The results of Figure 5.2a are re-plotted with vertical shifts of 0.2 (i.e., values of the ordinate are displaced vertically upwards by 0.0, 0.2, or 0.4).

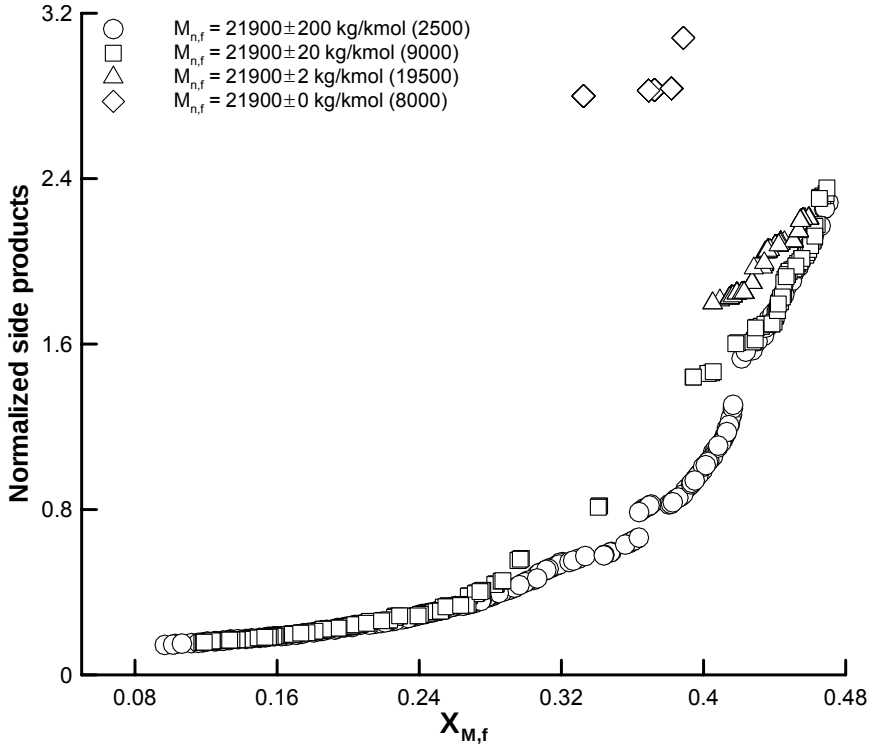

Figure 5.3 Converged Pareto sets for problems having different end-point constraints on $M_{n,f}$ using NSGA-II-aJG. Numbers in parenthesis indicate the generation numbers.

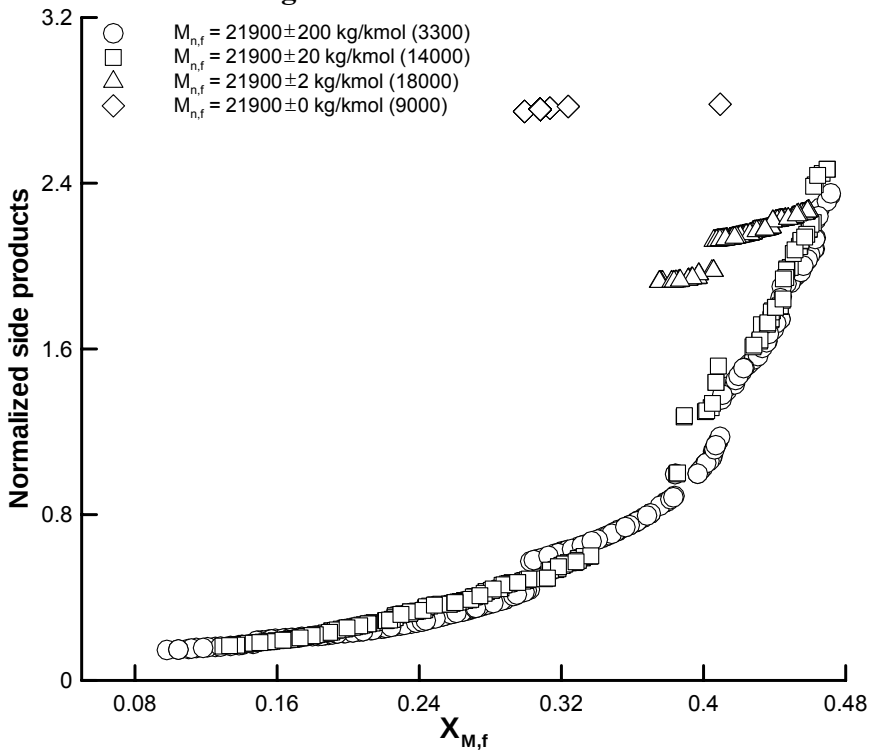

Figure 5.4 Converged Pareto sets for problems having different end-point constraints on $M_{n,f}$ using NSGA-II-JG. Numbers in parenthesis indicate the generation numbers.

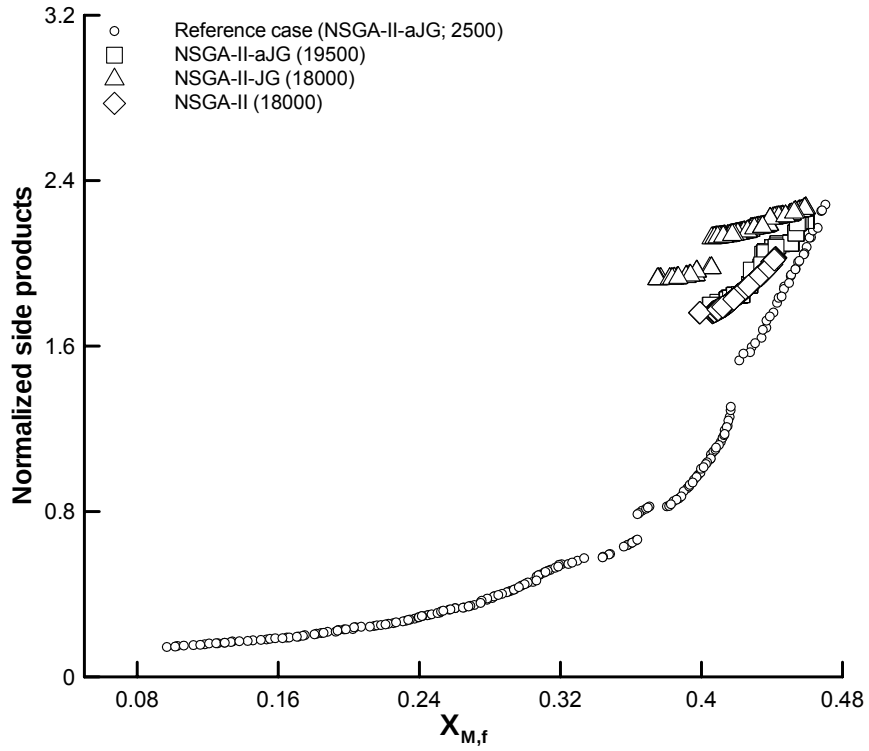

Figure 5.5 Converged Pareto sets for $M_{n,f}$ = 21900 ± 2 kg/kmol using NSGA-II and its JG adaptations. Numbers in parenthesis indicate the generation number. Results for NSGA-II-aJG (19500) and NSGA-II-JG (21000) are the same as those in Figures 5.3 and 5.4, respectively

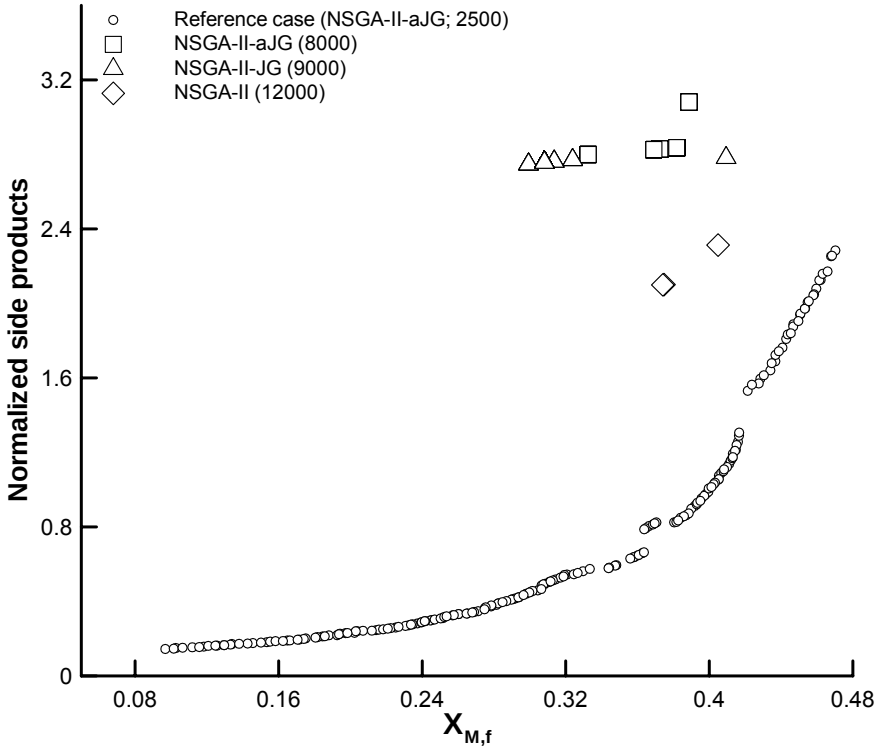

Figure 5.6 Solutions for $M_{n,f}$ = 21900 ± 0 kg/kmol using NSGA-II and its JG adaptations

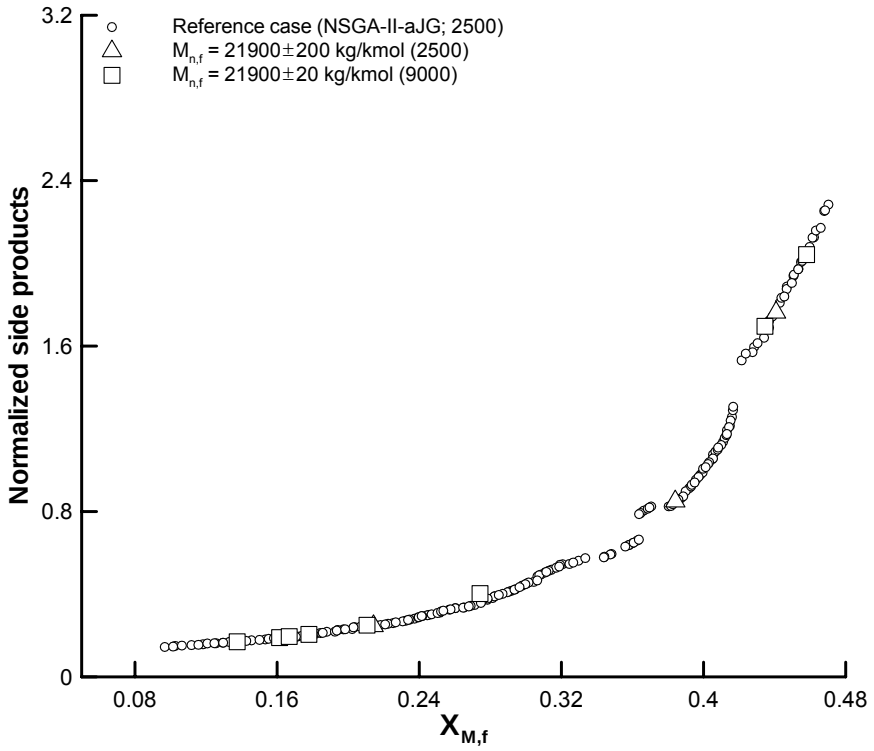

Figure 5.7 Points satisfying $M_{n,f}$ = 21900 ± 2 kg/kmol from among the Pareto sets of $M_{n,f}$ = 21900 ± 200 kg/kmol and $M_{n,f}$ = 21900 ± 20 kg/kmol cases using NSGA-II-aJG. These points are compared to the reference case.

A sudden jump (at $X_{M,f} \approx 0.42$) is observed in the Pareto-optimal set for the $M_{n,f}$ = 21900 ± 200 kg/kmol case using NSGA-II-aJG (Figure 5.3). Similar sudden breaks are also observed in the Pareto-optimal sets using different algorithms (NSGA-II and its JG variants) and constraint-handling techniques (these results are discussed later). The plots of decision variables corresponding to this Pareto-set are investigated. It is observed that the sudden jump in the optimal Pareto-set is due to jump in some decision variables, namely, F_S, $F_{I,1}$, and $F_{I,2}$ (Figures 5.11d – f; these are shown and discussed later) etc., which makes it difficult for the optimizer to choose non-dominated points in this region.

5.3.3 Constraint Handling by Constrained-dominance Principle

We tried to improve the performance of NSGA-II and its JG variants by incorporating *constrained-dominance principle* instead of penalty function for constraint handling. Deb (2001) showed that the penalty parameter for handling constraints plays an important role in multi-objective evolutionary algorithms. If the parameter is not chosen properly then it may create a set of infeasible solutions or a poor distribution of solutions. Therefore, the approach of *constrained-dominance principle* for handling constraints in MOO was proposed by Deb et al. (2002). The detailed description of this method can be found in Deb (2001). The *design* of an industrial LDPE tubular reactor is optimized for two objectives using NSGA-II and its JG variants with *constrained-dominance principle* to handle the constraints. The results obtained are compared with those obtained with the penalty function method for constraint-handling in NSGA-II-aJG.

The best values of computational parameters in NSGA-II-aJG, NSGA-II, and NSGA-II-JG were obtained for *constrained-dominance principle*, and these are listed in Table 5.2. These values were obtained by varying computational parameters, one by one, and keeping other parameters at their reference values. S_r, p_c, and p_{JG} were varied with the step size of 0.1, while p_m and L_{aJG} were varied with the step size of 0.005 and 40, respectively, to see the effect on the Pareto set. It was observed that the performance of NSGA-II-aJG was somewhat dependent on the random seed parameter (S_r) and jumping gene probability (p_{JG}) but was practically in-variant to other computational parameters. The converged Pareto-optimal set using the *constrained-dominance principle* has a slightly wider range of non-dominated points and is marginally better for the reference case ($M_{n,f}$ = 21900 ± 200 kg/kmol) (Figure 5.8); but, the *constrained-dominance principle* took more generations (3000) than the

penalty function approach (2500). Note that the Pareto set using penalty function approach was not improved even after 3000 generations; these results are shown in Figure 5.8 for both 2500 and 3000 generations but with a shift of 0.4 for clarity.

The Pareto-optimal set for the $M_{n,f}$ = 21900 ± 2 kg/kmol case using the *constrained-dominance principle* is closer to the reference Pareto-optimal set than that using penalty function (Figure 5.9). Similar results were obtained by the NSGA-II-JG upon inclusion of *constrained-dominance principle* for constraint handling. All these results indicate that the performance of NSGA-II-JG and NSGA-II-aJG has marginally improved when constraints are dealt with the systematic approach of *constrained-dominance principle* rather than the penalty function method. The points satisfying $M_{n,f}$ = 21900 ± 2 kg/kmol were collected from the converged Pareto-optimal sets of $M_{n,f}$ = 21900 ± 200 kg/kmol and $M_{n,f}$ = 21900 ± 20 kg/kmol cases using NSGA-II and its JG variants with *constrained-dominance principle* for constraint handling. These points (Figure 5.10) show uniform distribution along the reference Pareto set. This uniformity could not be captured by any algorithm along with *constrained-dominance principle* when the MOO problem with the constraint: $M_{n,f}$ = 21900 ± 2 kg/kmol, was solved using inequality (softer) constraints rather, non-dominated points were accumulated towards the higher end of conversion.

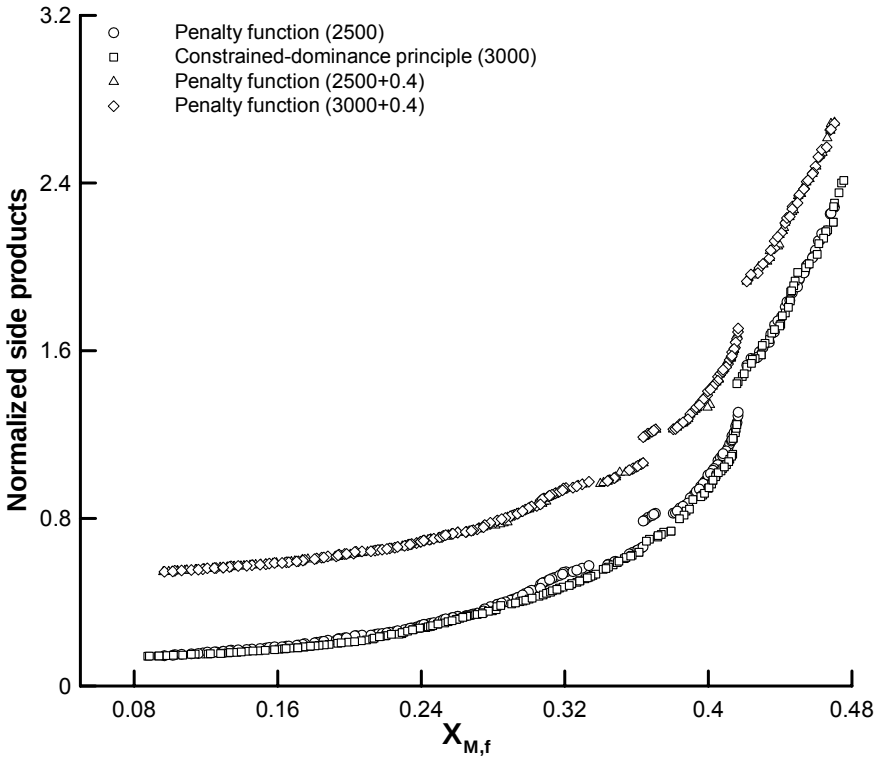

Figure 5.8 Converged Pareto-optimal sets for $M_{n,f}$ = 21900 ± 200 kg/kmol using NSGA-II-aJG for constrained-dominance principle and penalty function method. Pareto-optimal sets for 2500 and 3000 generations using the latter method are plotted with a vertical shift to show the convergence.

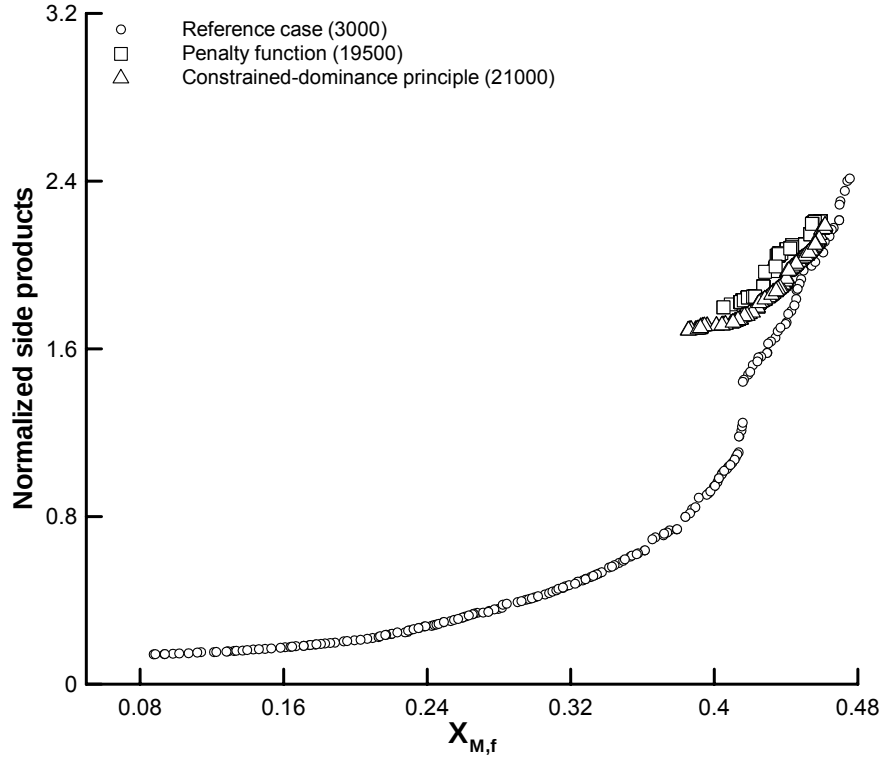

Figure 5.9 Pareto-optimal solutions for $M_{n,f}$ = 21900 ± 2 kg/kmol using NSGA-II-aJG for constrained-dominance principle and penalty function method. These solutions are compared to those for the reference case

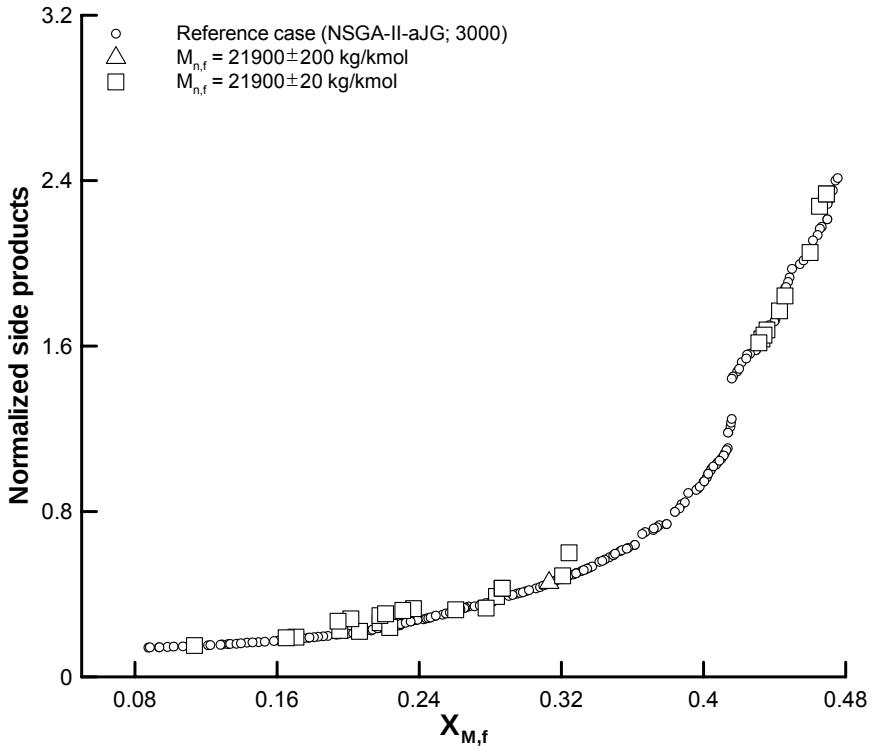

Figure 5.10 Points satisfying $M_{n,f}$ = 21900 ± 2 kg/kmol from among the Pareto sets of $M_{n,f}$ = 21900 ± 200 kg/kmol and $M_{n,f}$ = 21900 ± 20 kg/kmol cases using NSGA-II and its JG adaptations and constrained-dominance principle. These solutions are compared to those for the reference case.

The Pareto-optimal set for the reference case as well as plots of the decision variables and constraints corresponding to the points in the Pareto set obtained by NSGA-II-aJG are shown in Figure 5.11. The decision variables: T_{in}, $T_{J,2} - T_{J,5}$ are reaching their lower bounds whereas $L_{z4} - L_{z5}$, $V_{J,4}$ are at their upper bounds, and hence these variables are not plotted in Figure 5.11. It is clear that even better optimization results can be found by relaxing one or more of these bounds. However, this was not tried with the view of keeping the decision variables within the ranges inferred from the literature. When one goes from point A to point C on the Pareto-optimal set (Figure 5.11a), monomer conversion increases at the expense of increased side products. The two objectives, maximization of monomer conversion and minimization of normalized side products (branching and unsaturation), are contradictory in nature. Therefore, these were simultaneously optimized using multi-

objective evolutionary algorithms. The Pareto-optimal solutions show that much higher conversions can be obtained with the same normalized side product concentrations, as compared to current plants (Asteasuain et al., 2001b; Agrawal et al., 2006). Our study offers the scope for obtaining similar products but with higher productivity. The trends of decision variables: T_{in}, F_o, F_S, $F_{I,1}$, $F_{I,2}$, $T_{J,1} - T_{J,5}$, and P_{in} which were used in the operation optimization of LDPE tubular reactor by Agrawal et al. (2006), are almost similar to our earlier study.

The Pareto-optimal set (in Figure 5.11a) largely depends on three decision variables, P_{in}, F_S, and $F_{I,1}$. Initially, $X_{M,f}$ increases with P_{in} (Figure 5.11b) and, later on, $F_{I,1}$ contributes to higher conversion as shown in Figure 5.11e. The F_S (Figure 5.11d) decreases as $X_{M,f}$ increases, to maintain $M_{n,f}$ at the required value; at higher conversion, more and more polymer chains are formed which reduces $M_{n,f}$ and therefore less F_S is required. The flow rates of two other initiators, F_o, and $F_{I,1}$ (Figures 5.11c and f), are at their lower bounds. Machi et al. (1968) observed that the reaction temperature had profound effect on short chain branching and unsaturation; therefore, jacket fluid temperatures ($T_{J,1} - T_{J,5}$), T_{in}, L_{z2} (Figure 5.11i), $V_{J,2}$ and $V_{J,3}$ (Figures 5.11m and n) attain appropriate values to keep the reactor temperature optimum so as to minimize the side product concentrations and also maximize conversion. The optimal L_{z1}, L_{z3}, D_{int} and D_{Jacket} (Figures 5.11h, j, k, l) are somewhat scattered. Polymerization reaction generates enormous amount of heat which is removed by higher $V_{J,4}$ and $V_{J,5}$ (Figure 5.11o) and by larger L_{z4} and L_{z5}.

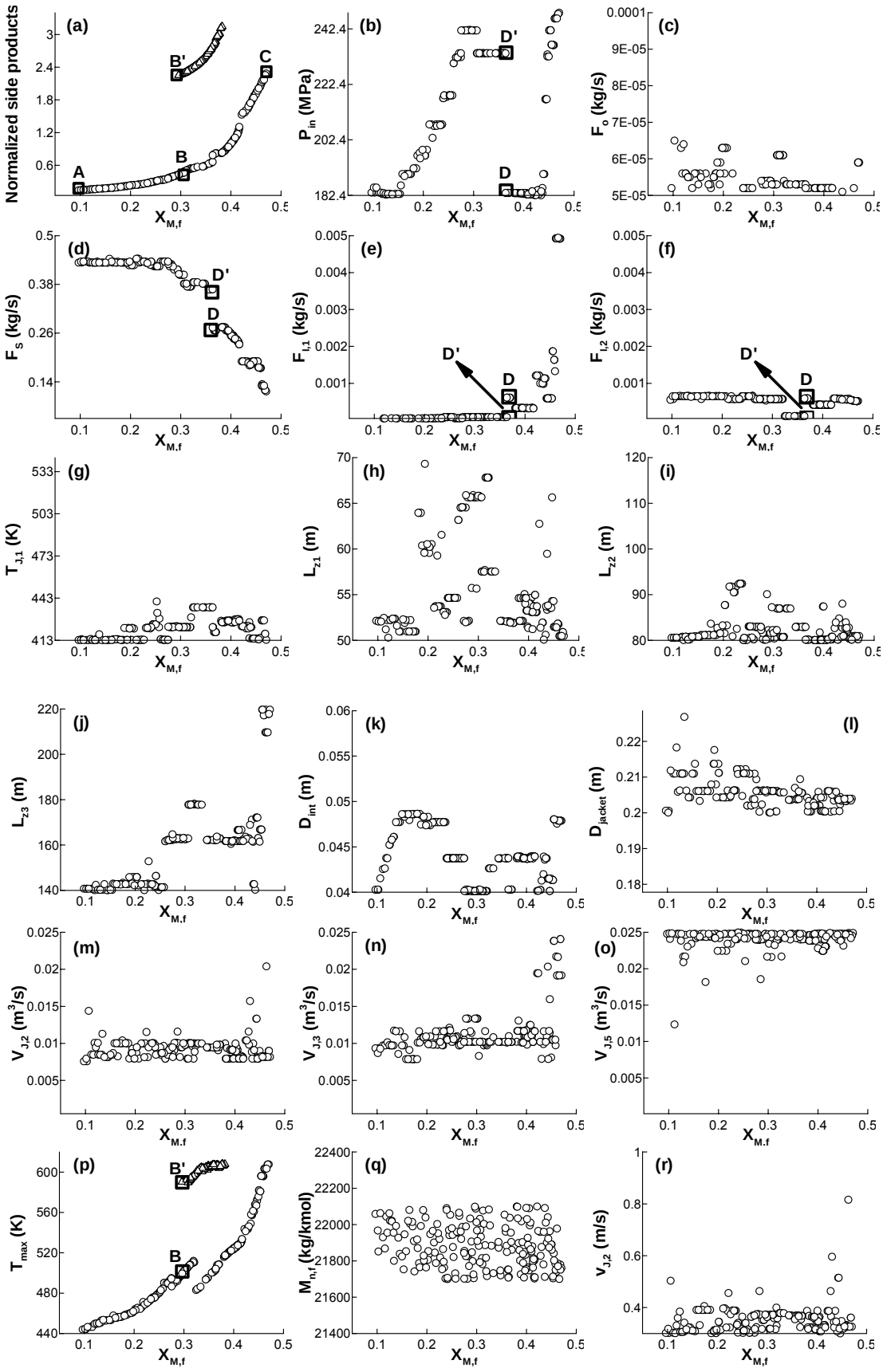
(a)
Normalized side products
A
B
B'
C
(b)
P_{in} (MPa)
D
D'
(c)
F_o (kg/s)
(d)
F_S (kg/s)
D
D'
(e)
$F_{l,1}$ (kg/s)
D
D'
(f)
$F_{l,2}$ (kg/s)
D
D'
(g)
$T_{J,1}$ (K)
(h)
L_{z1} (m)
(i)
L_{z2} (m)
(j)
L_{z3} (m)
(k)
D_{int} (m)
(l)
D_{jacket} (m)
(m)
$v_{J,2}$ (m^3/s)
(n)
$v_{J,3}$ (m^3/s)
(o)
$v_{J,5}$ (m^3/s)
(p)
T_{max} (K)
B
B'
(q)
$M_{n,l}$ (kg/kmol)
(r)
$v_{J,2}$ (m/s)
$X_{M,f}$

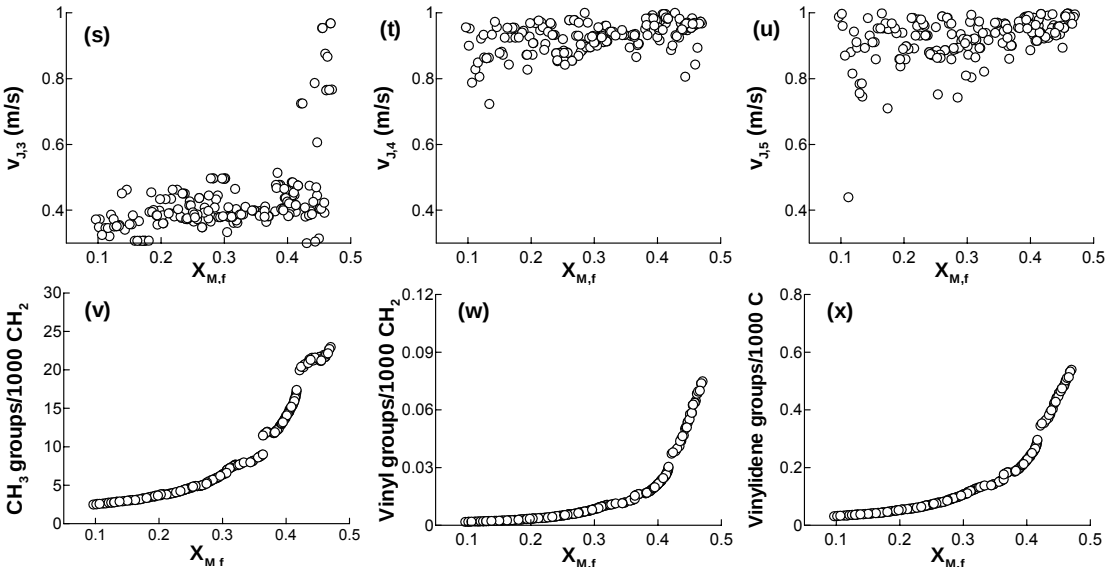

Figure 5.11 Pareto-optimal points and the corresponding decision variables and constraints for the reference case ($M_{n,f}$ = 21900 ± 200 kg/kmol) using NSGA-II-aJG. The Pareto-optimal points for design stage (○) are compared to those for the operation stage optimization (Δ) in Figures 5.11a and p.

The solutions for design optimization are compared to the Pareto-optimal set obtained at *operation* stage optimization for the same case using NSGA-II-aJG (Figure 5.11a). The results show significant improvement in the Pareto-optimal set for the design case. This improvement is attributed to the reactor temperature in design case where the maximum temperature (T_{max}; therefore temperature inside the whole reactor; Figure 5.11p) is lesser than that found in the operation stage. To illustrate this, chromosomes B and B' (identified in Figure 5.11a) are selected from the Pareto-optimal sets of design and operation optimization, respectively. Monomer conversion for each of these two chromosomes is similar but normalized side products are quite different (Figure 5.11a). Profiles for the temperature, monomer conversion, and initiator concentrations ($C_{I,1}$ and $C_{I,2}$) are generated for these chromosomes (along with for chromosomes A and C, identified in Figure 5.11a), as shown in Figure 5.12. (In Figure 5.12c, $C_{I,1}$ for chromosome A (– – –) is beyond the limits shown in the y-

axis and so its profile could not be shown completely; rather, two vertical dashed lines are shown.) Maximum temperature for chromosomes B and B' (Figure 5.12a) is 499 K and 590 K, respectively. Therefore, the side products concentration, which decreases with temperature, is very low in the design stage optimization. But, the same conversion is achieved due to gradual decomposition (unlike in the operation stage optimization) of initiators in the tubular reactor as shown in Figure 5.12c. Similar trends were observed for chromosome C giving highest conversion, where temperature in the fifth zone is below the optimum temperature for decomposition of second initiator (I_2) and then temperature of reactant-product mixture increases slowly and correspondingly monomer conversion increases (see Figures 5.12a and b).

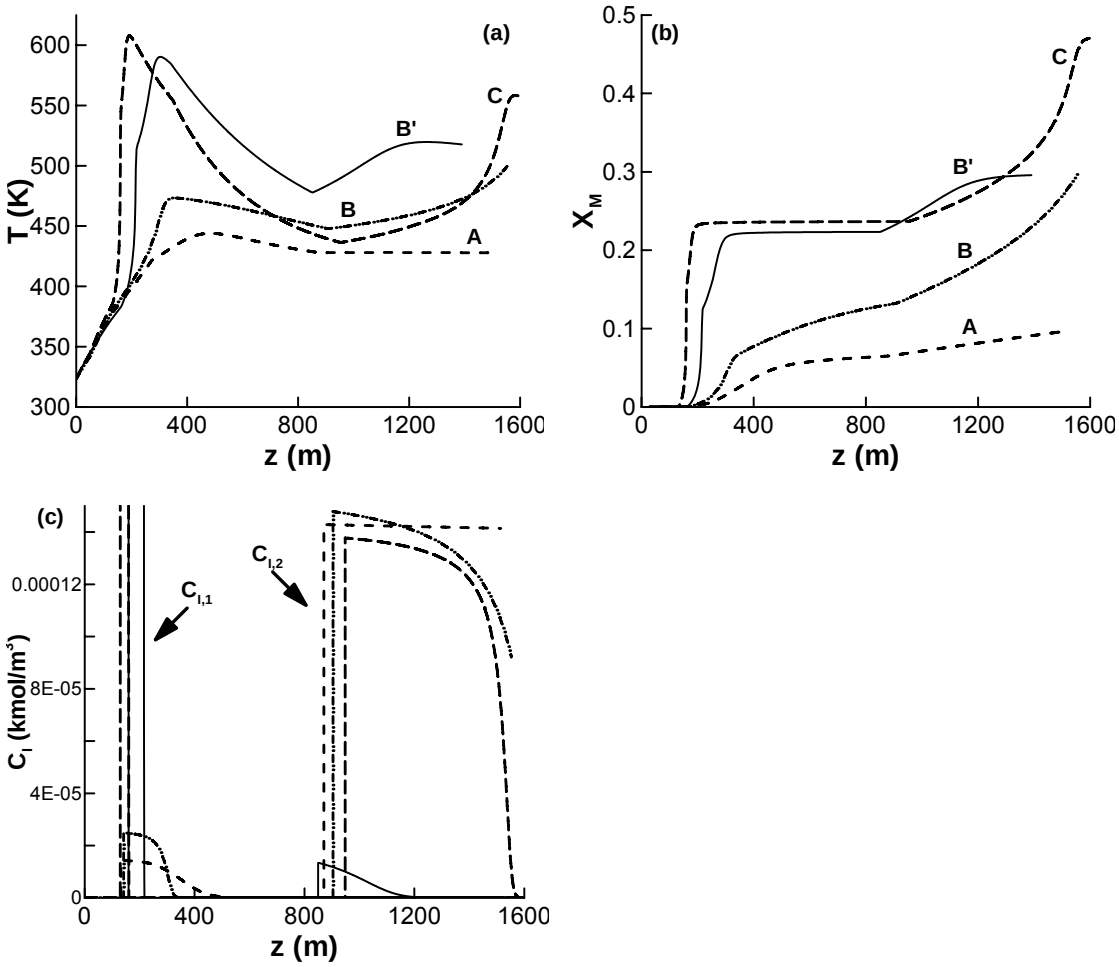

Figure 5.12 Temperature (T), monomer conversion (X_M), and initiator concentrations profiles for chromosomes A (---), B (-·-·-·-), B' (—) and C (− − −) shown in Figure 5.11a

In Figure 5.11b, it is observed that two chromosomes (say D and D') show a break in the inlet pressure, whereas the monomer conversion and normalized side products for these two chromosomes are nearly the same. For chromosome D, monomer conversion should have decreased, because the inlet pressure is lowered; but, the same conversion level is maintained by the sudden increase in $F_{I,1}$ and $F_{I,2}$ (Figures 5.11e and f). Also, solvent flow rate, F_S, is reduced to satisfy constraint on the number-average molecular weight (Figure 5.11d). These solutions (D and D') reveal that different sets of decision variables may give the same Pareto-optimal solutions. Therefore, they are possibly the multiple near-optimal solutions and could be produced due to random nature of the algorithm. To confirm, Pareto-optimal set and some associated decision variables obtained using NSGA-II-JG for the reference case are plotted (Figure 5.13). Results by NSGA-II-JG also showed a similar jump in the inlet pressure profile (Figure 5.13f) and associated changes in F_S and $F_{I,1}$ (Figures 5.13c and d), but at a different monomer conversion. Similarly, there are differences in the maximum temperature profiles obtained by NSGA-II-aJG and NSGA-II-JG (Figures 5.11q and 5.13(l)).

In the high pressure process, the product mixture passes through a let-down valve (used to reduce the pressure; Cervantes et al., 2000). Thereafter, this mixture is sent to a flasher (high-pressure separator). The half-life of the second initiator (I_2; tert-butyl 3,5,5 trimethyl-peroxyhexaonate) is about 1 s at the reaction temperature of 211°C. This means that the reaction will continue to take place in the pipes after the reactor (till before the flasher) for Pareto solutions that are associated with unreacted I_2 at the end. We solved the MOO problem with an additional constraint on the concentration of the second initiator at the reactor exit, i.e., $C_{I,2,f} \leq 0.0001 C_{I,2,O}$ (where $C_{I,2,O}$ is the concentration of the second initiator at its feed point in the fifth zone), for $M_{n,f}$ =

21900 ± 200 kg/kmol. The solutions are compared to the earlier Pareto-optimal set (without this constraint) in Figure 5.14. It is observed that the Pareto-optimal set in the presence of this extra constraint superimposes on the reference Pareto set (without the penalty on $C_{I,2,f}$), but that the optimal solutions extend only over monomer conversions of about 40% (the presence of this constraint on $C_{I,2,f}$ eliminates solutions corresponding to $X_{I,2,f} \leq 99\%$). Again, a decision maker can use only the relevant part of the Pareto set to select a preferred solution.

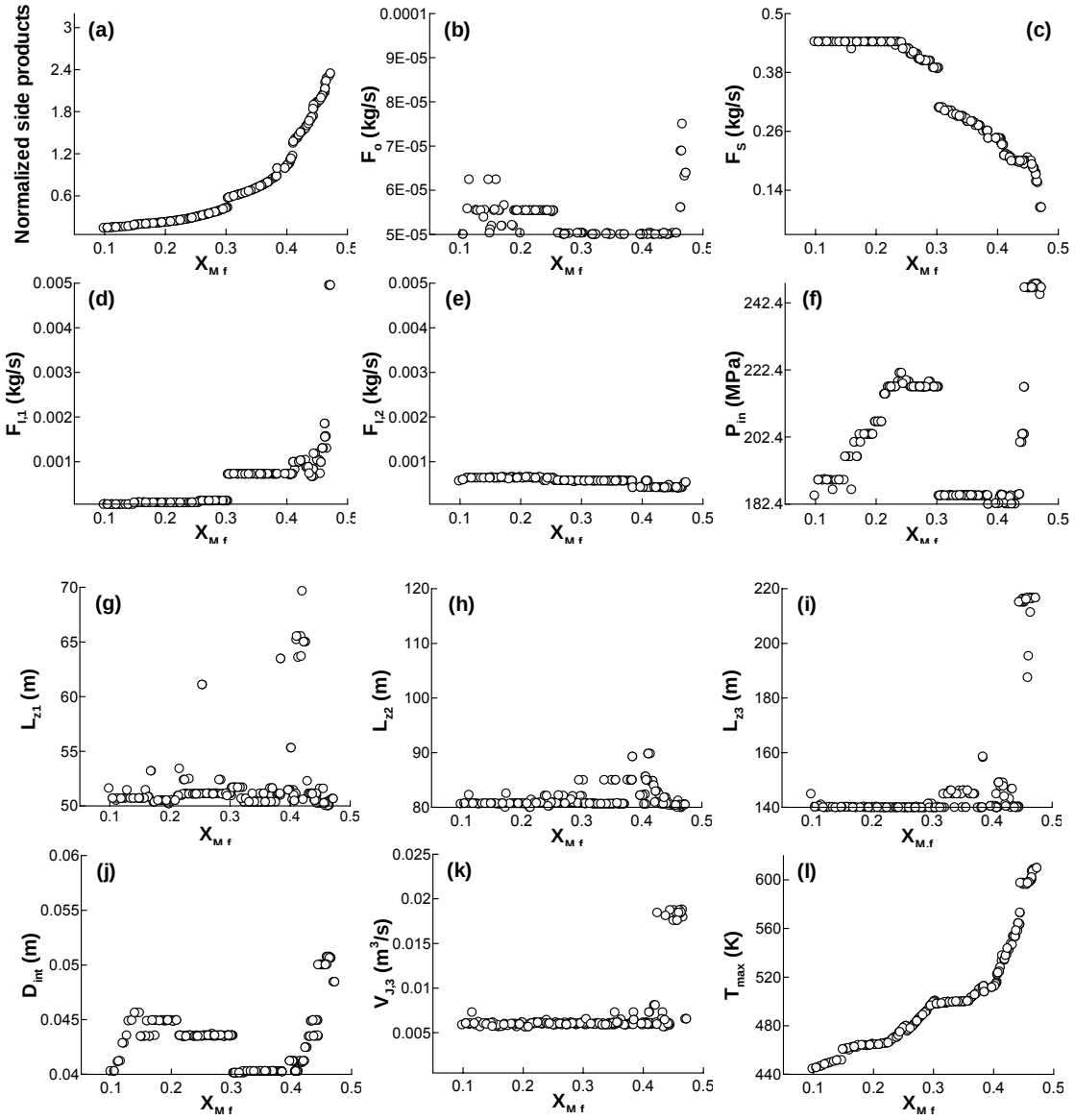

Figure 5.13 Pareto-optimal points and the corresponding decision variables and constraints for the reference case ($M_{n,f}$ = 21900 ± 200 kg/kmol) using NSGA-II-JG

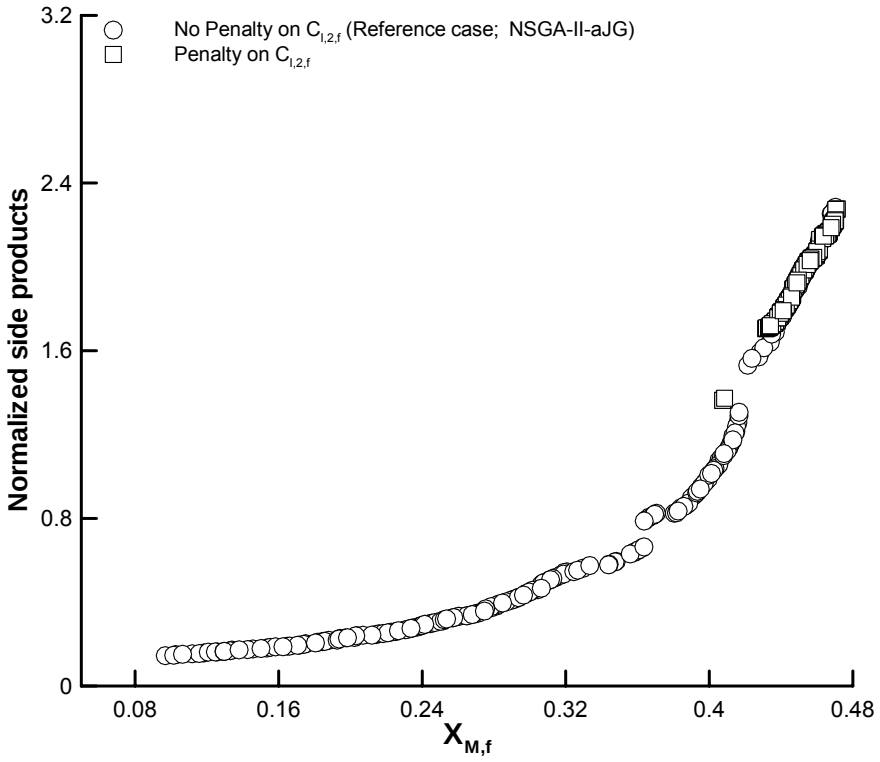

Figure 5.14 Pareto-optimal solutions for $M_{n,f}$ = 21900 ± 200 kg/kmol using NSGA-II-aJG with and without penalty on $C_{I,2,f}$

It is the lower density and crystallinity (inversely proportional to the SCB: short side-chain branching frequency) of LDPE that makes it soft. The value of SCB in LDPE also influences its heat softening point, yield strength, stiffness, impermeability to gases and liquids, film drawdown, and optical clarity (Luft et al., 1982), and, hence, determines its use for its *various* applications. LDPEs having an *extended range* of properties (SCBs) can be produced by the high pressure process. The range of SCBs (CH_3 per 1000 C) for the three *common* PEs are: LDPE: 10 – 50 [SCB = 30 per 1000C (Gupta et al., 1985) for typical LDPEs]; HDPE: 2 – 3; LLDPE: 3 – 30. Minimization of SCB in our study leads to values of SCB in the range of 2.5 - 23 CH_3 per 1000 C, corresponding to different points on the Pareto set (Figure 5.11a). If the decision maker wishes to produce LDPE with an SCB of, say, 5.0 (higher than that for HDPE, but lower than that for the LDPE produced usually, which will have properties

intermediate between LDPE and HDPE), he has to select the appropriate point on the Pareto set. Our study offers scope of producing additional grades of LDPE. If one does not wish to do so, all he has to do is to select an appropriate point in the Pareto set of optimal solutions, or solve another MOO problem with SCBs omitted in the objective function. Figure 5.15 gives the Pareto solutions without the SCB in the objective function.

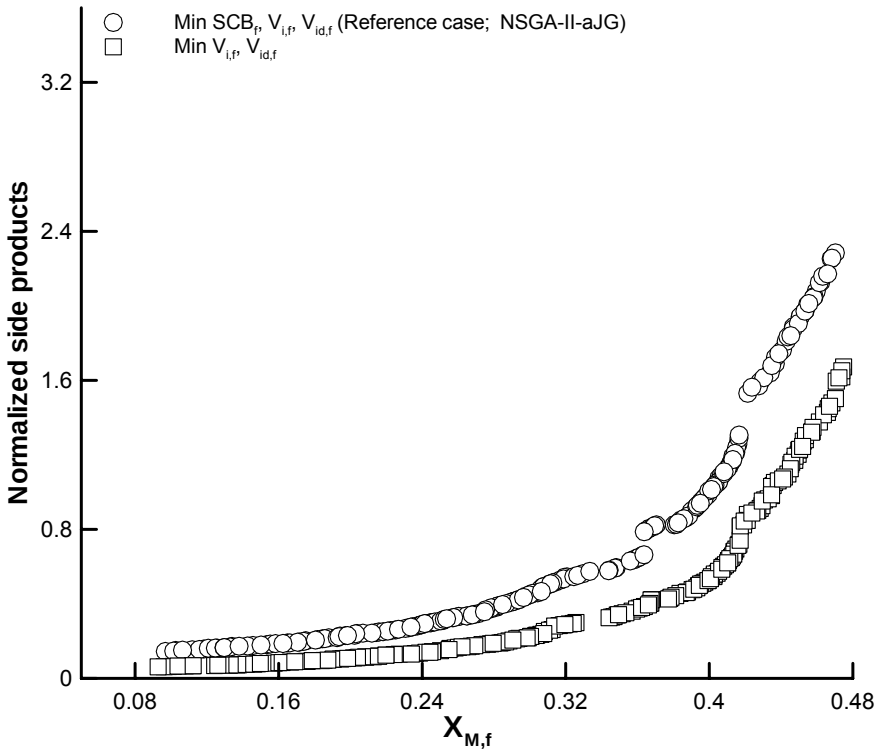

Figure 5.15 Pareto-optimal solutions for $M_{n,f}$ = 21900 ± 200 kg/kmol using NSGA-II-aJG with and without minimization of SCB

5.3.4 Three-objective Optimization

The three objectives: maximization of monomer conversion, $X_{M,f}$, minimization of the (weighted average value of the) undesirable side product contents ($[M_e]_f$, $[V_i]_f$, and $[V_{id}]_f$), and minimization of normalized compression power, are simultaneously optimized for the high-pressure polymerization of ethylene (case 2 in Table 5.1). To

understand the third objective, consider a simplified process flow sheet for LDPE production (Figure 5.16). Fresh make-up ethylene, at a flow rate of $F_M X_{M,f}$, available at 1 atm, is pressurized to 350 atm in the primary-compressor (Cervantes et al., 2000). It is then mixed with the recycled stream after the polymer is separated (it contains inert, un-reacted monomer and solvent), and fed to the hyper-compressor to be pressurized to reactor inlet pressure (~ 2250 atm). This reaction mixture produces polyethylene ($F_M X_{M,f}$) in the tubular reactor, which is removed from the product mixture in the high-pressure separator. The operating cost of primary- and hyper-compressors forms a major part of the total production cost. The compression power can be calculated from the equation given in Table 5.1 (case 2). This equation is derived based on several compression stages shown for an industrial LDPE process by Cervantes et al. (2000). These compression stages are confirmed to require minimum compression work before deriving the expression for compression power. A compression efficiency of 75% is assumed in deriving the expression. The binary-coded NSGA-II-aJG is used for solving the three-objective optimization problem. Penalty function approach is used to handle the inequality constraints. The computational parameter values used for the three-objective optimization were the same as those used for the two-objective optimization.

NSGA-II-aJG required 3000 generations to produce converged non-dominated solutions shown in Figure 5.17; in this figure, the three objectives are plotted against the chromosome number after rearranging the results so that the conversion increases with the chromosome number. Figure 5.17 shows that higher conversion is achieved only at the higher normalized side products and higher compression power. Some scatter is observed in the plots of normalized side products and compression power (Figures 5.17b and c). This scatter could not be reduced by increasing number of

generations or by changing values of the computational parameters. The scatter in Figures 5.17b and c could be attributed to the dominance criterion, which is satisfied even if any one of the three objectives has a better value and other two objectives are worsened (Tarafder et al., 2006).

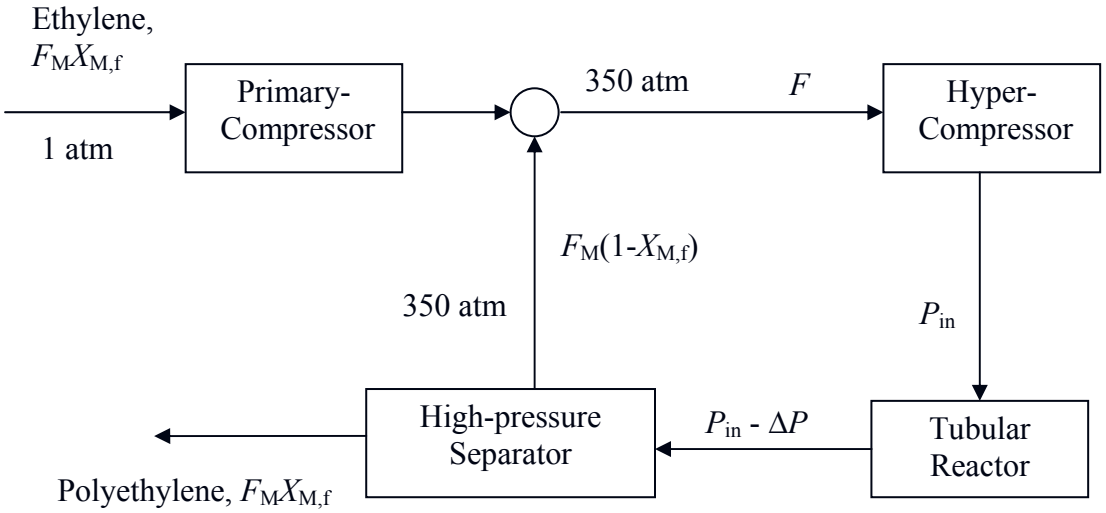

Figure 5.16 Simplified process flow diagram of the LDPE production (Cervantes et al., 2000)

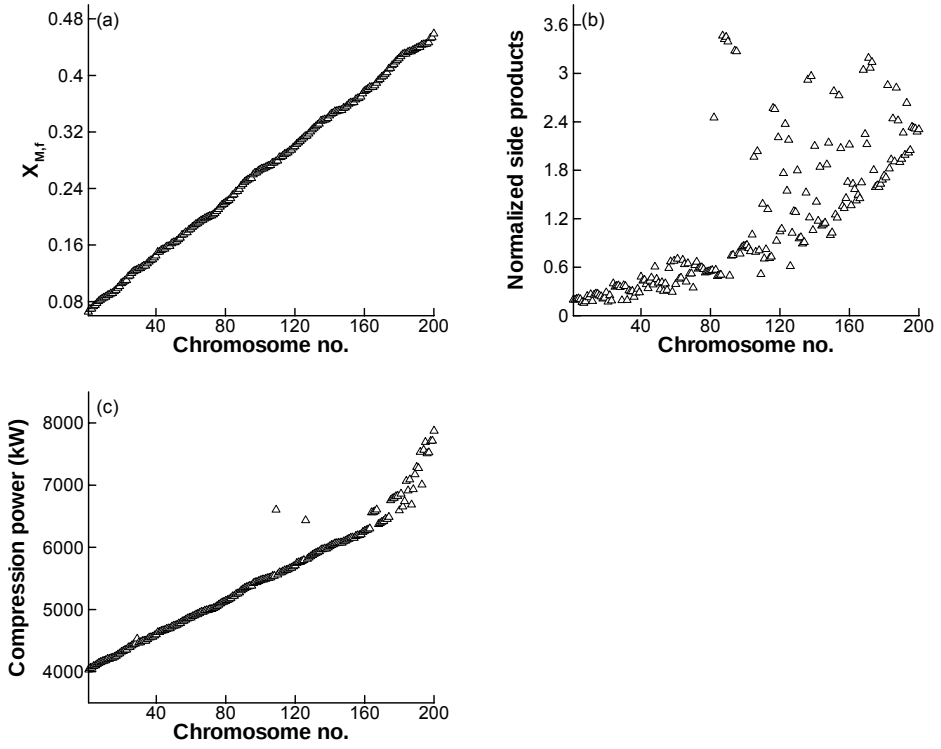

Figure 5.17 Results for the three-objective optimization problem using NSGA-II-aJG

The Pareto-optimal results obtained by three-objective optimization are also plotted in terms of two combinations of two-objectives: normalized side products vs. monomer conversion and compression power vs. monomer conversion (Figures 5.18 and 5.19). The results of three-objective optimization and those from the simultaneous maximization of monomer conversion and minimization of normalized side products are included in Figure 5.18 for comparing the results of two- and three-objective problems. Note that the compression power was calculated using the results of two-objective optimization. Although Figure 5.18a shows that the normalized side products-monomer conversion Pareto-optimal set of three-objective optimization problem is scattered and worse than the Pareto of two-objective optimization, this compromise was done to minimize the compression power, simultaneously. Similar observations were made by Tarafder et al. (2005) in three-objective optimization of styrene manufacturing process. Now, the two objectives – maximization of monomer conversion and minimization of compression power, are optimized and compared in Figure 5.19 with the Pareto-optimal set of three-objective optimization. The Pareto-optimal set of compression power vs. monomer conversion of two-objective optimization showed slightly faster convergence (with no scattering) than the Pareto-optimal set of compression power vs. monomer conversion of three-objective optimization (see Figure 5.19b). However, the three-objective optimization gives better objective values than the two-objective optimization, except at higher conversion. Thus, the simultaneous optimization of three-objectives is needed to obtain the best product quality with minimum compression cost and maximum throughput, simultaneously.

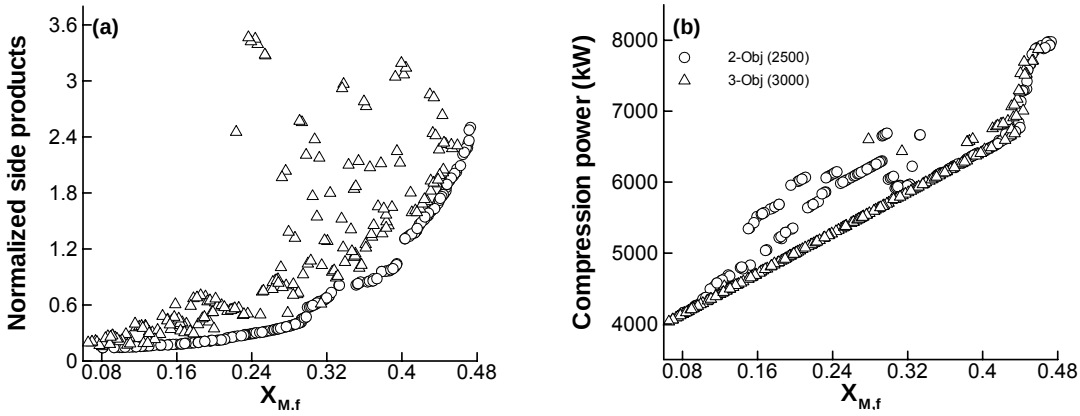

Figure 5.18 Comparison of Pareto sets obtained for (a) normalized side products Vs $X_{M,f}$ and (b) compression power Vs $X_{M,f}$, from the three-objective optimization (Δ) and two-objective optimization of normalized side products and $X_{M,f}$ (○)

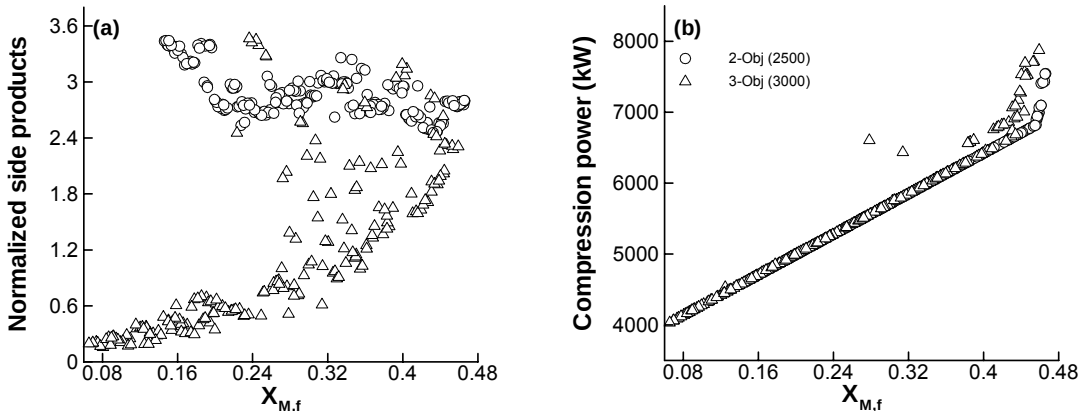

Figure 5.19 Comparison of Pareto sets obtained for (a) normalized side products Vs $X_{M,f}$ and (b) compression power Vs $X_{M,f}$ from three-objective optimization (Δ) and two-objective optimization of compression power and $X_{M,f}$ (○)

Figure 5.20 shows the plots of Pareto-optimal sets of three objective optimization problem and some decision variables and constraints corresponding to non-dominated solutions in these plots. Decision variables: T_{in}, F_o, $T_{J,1} - T_{J,3}$, $L_{z1} - L_{z5}$, $V_{J,2} - V_{J,5}$, D_{int}, and D_{Jacket}, and constraints: $v_{J,2}$ - $v_{J,5}$ are not plotted since their optimal values are scattered, and $T_{J,4} - T_{J,5}$ are reaching their lower bounds. It is observed from the Pareto-optimal sets (Figures 5.20a and b) that higher monomer conversions can be achieved only at the cost of higher side products and higher compression power. The

plots of decision variables in Figure 5.20 show that the optimal solutions depend, primarily, on three decision variables, P_{in}, F_S, and $F_{I,1}$ (Figures 20c - e). The dependency of the Pareto-optimal set in Figure 5.20a on these decision variables can be explained in a similar fashion as explained for the results of two objective optimization problem (Figure 5.11). For example, Figure 5.20c shows predominant effect of P_{in} on compression power. Thus, it is trying to reach the lower bound to minimize the compression power, as expected. But, higher inlet pressure (therefore higher pressure throughout the reactor) is required to lower the side product contents as discussed by Ehrlich and Mortimer (1970). Therefore, higher P_{in} is observed at higher monomer conversions to keep the check on side products concentration.

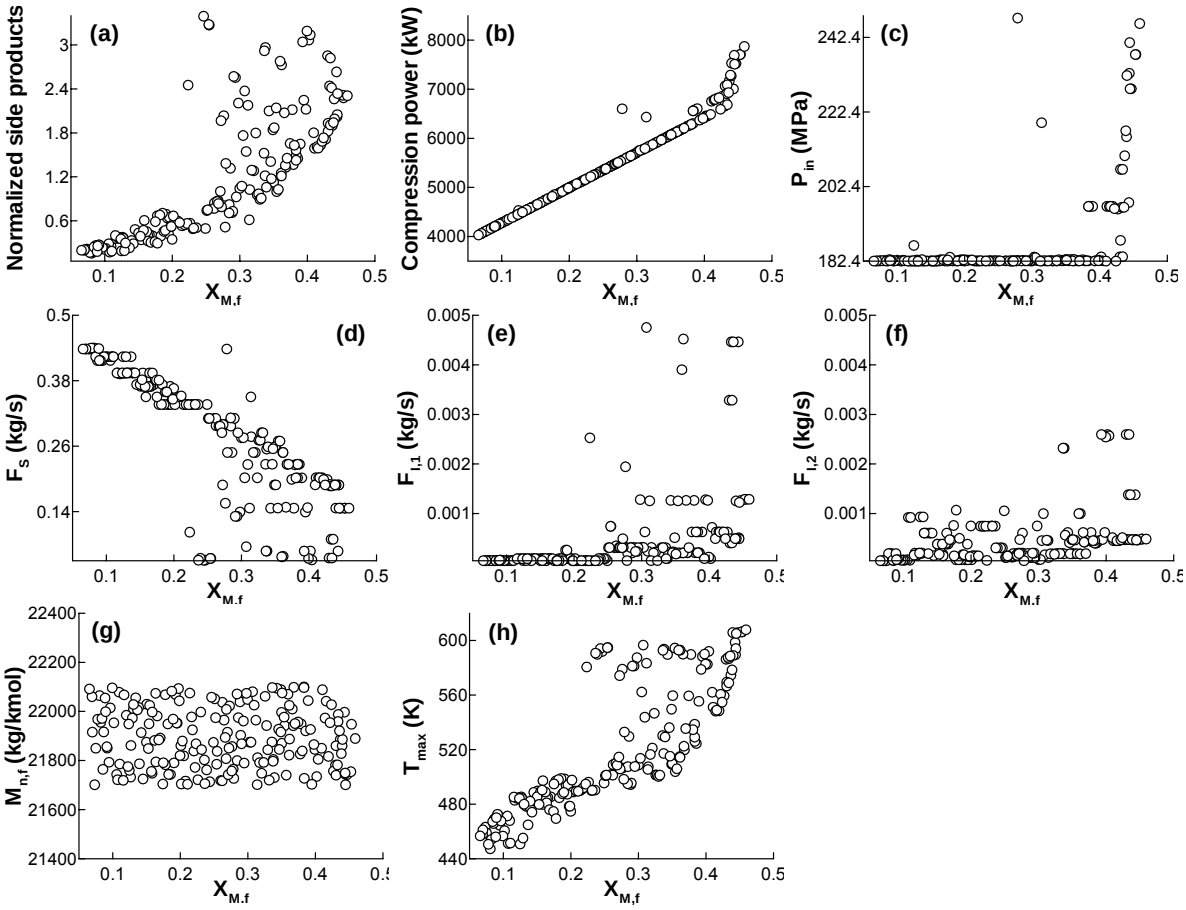

Figure 5.20 Objectives, selected decision variables and constraints corresponding to the Pareto-optimal points for the three-objective optimization problem for the reference case ($M_{n,f}$ = 21900 ± 200 kg/kmol) using NSGA-II-aJG.

5.4 Conclusions

Design of an industrial tubular reactor for high-pressure polymerization of ethylene to produce LDPE is optimized for multiple objectives using the elitist binary-coded NSGA-II and its JG adaptations. The monomer conversion is maximized and normalized side products are minimized, with constraints on $M_{n,f}$, reactor temperature, and jacket fluid velocities. The design stage optimization showed significant improvement in the reactor performance, when compared with the operation stage optimization. The correct global Pareto-optimal solutions could not be obtained by any of the NSGA-II, NSGA-II-JG, and NSAG-II-aJG algorithms tried, when the hard equality constraint on $M_{n,f}$ is imposed. Comparison of the Pareto-optimal sets for $M_{n,f}$ = 21900 ± 2 kg/kmol case obtained by the three algorithms showed that NSGA-II-aJG and NSGA-II are better than NSGA-II-JG. However, solution of this problem by any algorithm requires a lot of CPU time and the converged Pareto is limited to a small range. For the near hard end-point constraints, for instance, $M_{n,f}$ = 21900 ± 2 kg/kmol, Pareto-optimal solutions over a wider range can be assembled from among the Pareto-optimal sets of several MOO problems with softer constraints, optimized by NSGA-II and its JG adaptations. This approach takes less CPU time too. For the LDPE design problem, constrained-dominance principle worked marginally better than the penalty function approach for handling constraints in the binary-coded NSGA-II-JG and NSGA-II-aJG. The three-objective optimization of the LDPE design problem produced optimal solutions comparable to or better than those by the two-objective optimization.

Chapter 6

Dynamic Modeling, Simulation and Optimal Grade Transition

6.1 Introduction

Low-density polyethylene (LDPE) is one of the most highly used polymers in the world. It is produced in autoclave and tubular reactors using high pressure technology. In this study, dynamic optimization of an industrial tubular reactor for LDPE production is considered. The operating conditions in the reactor are very extreme, namely, 150–250 MPa and 325–625 K. Because of these extreme conditions, the polymerization kinetics is quite complex and undesired products are generated. Initiators such as azo compounds, organic peroxides, and oxygen are used to generate free-radicals which react with the monomer (ethylene) to produce polyethylene. The polymerization reaction is highly exothermic. Therefore, the tubular reactors are very long with coolant flowing counter-currently in the jackets to remove the heat of reaction. The monomer conversion per pass is low (for a single-injection of the monomer-initiator mixture at the feed end), but is enhanced by multiple injections of monomer and initiators along the reactor axis. Nevertheless, the monomer conversion per pass is reported to be 30 – 35 % in industrial reactors. The unconverted monomer is separated using high- and low-pressure separators in downstream operations and recycled to the reactor.

Polymer industries are subject to market fluctuations. This necessitates producing as many as thirty to forty different grades of polymer in a single polyolefin plant (Chatzidoukas et al., 2003). Indeed, the production of LDPE in tubular reactors is a typical example of a process where unsteady states during plant operation are commonly observed. Also, the cost of maintaining large inventories is huge. Thus,

what is required for the market should be produced just-in-time. So, frequent grade changes are expected in an LDPE plant. In addition, LDPE plants are connected to upstream and downstream processes which influence the throughput of the plant directly (Hafele et al., 2006). Therefore, grade-change of polymers while ensuring high quality becomes an essential and important issue in a polymer plant. Off-specification (off-spec) product is produced during grade change. This leads to loss of revenue. Thus, a change in the polymer grade should be made with the minimum production of the off-spec polymer and in the minimum time required for grade changeover.

The different grades of LDPE having desired specifications are obtained by switching between appropriate steady states (Cervantes et al., 2000). Grade-change, coupled with control strategies, can be carried out in two steps in any polyolefin industry. First, the optimal grade-change procedures are identified off-line to obtain the decision variables. This is done using appropriate constraints on the input, output and state variables of the process, using a good dynamic model. In the second step the optimal solutions are implemented using properly designed (values of their parameters) feed-forward and feed-back controllers (Chatzidoukas et al., 2003). This study focuses on the first aspect where optimal grade-change trajectories are obtained using off-line optimization.

LDPE production using tubular-reactor technology at high pressures is well established in industry. Many steady state models are available in the open literature (e.g., Zabisky et al., 1992; Kiparissides et al., 1993a; Brandolin et al., 1996; Agrawal et al., 2006), but only a few of these deal with dynamic models (e.g., Kiparissides et al., 1994; Cervantes et al., 2000; Asteasuain et al., 2001b). These dynamic models are fairly simple. Kiparissides et al. (1994) carried out on-line optimization of a high-

pressure tubular reactor. But, they used a steady state model, assuming that the dynamic response of this process is an order of magnitude faster than the grade-change. Their assumptions are not justified, as discussed by Hafele et al. (2006). Cervantes et al. (2000) minimized the grade-change time between two steady-states in a large-scale industrial LDPE plant, for two polymer grades. Asteasuain et al. (2001b) presented a dynamic model of an LDPE reactor and then obtained the optimal start-up policies. They maximized the outlet conversion and minimized the time required for the reactor to stabilize, while forcing the polymer properties to have some desired values during start-up. Again, these studies did not account for the spatial and time variations of the physico-chemical properties. Also, some reactions were not included in their reaction scheme. These are important for defining the polymer quality. Hafele et al. (2005) simulated an industrial tubular reactor for LDPE production using an adaptive method of lines where the adaptation of grid nodes was done dynamically. Hafele et al. (2006) used their model to study the effects of the thickness of the reactor wall and the recycle of the materials on the dynamics of the plant. However, they did not provide complete details of their approach for proprietary reasons. In the present study, a very comprehensive dynamic model for the production of LDPE in tubular reactors is presented and simulation results using it are discussed in detail.

In this work, the steady-state model of Agrawal et al. (2006) is modified to study the dynamic behavior of an industrial tubular reactor. The dynamic model comprises of a set of partial differential and algebraic equations, and uses a detailed reaction scheme and kinetics. The variations in the physical and transport properties are also included in the model. The dynamic model is used to study the effects of step-changes of the inlet pressure and of the concentrations of initiators and telogen, on the transient profiles of the monomer conversion, polymer properties and the reactor

temperature. Complete details of the model parameters and the simulation results for the industrial tubular reactor are provided. Thereafter, the dynamic model is used to optimize the grade-change policies. The objectives used are the time taken for grade changeover and the specifications on the quality of the product (M_n and the normalized concentration of the side-products in the exit stream). An end-point constraint on exit value, $M_{n,exit}$, is also used. These two objectives are simultaneously optimized using the binary-coded elitist non-dominated sorting genetic algorithm (NSGA-II; Deb, 2001) with the jumping gene (JG) adaptation (Simoes et al., 1999; Kasat and Gupta, 2003; Man et al., 2004; Guria et al., 2005). The details of NSGA-II-aJG are described in Guria et al. (2005). A multi-objective optimization (MOO) problem will not have a unique solution unless the objectives are non-conflicting. It will have several equally-good optimal solutions, which are known as Pareto-optimal or non-dominated solutions; i.e., each of the solutions is better than the others in the Pareto set in terms of at least one objective. However, the Pareto solutions are better than all *other* feasible solutions as far as all the objectives are concerned. Interested readers are referred to Deb (2001) and Rangaiah (2007) for more details on MOO and its applications.

6.2 Dynamic Modeling and Simulation

The industrial high-pressure tubular reactor for LDPE production contains several tubes which are inter-connected by 180 ° bends. The steady-state model of Agrawal et al. (2006) is modified to give a dynamic model for optimal grade-change studies. The detailed description of the tubular reactor, the kinetic scheme, and the process parameters are reported in Agrawal et al. (2006). The design features and model parameters are summarized in Table 6.1. In brief, the steady state model is based on

the plug flow assumption, and incorporates the axial variation of the concentrations, temperature and pressure (and the physical properties). In addition, several main (Asteasuain et al., 2001b) and side reactions, e.g., intra-molecular chain transfer, chain transfer to polymer, β-scission of secondary and tertiary radicals, etc. (the latter give the extent of long- and short-chain branching and the amount of unsaturation in the polymer) are included.

During grade-change, the concentrations, $C_j(z, t)$, and the temperature, $T(z, t)$, of the polymerizing mixture are functions of both the axial location, z, and the time, t. It is assumed that there are no radial gradients present in view of the high velocity of the reaction mass. The model equations for $C_j(z, t)$ and $T(z, t)$ can be written for a differential length, dz, as

$$v\frac{\partial C_j}{\partial z}=\left(r_j-\frac{\partial C_j}{\partial t}-C_j\frac{\partial v}{\partial z}\right) \quad \text{for } C_j = C_{I_1},\ C_{I_2},\ C_{O_2},\ C_S,\ C_M,\ C_{M_e},\ C_{V_i},C_{V_{id}},C_{R_1(0)},$$

$$\lambda_{np},\ \mu_{np};\ n = 0, 1;\ p = 0, 1, 2 \tag{6.1}$$

$$\rho C_P v\frac{\partial T}{\partial z}=-\left\{\rho C_P\frac{\partial T}{\partial t}+\frac{4U\left(T-T_J\right)}{1000D_{int}}+k_p C_M\lambda_{00}(\Delta H)\right\} \tag{6.2}$$

In Equation (6.1), C_j is the concentration of the j^{th} species, and its subscripts denote the various species: initiator 1, initiator 2, oxygen, solvent, monomer, methyl, vinyl, vinylidene, free-radicals without monomer unit, n^{th}- and p^{th}-order moments for the chain length distribution of macro-radicals and dead polymer molecules, respectively. The other symbols in Equations (6.1) and (6.2) are: r_j is the rate of generation of the j^{th} species, v is the axial velocity, ρ, C_p and T are the density, specific heat and the temperature of the reaction mixture, respectively, U is the over-all heat transfer coefficient, T_J is the jacket fluid temperature, D_{int} is the inside diameter of the reactor, k_p is the propagation rate constant, and ΔH is the heat (enthalpy) of polymerization.

The expressions for the reaction rate and the parameters are given in Agrawal et al. (2006) and are not repeated here. Constant (average) values of the temperature of the jacket fluid in each zone, and of the specific heat of the reaction mixture are assumed. The velocity of the reaction mixture is calculated by the over-all mass balance equation:

$$\frac{\partial v}{\partial z} = -\frac{v}{\rho}\left(\frac{\partial \rho}{\partial z}\right) \tag{6.3}$$

Since ρ depends on the monomer concentration, $C_M(z, t)$, and the temperature of the reaction mass, $T(z, t)$, its variation with respect to the axial position, z, is given by

$$\frac{\partial \rho}{\partial z} = \frac{\partial \rho}{\partial T}\frac{\partial T}{\partial z} + \frac{\partial \rho}{\partial C_M}\frac{\partial C_M}{\partial z} \tag{6.4}$$

The pressure at the axial location, z, and time, t, is computed using the following equation in fluid-mechanics

$$\frac{\partial P}{\partial z} = -10^{-6}\left(\frac{2 f_r \rho v^2}{D_{int}} + \rho v \frac{\partial v}{\partial z}\right) \tag{6.5}$$

There are a total of twenty five partial differential equations (PDEs) in the dynamic model. The model also contains fifteen algebraic equations given in Agrawal et al. (2006) (Equations T2-1 to T2-15). The initial conditions (at $t = 0$) and the boundary conditions (at $z = 0$) are given by:

$$\left\{\begin{array}{l} C_j(t=0,\, z) = C_j^{SS}(z) \\ T(t=0,\, z) = T^{SS}(z) \\ \rho(t=0,\, z) = \rho^{SS}(z) \\ v(t=0,\, z) = v^{SS}(z) \\ P(t=0,\, z) = P^{SS}(z) \end{array}\right\} 0 \le z \le L \tag{6.6}$$

$$\begin{Bmatrix} C_j(t,\ z=0) = C_{j,\text{in}}(t) \\ T(t,\ z=0) = T_{\text{in}}(t) \\ \rho(t,\ z=0) = \rho_{\text{in}}(t) \\ v(t,\ z=0) = v_{\text{in}}(t) \\ P(t,\ z=0) = P_{\text{in}}(t) \end{Bmatrix} \tag{6.7}$$

The quantities, C_j^{SS}, T^{SS}, etc., in Equation (6.6) are the steady-state (SS) profiles that can be obtained using the steady-state model of Agrawal et al. (2006). It is assumed that the tubular reactor is operating at steady-state for $t \leq 0$, and that changes in the operating conditions are introduced from $t = 0$.

The PDEs describing the homogeneous reaction mixture in the tubular reactor are converted into ordinary differential equations (ODEs) using the finite difference method (method of lines; Gupta, 1995) using equally spaced grid points. The PDEs are discretized in time, t, using the backward finite difference technique, with an accuracy of O(z). The resulting coupled non-linear ODEs (in z) are integrated using the D02EJF subroutine in the NAG library. This subroutine uses Gear's technique for integrating the stiff equations. A tolerance (TOL) of 10^{-5} is used for solving the ODEs. The discretization in t (instead of the commonly used space variable, z) is chosen in this work so as to decrease the computational time for each simulation, enabling the model to be used for optimization. Note that a typical LDPE tubular reactor is very long (more than 1000 m) and has several zones, whereas the grade-change time is small (~ 5 minutes). To obtain the steady-state profiles for the state variables [C_j^{SS}, T^{SS}, etc., in Equation (6.6)], the steady-state model of Agrawal et al. (2006) is coupled with the dynamic model. Owing to the discretization in t, values of the state variables, $\boldsymbol{x}$, are needed at the feed end ($z = 0$) at different times. These values, $\boldsymbol{x}$ (t, $z = 0$), are the same as those at $t = 0$ and $z = 0$, i.e., $\boldsymbol{x}$ ($t = 0$, $z = 0$) until step changes are introduced. Thereafter, they are given by the boundary conditions [Equation (6.7);

step inputs]. Then, the integration of the ODEs in z (as the independent variable) will produce profiles (function of the axial length) of the state variables at different times.

Table 6.1 Design and operating conditions of the industrial LDPE tubular reactor studied (Asteasuain et al., 2001b; Agrawal et al., 2006)

Quantities	Numerical values
Total reactor length, L_t	1390 m
Inside diameter of reactor, D_{int}	0.05 m
Wall thickness of reactor	0.0254 m
Number of zones, N_z	5
Inner diameter of outer (jacket) wall, D_{Ji}	0.2032 m
Axial lengths of zones, L_{zm}, $m = 1, \ldots, 5$	60, 100, 180, 510, 540 m
Specific heat of reaction mixture, C_{Pm}, $m = 1, \ldots, 5$	2.428, 2.428, 3.140, 3.1401, 4.019 kJ/kg-K
Initial conditions for moments, λ_{np}, μ_{np}; $n = 0, 1$; $p = 0, 1, 2$	0.0 kmol/m^3
Flow rate of monomer, F_M	11 kg/s
Flow rate of inert, F_{inert}	0.22 kg/s
Flow rates of jacket fluids, V_{Jm}, $m = 2, \ldots, 5$	4.03×10^{-3}, 3.94×10^{-3}, 3.32×10^{-3}, 0.26×10^{-3} m^3/s

The computer code for solving the differential equations for the dynamic simulation of the LDPE reactor was written in FORTRAN 90. The computer code was run on an HP workstation (3.60 GHz and 3.25GB RAM). The CPU time required on this machine was nearly 8.5 min for a typical dynamic simulation run using a time step of 0.2 min (referred to as $\Delta t_{0.2}$) and $t_f = 8$ min. This workstation can perform 325 MFlops according to the LINPACK program (available at http://www.netlib.org) for a matrix of order 500 × 500. The code was tested by solving the dynamic model with no perturbations and comparing the final results with those obtained from the SS code of Agrawal et al. (2006). The two sets of results were found to match exactly. Thereafter, a perturbation (step change) was introduced in *one* of the operating variables in the dynamic model and the differential equations were solved until the final SS was attained. The results generated at large values of t from the dynamic code matched those generated from the SS code under corresponding conditions.

The step size, Δt, for discretization the time, t, is selected carefully such that transient responses of acceptable accuracy are obtained within reasonable computational times. For this, step changes were introduced in four operation variables simultaneously: the solvent flow rate, F_S, the flow rates, $F_{I,1}$ and $F_{I,2}$, of both the initiators and the inlet pressure, P_{in}. The initial operating conditions used were those given in Table 6.2 for the initial grade, and the values of the above four variables were changed later to the values corresponding to the final grade in Table 6.2. The time dependence of the temperature, number average molecular weight, monomer conversion and the normalized side-product content at the reactor exit (T_{exit}, $M_{n,exit}$, $X_{M,exit}$ and NSP_{exit}) are shown in Figure 6.1 for several different values of Δt: 1.0, 0.5, 0.2, 0.1 and 0.05 min. NSP_{exit} is calculated using $\left(\frac{C_{M_e,exit}}{30} + \frac{C_{V_i,exit}}{0.1} + \frac{C_{V_{id},exit}}{0.7} \right)$. The final steady states for these values of Δt are reached in 12, 10, 8, 5 and 3 min, respectively, and the corresponding CPU times are 0.5, 1.5, 8.5, 16.5 and 30 min. These data show that simulations with higher step sizes, for instance, 1 min and 0.5 min (Δt_1 and $\Delta t_{0.5}$), took the least CPU time to reach the final SS. But, these results do not show all the dynamic characteristics shown by simulations using $\Delta t_{0.2}$, $\Delta t_{0.1}$ and $\Delta t_{0.05}$, as shown in Figure 6.1b for $X_{M,f}$. Though results obtained using $\Delta t_{0.05}$ show the best dynamic results, the CPU time is exorbitant, and so such a small step size is not practical for multi-objective optimization which requires numerous simulations of the dynamic model. Hence, $\Delta t_{0.2}$, which produces results close to those generated using $\Delta t_{0.05}$, is chosen for subsequent simulations and optimization.

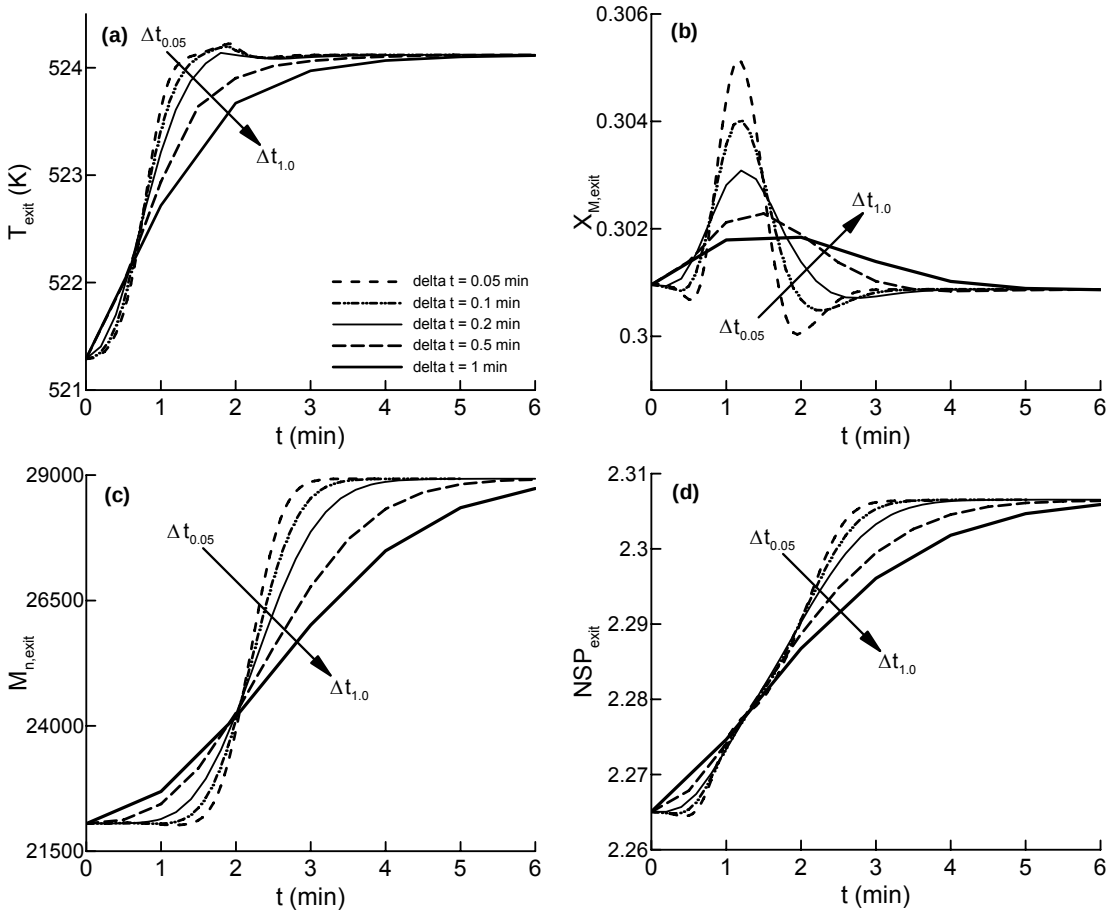

Figure 6.1 Effect of step size on the histories of the values at the exit of the reactor: (a) temperature (T_{exit}), (b) monomer conversion ($X_{M,exit}$), (c) number-average molecular weight ($M_{n,exit}$), and (d) normalized side products (NSP_{exit}) at the reactor exit

6.3 Effects of Changes in the Operation Variables

Having established a suitable value of Δt, we now generate results for step changes in the operation variables. The changes are carried out one by one. First, the solvent flow rate, F_S, is changed from 0.13 kg/s to 0.049 kg/s as a step. The variation of the concentration, C_S, of the solvent along the axis of the reactor is shown in Figure 6.2a for different times. The decrease of the solvent concentration at the reactor exit with time is shown in Figure 6.2b. The solvent is used in the feed to control the propagation of the chains. Therefore, it affects $M_n(z, t)$ as well as $M_{n,exit}(t)$, as observed in Figures 6.2c and d.

The flow rate, $F_{I,1}$, of initiator 1 is decreased (alone) next from 2.23×10^{-3} kg/s to 1.7×10^{-3} kg/s. This initiator is introduced in the third zone (the propagation reaction is highly exothermic and the temperature peaks in the third zone) where it decomposes into free-radicals which react with the monomer present at that point. When the quantity of initiator is decreased, the temperature peak is lowered from 590.2 to 589.4 K and shifts towards the end of the reactor (from z = 305 to 320 m). These results are not shown here but are available from the authors. On the contrary, the temperature peak becomes steeper on increasing $F_{I,2}$ from 6.8×10^{-5} kg/s to 8.2×10^{-5} kg/s, as shown in Figure 6.3a. Similarly, T and X_M at the reactor exit increase as shown in Figures 6.3b and c, whereas M_n remains unaffected (not shown). Similar effects are observed when P_{in} is increased from 183.11 MPa to 187.53 MPa. These results are not shown here for the sake of brevity but can be provided on request.

In any industrial plant, changes in more than one variable can occur simultaneously. This complex problem is studied next. Step changes in F_S, $F_{I,1}$, $F_{I,2}$ and P_{in} are introduced simultaneously, with values as mentioned in the earlier cases. The transient behaviors of M_n, X_M and T at the reactor exit have already been shown in Figure 6.1. The profiles of X_M and M_n along the reactor axis at different times are plotted in Figures 6.4a and 6.4b. The effect of a decrease in F_S is observed in Figure 6.4b where M_n starts increasing as soon as the solvent concentration is lowered and a sudden dip in M_n is seen at the point of injection of the first initiator in the third zone. This is due to the generation of free-radicals. Similarly, the monomer conversion at the reactor exit first increases due to the sudden increase in $F_{I,2}$ and then decreases to account for the reduction in $F_{I,1}$.

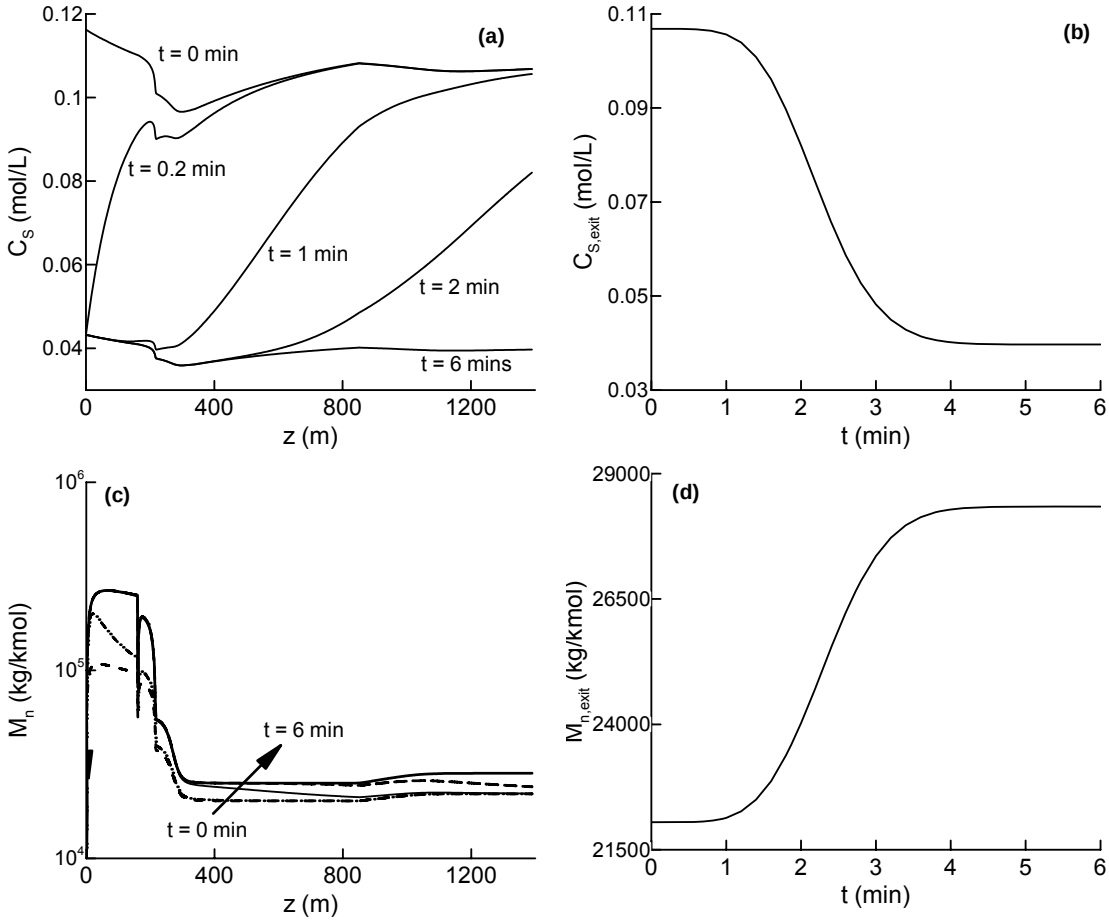

Figure 6.2 Transient profiles for a step decrease in F_S alone: (a) variation of the solvent concentration along the reactor axis at different times, (b) variation of the solvent concentration at the reactor exit, (c) variation of M_n along the reactor axis at different times, and (d) variation of M_n at the reactor exit

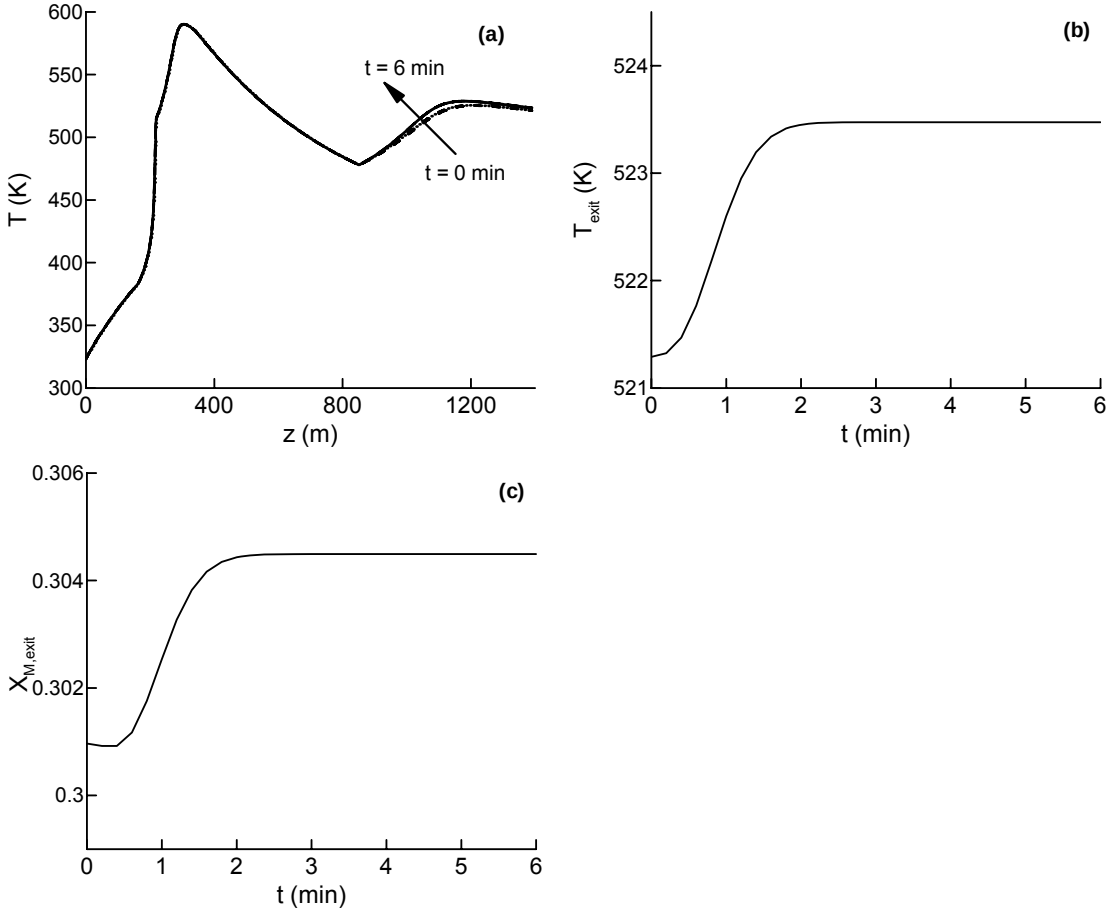

Figure 6.3 Transient data for a step increase in $F_{I,2}$: (a) variation of T along the reactor axis at different times, (b) T_{exit}, and (c) $X_{M,exit}$

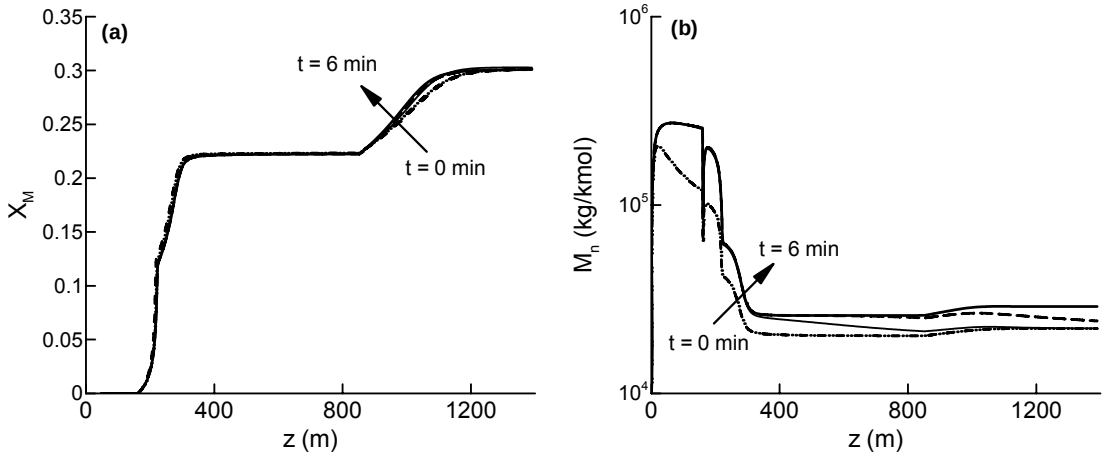

Figure 6.4 Transient profiles of (a) X_M and (b) M_n along the reactor axis, for simultaneous step changes in F_S, $F_{I,1}$, P_{in}, and $F_{I,2}$

6.4 Optimal Grade-change for LDPE Tubular Reactor

6.4.1 Formulation

Optimal grade-change of polymers in a polymer plant is an important issue. During grade change, off-spec product is produced which leads to a loss of revenue. Thus, changes in the polymer grade should be made with the minimum amount of off-spec material being produced, as also in as short a grade-change time as possible. It is expected that the minimization of the grade-change time would simultaneously minimize the amount of off-spec products. The grade of the polymer is typically characterized by several physical properties of the product, namely, the average molecular weight, density, melt-index, etc. In this study, the molecular variables that represent these physical properties, the number-average molecular weight, M_n, and the normalized side products, *NSP*, etc., are used for characterizing the off-spec product during the grade change period. The integral of the squared deviations/errors (ISE) of $M_{n,exit}$ and NSP_{exit} from their desired values over the grade-change period can be used as objective functions. The minimization of these objective functions not only ensure the specs on the polymer quality but also minimizes the grade-change period, t_f, since the latter is treated as an additional optimization variable (Chatzidoukas et al., 2003). Padhiyar et al. (2006) and Asteasuain et al. (2006) also used the deviation of M_n for optimizing the grade-change period. Chatzidoukas et al. (2003) used an objective function in terms of the squared deviation of the polymer density and the melt index from their corresponding desired values. These two properties were related to M_n through empirical correlations.

The SS model of Agrawal et al. (2006) was first used to obtain the optimal operating conditions at steady state, both before and after grade-change. Two objective functions were considered: the monomer conversion, $X_{M,exit}$, was maximized

and the normalized side product concentration was minimized, both at the exit of the reactor. These were carried out for two different desired values of $M_{n,exit}$, 21900 kg/kmol (initial grade, A) and 29000 kg/kmol (final grade, B). These runs provide information on the manipulated (decision) variables to be used for optimization of the grade-change problem. The product specifications and the steady-state operating conditions for grades A and B are reported in Table 6.2. The *NSP* for these two grades are 2.265 and 2.307, respectively. It should be mentioned that soft constraints (Agrawal et al., 2006) on $M_{n,exit}$, with a 1 % variation around the desired value permitted, were used to obtain the Pareto-optimal solutions and so the values of $M_{n,exit}$ given in Table 6.2 are very slightly different from the desired values.

The Pareto optimal solutions and the associated decision variables for these two grades of LDPE are shown in Figures 6.5 and 6.6. Chromosomes 'a' and 'b' (Figures 6.5a and 6.6a) are selected for grade-change optimization. These have the same values of the monomer conversion. After comparing Figures 6.5 and 6.6, seven of the eleven decision variables (F_S, $F_{I,1}$, $F_{I,2}$, $T_{J,1}$, $T_{J,2}$, $T_{J,3}$ and P_{in}) were found to be different in the two steady-state optimizations, corresponding to grades A and B (Table 6.2). However, $T_{J,1} - T_{J,3}$ do not differ much and also do not affect the Pareto optimal set significantly. This was also confirmed, when plots of Pareto optimal results for two other polymer grades ($M_{n,exit}$ = 16000 kg/kmol and $M_{n,exit}$ = 25000 kg/kmol) were compared with that for grade A. These results are not presented here but can be presented on request. Therefore, $T_{J,1} - T_{J,3}$ can be eliminated from the set of decision variables so as to reduce the complexity of the dynamic optimization problem. Steady-state optimization, using only four decision variables (F_S, $F_{I,1}$, $F_{I,2}$, P_{in}) for $M_{n,exit}$ = 29000 kg/kmol, and with the remaining decision variables kept constant at their optimal values corresponding to grade A, produced Pareto optimal solutions for

grade B that were quite similar to those obtained with eleven decision variables. Hence, only the five decision variables, F_S, $F_{I,1}$, $F_{I,2}$, P_{in} and t_f, are used for the optimal grade-change problem.

The first four decision variables, F_S, $F_{I,1}$, $F_{I,2}$, and P_{in}, are changed *continuously* with time, over $0 \le t \le t_f$ (where $t = 0$ is the beginning of the grade change operation and t_f is the end). The starting values of each of the four decision variables at $t = 0$ are those corresponding to grade A, while the values at t_f and thereafter are those for grade B. To simplify the problem, however, each of these four decision variables, ξ_i, are represented by two discrete (intermediate) values, $\xi_{i,j}$, at times, $t_{i,j}$ (i^{th} decision variable at the j^{th} time; j = 1 and 2), with a ramp function connecting these discrete points. Thus, the continuous functions are represented by a set of three ramps over three intervals, $\Delta t_{i,j}$; (j = 1, 2, 3), used for discretization of the i^{th} decision variable (hence, $t_{i,0} = 0;\ t_{i,k} = \sum_{j=1}^{k} \Delta t_{i,j};\ k = 1,2;\ t_{i,3} = t_f = \sum_{j=1}^{3} \Delta t_{i,j}$). This is done to keep the algorithm simple.

The mathematical formulation of the MOO grade-change problem is as follows:

$$J_1[F_S(t), F_{I,1}(t), F_{I,2}(t), P_{in}(t), t_f] = \int_0^6 \left(\frac{M_{n,exit}(t) - M_{n,exit(f)}}{M_{n,exit(0)} - M_{n,exit(f)}} \right)^2 dt \tag{6.8a}$$

$$J_2[F_S(t), F_{I,1}(t), F_{I,2}(t), P_{in}(t), t_f] = \int_0^6 \left(\frac{NSP_{exit}(t) - NSP_{exit(f)}}{NSP_{exit(0)} - NSP_{exit(f)}} \right)^2 dt \tag{6.8b}$$

subject to

$$0.02 \le F_S(t) \le 0.5 \text{ kg/s} \tag{6.8c}$$

$$5 \times 10^{-5} \le F_{I,1}(t) \le 5 \times 10^{-3} \text{ kg/s} \tag{6.8d}$$

$$5 \times 10^{-5} \le F_{I,2}(t) \le 5 \times 10^{-3} \text{ kg/s} \tag{6.8e}$$

$$182.39 \le P_{in}(t) \le 248.25 \text{ MPa} \tag{6.8f}$$

$$0.4 \le t_f \le 3 \text{ min} \tag{6.8g}$$

$0.2 \le \Delta t_{i,j} \le 2.6$ min ; $i = 1, 2, 3, 4; j = 1, 2$ (6.8h)

$T_{max}(z, t) \le 610.15$ K (6.8i)

$M_{n,exit}(t) \ge 22050 - 200$ kg/kmol (6.8j)

$M_{n,exit}(t) \le 28970 + 200$ kg/kmol (6.8k)

Model equations (6.8l)

In Equations (6.8a) and (6.8b), subscripts '0' and 'f' represent the values of $M_{n,exit}$ and NSP_{exit} at the initial and final times of the grade change-over. The bounds of the decision variables have been chosen based on information in the literature (Asteasuain et al., 2001b; Brandolin et al., 1988; Agrawal et al., 2007).

It may be emphasized that even though the decision variables have been indicated as continuous *functions* of t in Equation (6.8), only the set of discretized values, $\xi_{i,j}$ ($i = 1, \ldots, 4; j = 1, 2$) and $\Delta t_{i,j}$ ($i = 1, \ldots, 4; j = 1, 2$) are *actually* to be used. Note that the values of $\xi_{i,j}$ at $t = 0$ and $t = t_f$ are fixed at the initial and final SS values and so cannot be used for optimization. The third discretization interval, $\Delta t_{i,3}$ for each decision variable is *calculated* using $\Delta t_{i,3} = t_f - \Delta t_{i,1} - \Delta t_{i,2}$. The lower bound on $\Delta t_{i,j}$ is decided based on the integration step size of 0.2 min used in the dynamic model, while the upper bound (Equation 6.8h) is selected so as to allow two additional intervals, each of 0.2 min, before t_f. The ramp trial function for the parameterization of a typical decision variable, say, $F_S(t)$, is shown in Figure 6.7. Two values (referred to as the amplitudes), $F_{S,1}$ and $F_{S,2}$, and two 'discretization' intervals, $\Delta t_{1,1}$ and $\Delta t_{1,2}$, (and t_f, it being a decision variable, too) are used to define the solvent flow rate as a function of time. Thus, there are a total of 17 (including t_f) decision variables for the dynamic optimization problem. The upper bound on t_f is chosen as 3 min (Cervantes et al., 2000). However, the upper bound (horizon of the dependent variables) on the two integrals in Equations (6.8a and 6.8b) is taken to be larger (= 6 min) than t_f

(horizon of the decision variables), so that the final optimal steady state is attained after the introduction of the inputs. A local constraint is imposed on the reaction mass temperature to ensure safety (Equation 6. 8i). The inequality constraints on $M_{n,exit}(t)$ (Equations 6.8j and 6.8k) are imposed to avoid undershoot and overshoot. The constraints (Equations 6.8i – 6.8k) are handled using the constrained dominance principle (Deb et al., 2001; Agrawal et al., 2007). Chromosomes with the computed value of $\Delta t_{i,3} < 0$ are not passed on to the dynamic model so as to save computational time, and the values of their objective functions are assigned very low values (-1.0×10^{12}) so that they are killed in subsequent generations.

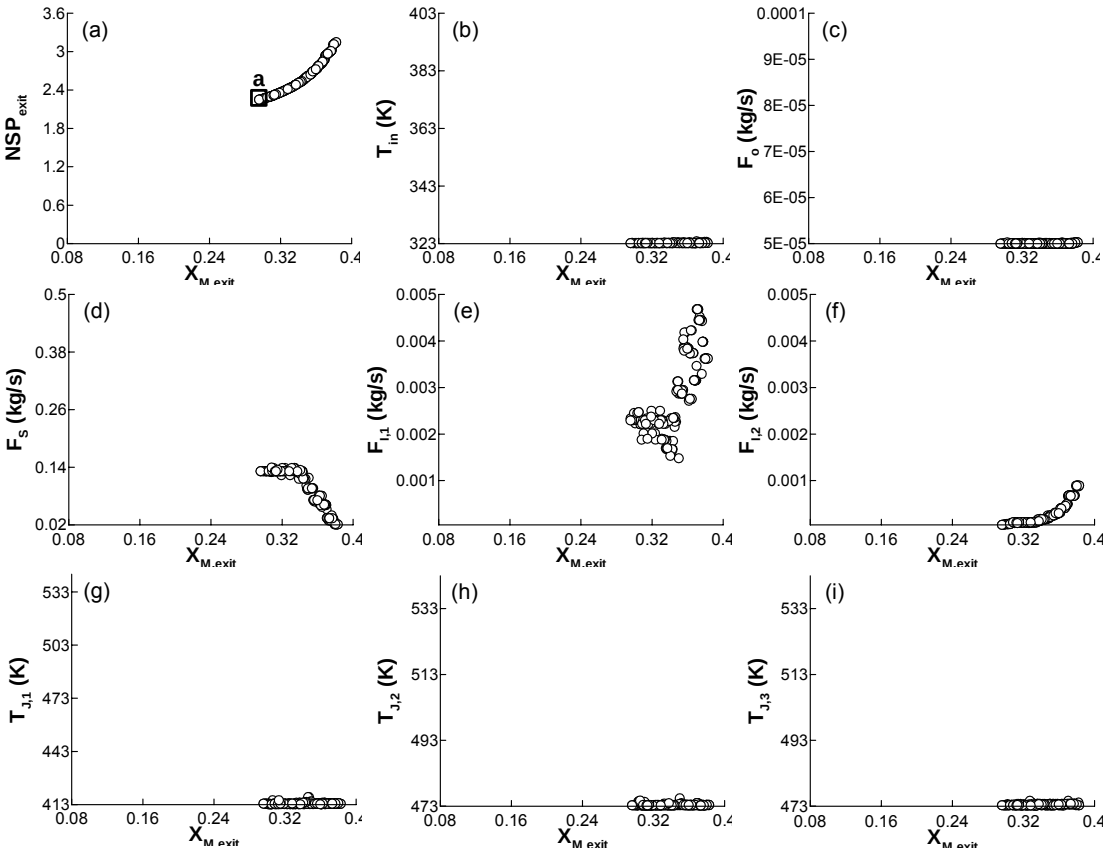

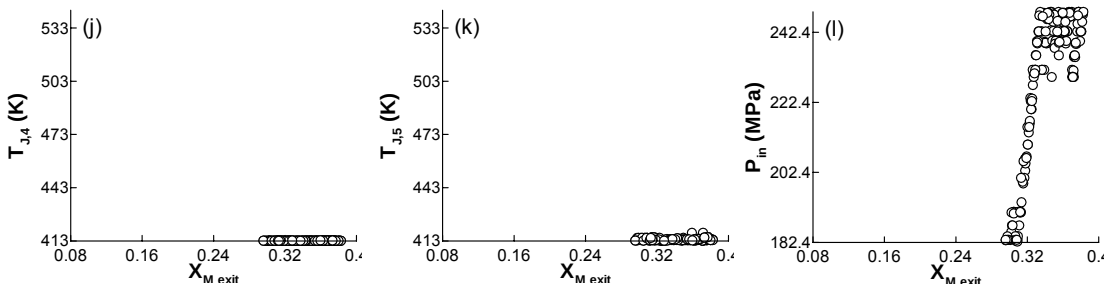

Figure 6.5 Pareto optimal solutions and the corresponding decision variables for the initial grade, A ($M_{n,exit}$ = 21900 ± 200 kg/kmol) using NSGA-II-aJG

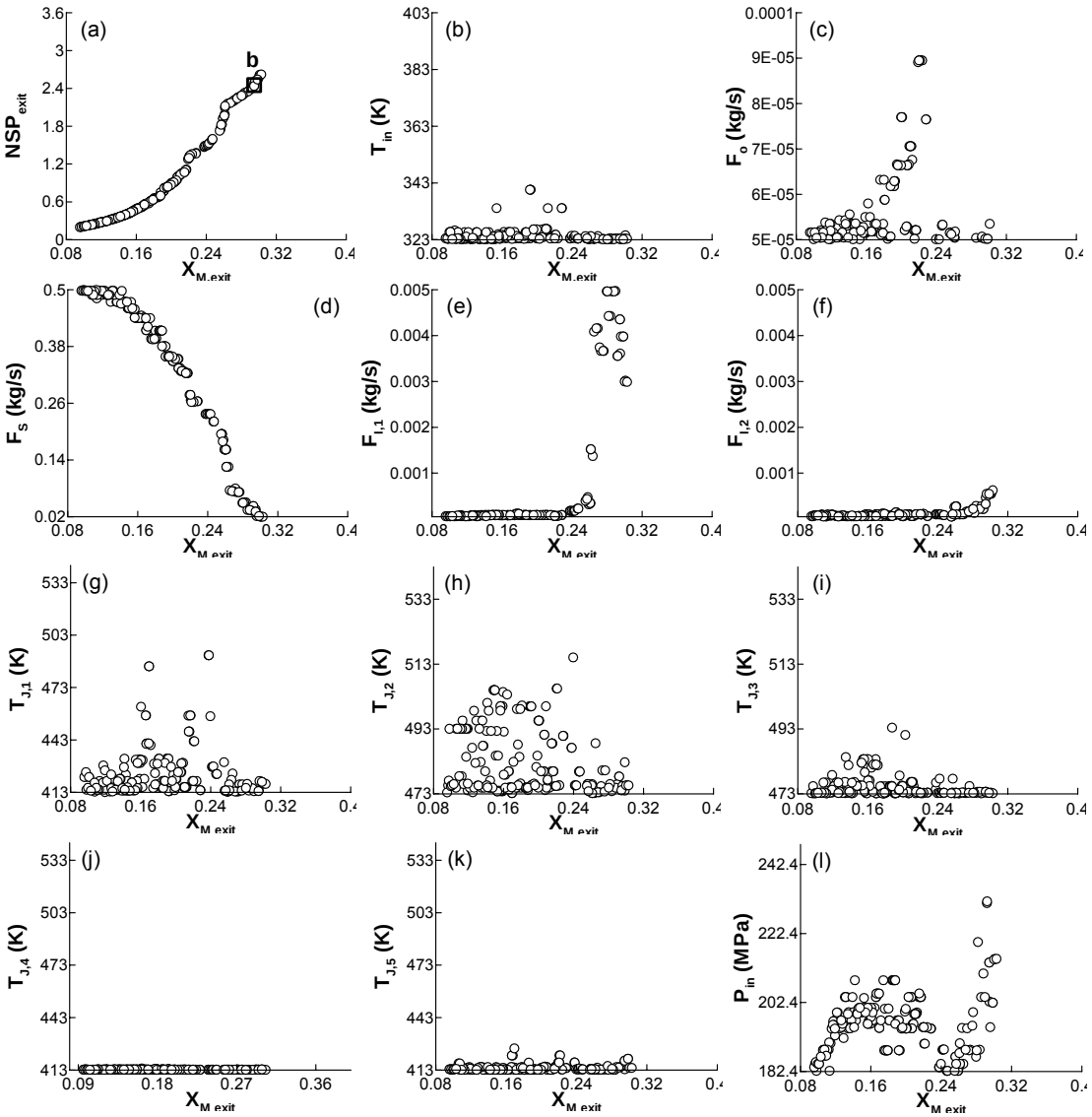

Figure 6.6 Pareto optimal solutions and the corresponding decision variables for the final grade, B ($M_{n,exit}$ = 29000 ± 300 kg/kmol) using NSGA-II-aJG

Table 6.2 Steady-state operating conditions and product specifications for the initial (A) and final (B) grades

Operating conditions	Initial: Grade A	Final: Grade B
T_{in} (K)	323.20	323.20
F_o (kg/s)	5×10^{-5}	5×10^{-5}
F_S (kg/s)	0.1319	0.049
$F_{I,1}$ (kg/s)	2.23×10^{-3}	1.7×10^{-3}
$F_{I,2}$ (kg/s)	6.8×10^{-5}	8.2×10^{-5}
$T_{J,1}$ (K)	413.25	413.48
$T_{J,2}$ (K)	473.36	473.36
$T_{J,3}$ (K)	473.27	473.19
$T_{J,4}$ (K)	413.19	413.16
$T_{J,5}$ (K)	414.47	413.41
P_{in} (MPa)	183.11	187.53
Product Specifications		
$M_{n,exit}$ (kg/kmol)	22050	28970
$X_{M,exit}$	0.30096	0.30009
NSP_{exit}	2.265	2.307

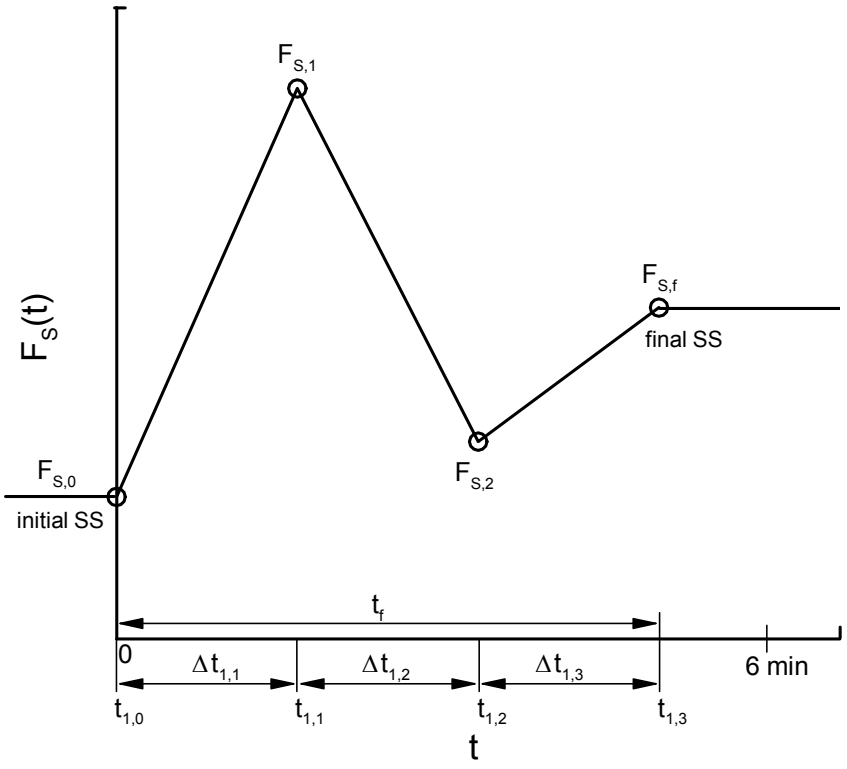

Figure 6.7 Ramp trial function for the discretization of the decision variable, $F_S(t)$

6.4.2 Results and Discussion

The MOO problem described above is solved using the binary-coded NSGA-II-aJG (Guria et al., 2005). The best values of the computational parameters in NSGA-II-aJG are obtained by trial and are given in Table 6.3. These values are the same as used in the design-stage MOO of the LDPE reactor using the constrained dominance principle, as reported in Agrawal et al. (2007). The CPU time on the HP workstation (3.60 GHz and 3.25 GB RAM) was about 200 hr for a typical optimization run with 50 chromosomes and for 250 generations (the CPU time for the first 200 generations is not accounted due to infeasible solutions; these are discussed later). Because of large computational time, it becomes difficult to run the optimization for more generations and/or chromosomes. Therefore, attainment of *reasonable* non-dominated solutions is considered to be satisfactory. Nandasana et al. (2003) also faced a similar problem of high computational times for the MOO of unsteady state operation of an industrial steam reformer.

It may be noted that the first *feasible* solution (chromosome) was obtained in the 205^{th} generation and all fifty chromosomes were feasible only in the 220^{th} generation. This occurs due to infeasible chromosomes associated with $\Delta t_{i,3} < 0$ for any of the decision variables. It may be noted that only one non-dominated solution ($J_1 = 3.21$, $J_2 = 1.86$) could be obtained in the 220^{th} generation while all others were dominated solutions. Values of the objective functions, J_1 and J_2, obtained using a step change in all four decision variables, $\xi_i(t)$, from their initial optimal SS values to their final SS values, starting right from $t = 0$, are obtained by solving the dynamic model. These integrals are found to be 1.86 and 1.22, respectively. These are shown as inverted filled triangle in Figure 6.8 and are non-optimal (note that optimal grade change involves continuous changes of the decision variables over time, rather than step

changes). Interestingly, these values are better than the results obtained with MOO in the 220th generation. This shows that optimization needs to be run for more generations.

Table 6.3 Values of the computational parameters used in the binary-coded NSGA-II-aJG for the two-objective dynamic optimization problem

Parameter	Values
N_{gen}	350
N_{pop}	50
l_{substr}	30
l_{chrom}	510
l_{aJG}	70
p_c	0.8
p_m	0.01
p_{JG}	0.3
S_r	0.1

Non-dominant solutions at four selected generations are shown in Figure 6.8. One objective, J_1, increases and the other, J_2, decreases as one goes from the left-most point in any generation to the right. Hence, the solutions in a generation are non-dominated. *Reasonable* convergence to the Pareto optimal set can be seen at about the 330th generation. The distribution (spread) of points in the Pareto optimal set could possibly be improved by solving for more generations and/or using more chromosomes, but excessive CPU times limits doing this. The Pareto optimal solutions show that smaller amounts of off-spec product (i.e., lower J_1) is obtained but at the cost of a higher value of the normalized side products in the polymer (i.e., higher J_2) during the grade-change. The non-dominated optimal solutions are better than and dominate over the single step-change policy (shown with a filled inverted triangle). This shows the usefulness of using MOO for this problem.

The histories of the two squared deviations used in the two objectives (not the values of the integrals) for chromosome C in Figure 6.8 (corresponding to a maximum

value of J_1 and a minimum value of J_2) over the grade-change period, are shown in Figures 6.9a and 6.9b, respectively. The integral of the squared deviation in the objective functions emphasizes considerably on the large errors at the beginning of the grade-change period. The relatively smaller deviations near the final steady state do not contribute much to the objective function, due to the squaring of the error. This can be seen in Figure 6.9a. The value of the square of the deviation in $M_{n,exit}$ approaches zero as soon as $M_{n,exit}$ increases to the proximity of the final steady-state value. Though $M_{n,exit}$ differs by 500 kg/kmol from the final steady-state value (Figure 6.9c), its contribution to the objective function, J_1 is negligible (Figure 6.9a). Similar comments are applicable for the squared deviations of NSP_{exit} (Figures 6.9b and 6.9d).

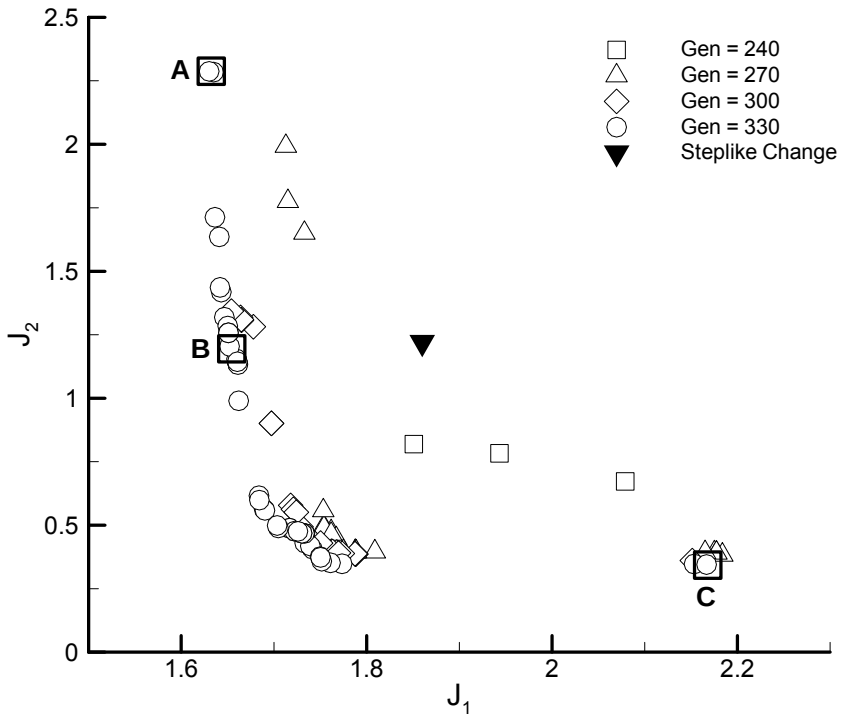

Figure 6.8 Non-dominated solutions for the 2-objective optimization problem in Equation (6.8) (ISE approach) using NSGA-II-aJG, at different number of generations

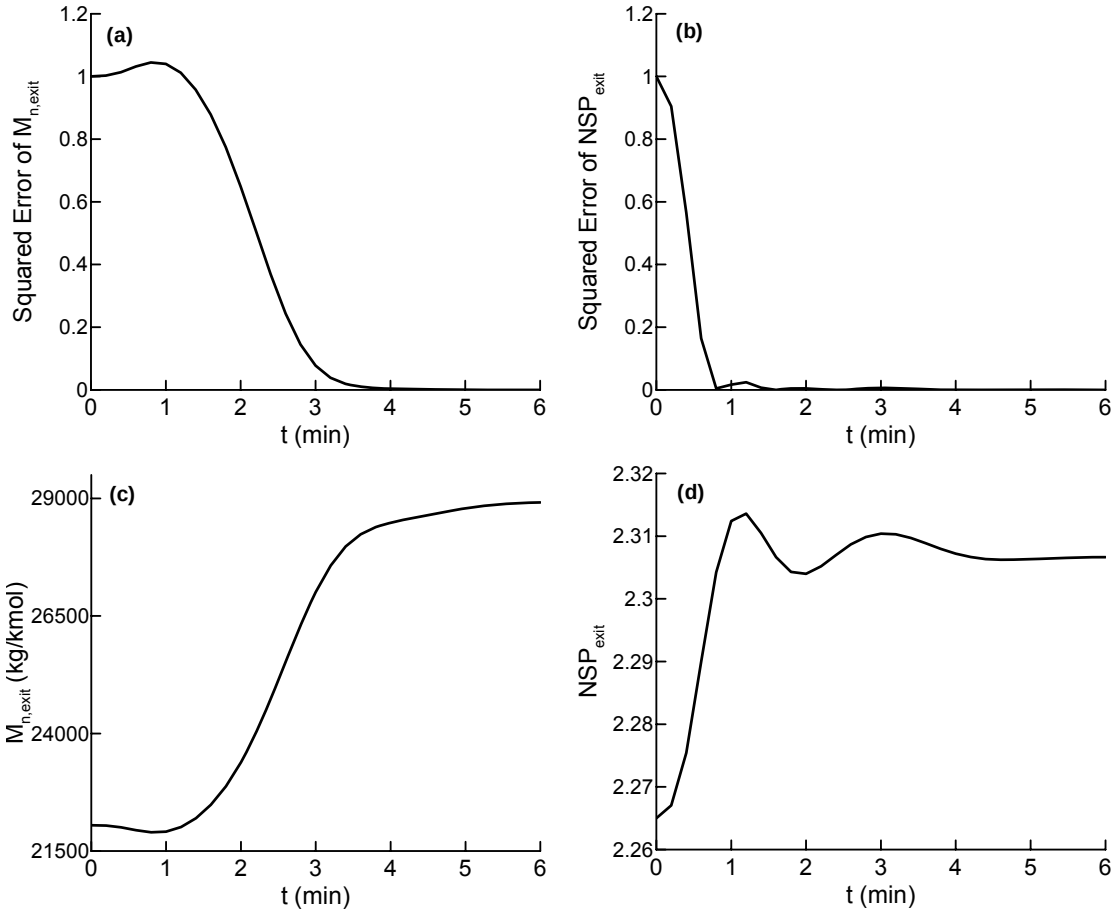

Figure 6.9 Histories of the squared errors of: (a) $M_{n,exit}$, (b) NSP_{exit}, and the optimal histories of: (c) $M_{n,exit}$, and (d) NSP_{exit}, over the grade-change period for chromosome C in Figure 6.8.

It is more important to emphasize deviations near the final steady state during grade-change. This can be achieved by using the integral of the product of time and the absolute error (ITAE) in the two objectives. The two objectives can then be defined as

$$I_1 = \int_0^6 t \left| \frac{M_{n,exit}(t) - M_{n,exit(f)}}{M_{n,exit(0)} - M_{n,exit(f)}} \right| dt \tag{6.9a}$$

$$I_2 = \int_0^6 t \left| \frac{NSP_{exit}(t) - NSP_{exit(f)}}{NSP_{exit(0)} - NSP_{exit(f)}} \right| dt \tag{6.9b}$$

The non-dominated solutions for the MOO problem using these objectives (along with Equations 6.8c – 6.8l), after the 250th, 280th and 310th generations, are shown in

Figure 6.10. The Pareto solutions occur at larger values of both the objective functions when compared to the results in Figure 6.8. Note that, as before, the first feasible chromosome was found only in the 202nd generation and all chromosomes in the population were found to be feasible only after 222 generations.

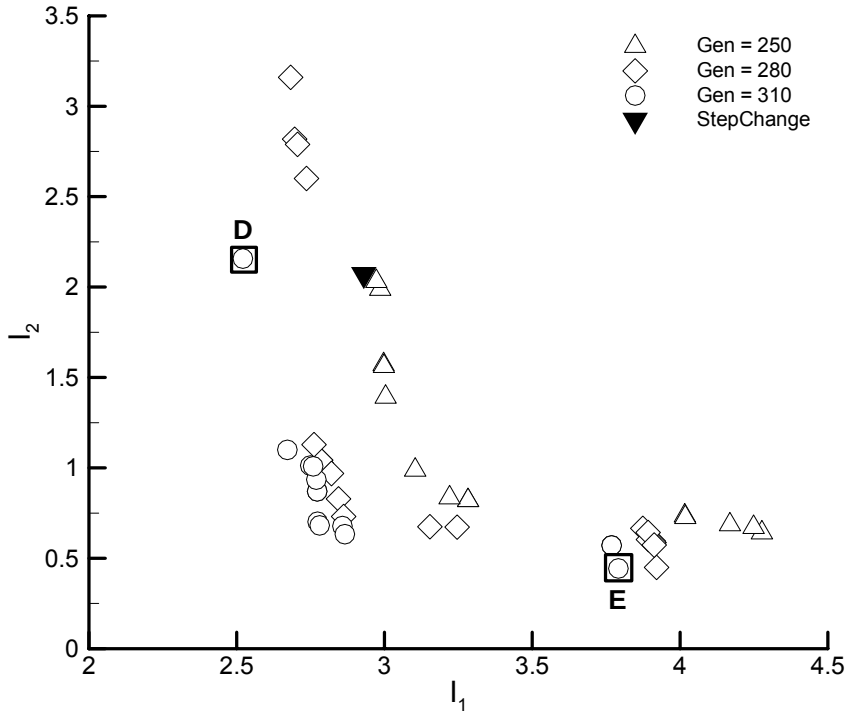

Figure 6.10 Non-dominated sets for the two objectives in Equation (6.9) (ITAE approach) using NSGA-II-aJG, at different number of generations

The histories of the product of the time and the absolute error (TAE) (used as the integrand in Equation 6.9) corresponding to the two objectives in Equation (6.9) for chromosomes D (I_1 is minimum, I_2 is maximum) and E (I_1 is maximum, I_2 is minimum), are plotted in Figures 6.11a and 6.11b, respectively. The corresponding histories of $M_{n,exit}$ and NSP_{exit} are also plotted in Figures 6.11c and 6.11d. It is evident from these plots that the TAE becomes zero only when $M_{n,exit}$ (or NSP_{exit}) becomes extremely close to the final steady-state value of the new grade. In the ITAE approach, polymer properties ($M_{n,exit}$ and NSP_{exit}) reach their new steady state quickly

(~ 3.2 min). On the other hand, in the ISE approach, errors near the final steady state are not penalized in the objectives, and the final steady state for the two attributes ($M_{n,exit}$ and NSP_{exit}) of the polymer is attained quite late (~ 5 min). Thus, it can be concluded that the ITAE approach (and not the use of the ISE) should be used in formulating the objectives for polymer grade-change so as to reach to the new grade quickly, with the least off-spec product produced during the grade-change period.

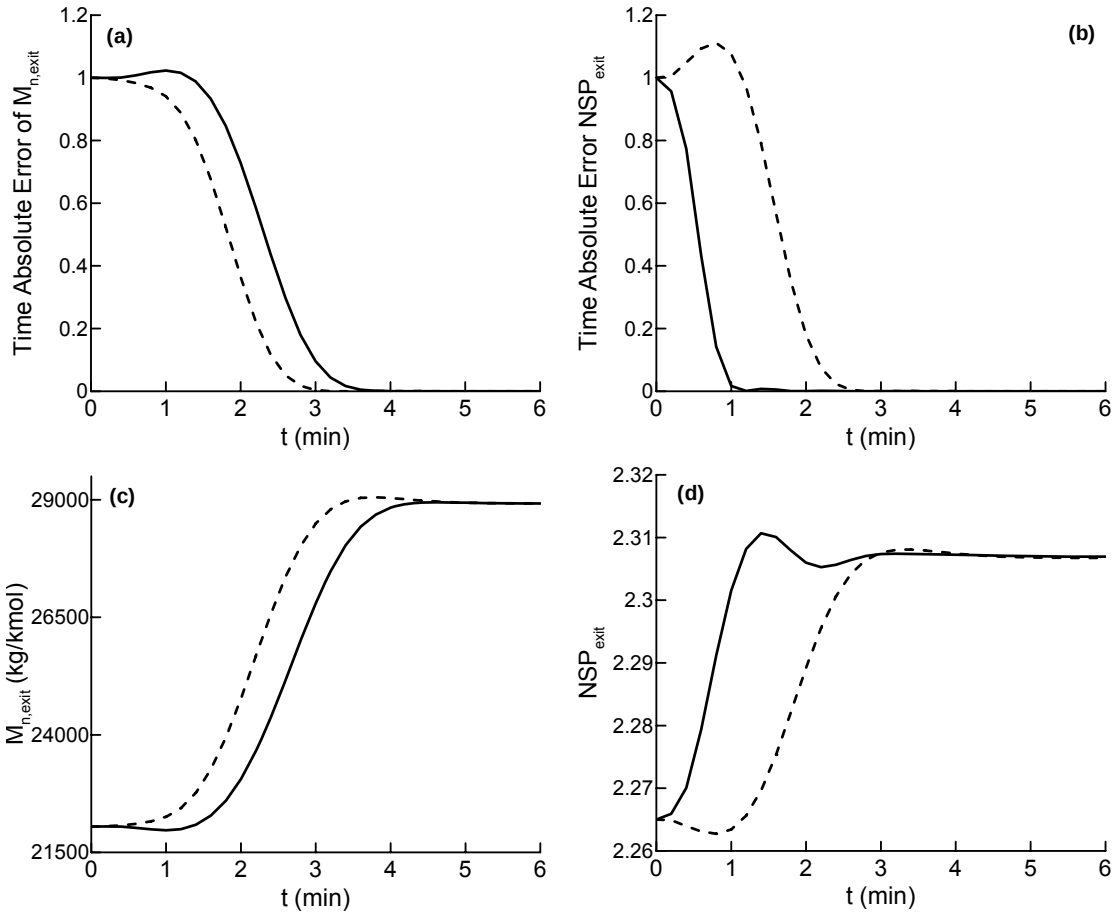

Figure 6.11 Histories of the product of the time and the absolute error (TAE) of: (a) $M_{n,exit}$, (b) NSP_{exit}, and the optimal histories of: (c) $M_{n,exit}$, and (d) NSP_{exit} over the grade-change period for chromosomes D (---) and E (—) in Figure 6.10

The history of the molecular weight of the product in Figure 6.11c shows that, initially, $M_{n,exit}$ remains unchanged till about 1.4 min and then it starts rising until about 4.2 min to reach a value within ±100 kg/kmol of the new grade of the polymer.

This causes the TAE for $M_{n,exit}$ to be quite high initially whereas NSP_{exit} rises quickly in about 1 min (see Figure 6.11d). Thus, I_2 equals the minimum value since NSP_{exit} does not show the same sluggish response initially as for $M_{n,exit}$. On the other hand, the history of NSP_{exit} for chromosome D (Figure 6.10; I_1 is minimum and I_2 is maximum) shows a sluggish nature at the start of the grade-change and large errors are accumulated in I_2 (Figure 6.11d). Thus, the objective function, I_2, attains a large value. The rise time for the molecular weight plot is ~ 3.2 min and the new steady-state is attained quickly, as shown in Figure 6.11c.

Plots of the decision variables for chromosomes D and E are shown in Figure 6.12. As can be seen from the points in these plots, the discretization time intervals are different for each decision variable. The optimal 'recipes' generated by NSGA-II-aJG using the ITAE approach involve large changes at the beginning of the grade-change period. The plots of the decision variables for chromosome E are now discussed. Figure 6.12a shows that the optimal F_S first decreases to close to its lower bound in the first discretization interval ($\Delta t_{1,1}$ ~ 1 min) so that the value of $M_{n,exit}$ comes close to that for the new grade. But, decrease in the solvent concentration also leads to higher monomer conversion. So, to retain the same level of the monomer conversion, the amount of the first initiator, $F_{I,1}$, decreases during this time ($\Delta t_{2,1}$ ~ 1 min; see Figure 6.12b). However, $F_{I,2}$ increases sharply (Figure 6.12c) in this interval ($\Delta t_{3,1}$ ~ only 0.3 min, different from 1 min). This generates more free radicals in the reaction mixture to increase the monomer conversion at the end of the reactor. The increase in the monomer conversion also corresponds to higher values of NSP_{exit} (Agrawal et al., 2006). Also, increase in the inlet pressure helps in lowering the SCB, vinyl, and vinylidene group concentrations and therefore the value of NSP_{exit} (Ehrlich and Mortimer, 1970; Agrawal et al., 2006). Hence, the inlet pressure, P_{in}, also

increases sharply almost in the same discretization interval ($\Delta t_{4,1}$ ~ 0.3 min), so as to keep the concentrations of the side products in check, as shown in Figure 6.12d. Similarly, the amplitudes and the discretization intervals for the decision variables occur optimally such that the amount of off-spec product is minimized. Results for chromosome D can be explained similarly.

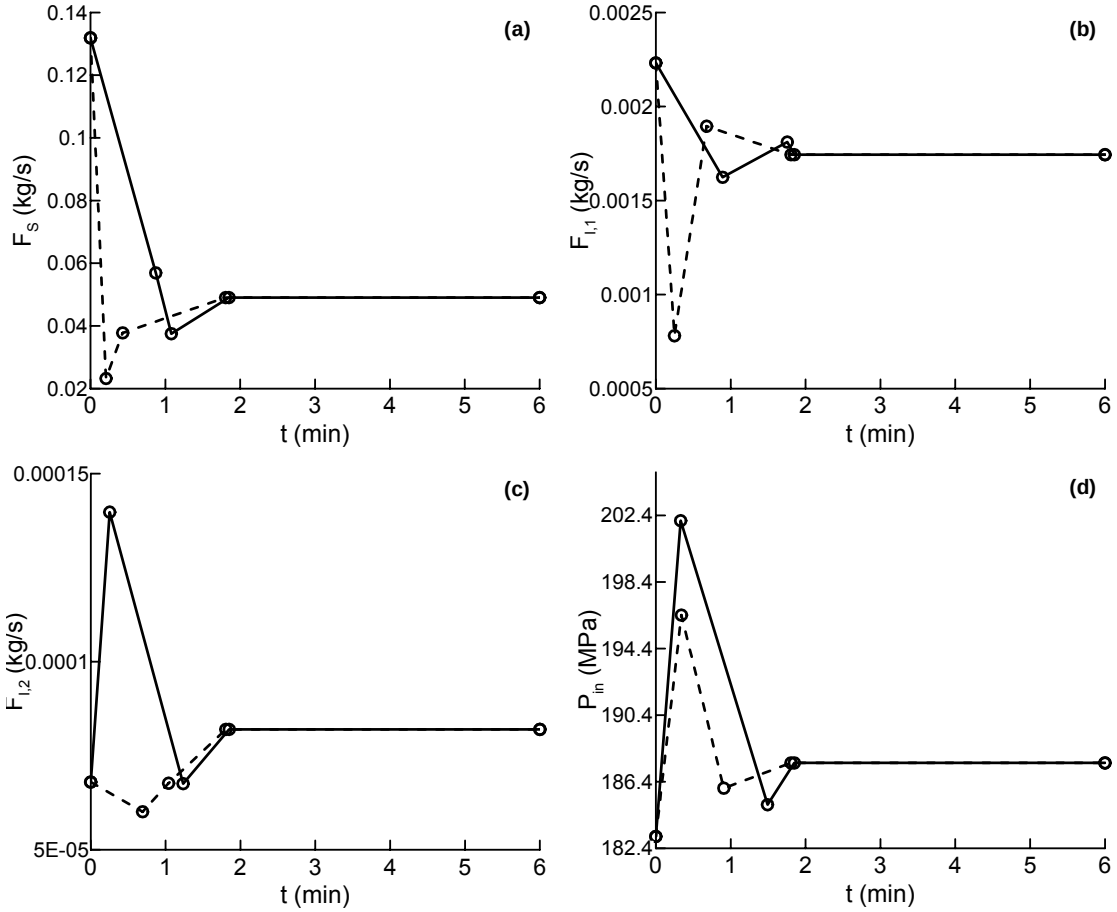

Figure 6.12 Optimal grade-change histories of the four decision variables for the MOO problem in Equation (6.9) (ITAE approach): flow rates of solvent (F_S), initiator 1 ($F_{I,1}$), and initiator 2 ($F_{I,2}$) and the inlet pressure (P_{in}) for chromosomes D (---) and E (—) in Figure 6.10

6.5 Conclusions

A comprehensive dynamic model for the production of LDPE in high-pressure tubular reactors is developed and validated by comparing its predictions with those of

the SS model. Complete details of the dynamic model are provided for use by other workers. The effects of changes in the operation variables are first studied. Thereafter, optimal 'recipes' for grade-change using two objective functions are obtained. The binary-coded NSGA-II-aJG is used for solving the multi-objective optimization problem. A set of Pareto optimal solutions is obtained. These provide several choices to the decision maker for grade-change in the LDPE reactor. Two approaches were used, one using the ISE and the other using the ITAE. The latter is better.

Chapter 7

Conclusions and Recommendations

7.1 Conclusions

The present work was on modeling, simulation and optimization of an industrial tubular reactor for LDPE production so as to improve its overall performance. Operation, design and grade-change optimization of an LDPE reactor for multiple objectives were successfully carried out using NSGA-II and its JG adaptations. The conclusions and contributions of this work are outlined in following paragraphs.

A comprehensive, steady-state model for LDPE production in high-pressure tubular reactors was developed. A review of available models in open literature showed inconsistency in the values of the rate constants (possibly due to different operating conditions) and/or unavailability of a few rate constant values (due to proprietary reasons). Hence, the steady-state model in our study was tuned using the reported industrial data (Asteasuain et al., 2001b). We assumed and provided reasonable values for all the missing information. Our model description and details are complete and useful for researchers (Chapter 4).

Thereafter, the developed model is used for operation optimization of the LDPE tubular reactor for the industrially important objectives: maximization of monomer conversion and minimization of normalized side products concentration (SCB and unsaturated products) in the product. The binary-coded NSGA-II and its JG adaptations were used to solve this constrained MOO problem for LDPE tubular reactor operation. The resulting Pareto-optimal solutions show that higher monomer conversions (close to 38%) can be achieved with almost similar concentrations of the side products of current industrial operation ($X_{M,f}$ = 30% for the actual operating

point). Thus, this study offers considerable scope for improving the operation of industrial LDPE reactors.

It was found that NSGA-II and its JG adaptations failed to converge to the global optimal solutions when an equality constraint on number-average molecular weight at reactor exit, $M_{n,f} = M_{n,d}$ kg/kmol, is placed. Thus, it was suggested that solutions of problems involving hard (equality) end-point constraints should be assembled by obtaining solutions of several MOO problems with softer constraints, rather than by solving the problem only once; otherwise, erroneous results could be obtained (Chapter 4). In addition, it was observed that the binary-coded NSGA-II-aJG and NSGA-II-JG performed better than NSGA-II near the hard end-point constraints. We also studied a four-objective problem (with each of the three normalized side product concentrations taken individually as objectives), and demonstrated that the resulting non-inferior solutions were comparable to those for the two-objective problem (Chapter 4).

Thereafter, optimal design of a LDPE tubular reactor for two objectives: maximization of monomer conversion and minimization of normalized side products concentration was investigated. This complex problem involved 22 decision variables and several constraints on average molecular weight, reactor temperature and jacket fluid velocities. Binary-coded NSGA-II, NSGA-II-JG, and NSGA-II-aJG could not converge to the correct global Pareto-optimal solutions for the case of equality constraint on $M_{n,f}$. However, for the near equality constraints, for instance, $M_{n,f} = M_{n,d} \pm 2$ kg/kmol, the Pareto-optimal solutions were obtained but these were limited to higher monomer conversion and required intensive computational time. Thus, solutions satisfying the above constraint were picked up from among the Pareto-optimal sets corresponding to several MOO problems with more relaxed bounds on

$M_{n,f}$. These solutions are spread over a wider range and can be obtained with less total CPU time. Also, NSGA-II-aJG and NSGA-II performed better than NSGA-II-JG in terms of convergence to and diversity of the Pareto-optimal sets for the near equality constraints (Chapter 5).

A three-objective optimization of the LDPE design problem, which included minimization of normalized compression power along with the earlier mentioned two objectives, was also solved using NSGA-II-aJG. The results show that the Pareto-optimal solutions for this problem were comparable to or better than those obtained by the two-objective optimization (Chapter 5).

In view of the difficulty in handling the equality constraint on molecular weight in the LDPE optimization, a systematic approach of constrained-dominance principle for handling the constraints was implemented and tested in the binary-coded NSGA-II-JG and NSGA-II-aJG for the first time (Chapter 3). This approach performed marginally better than the penalty function approach for these algorithms for handling the constraints in the LDPE design problem (Chapter 5).

Now, to optimize the frequent changes in polymer grades encountered in a LDPE plant, a comprehensive dynamic model for the reactor is developed (Chapter 6) and its complete details are provided. Thereafter, this model is used to find the optimal grade-transition policies for two objectives (namely, specifications on the quality of the product, M_n and the normalized concentration of the side-products in the exit stream) and in the presence of constraints. These profiles were presented and discussed. It was observed that the ISE approach is not sensitive to errors near to the steady-state of new grade whereas the ITAE approach penalizes these errors and is better. Hence, the optimal trajectories for grade transition should be obtained using the ITAE approach and to reach the final steady state quickly.

In this study, two conflicting objectives which are industrially important are identified for LDPE reactor optimization, and reactor performance is significantly improved using MOO. Thus, our study provides sufficient value addition to the research and scientific community. The lessons learnt from these optimizations include the ability of formulating the reactor optimization problems and solving them with complex multivariate optimization techniques such as binary-coded NSGA-II and its JG adaptations. The major constraint to be considered and dealt with is the heat generation since the polymerization is extremely exothermic and the reaction temperature is very high. These issues are discussed in the thesis. The vector optimization approach is never studied for optimizing this process system prior to our study. The quality and usefulness of this work are evident by our journal publications (Agrawal et al., 2006 and 2007).

7.2 Recommendations for Future Work

Based on experience gained and outcomes of the present work, several suggestions to further extend this work are outlined below.

A comprehensive dynamic model is presented in this work to study the dynamics of LDPE tubular reactor. It was limited to the tubular reactor only; however, scope of the model can be expanded by considering the associated down-stream units (high- and low pressure separators and primary- and hyper compressors typically found in the LDPE plant) and recycle of unconverted ethylene. It will then be useful to understand the plant-wide behavior including instabilities and multiple steady-states caused by recycles as observed by Hafele et al. (2006).

Grade-change, coupled with control strategies, can be carried out in two steps in any polyolefin industry. First, the optimal grade-change procedures are identified off-

line to obtain the decision variables. This is done using appropriate constraints on the input, output and state variables of the process, and a good dynamic model. In the second step the optimal solutions are implemented using properly designed (values of their parameters) feed-forward and feed-back controllers (Chatzidoukas et al., 2003). This study focuses on the first aspect where optimal grade-change trajectories are obtained using off-line optimization. The second step of implementing the optimal solutions should be investigated, possibly for multiple objectives to maintain the process within a safe operating envelope and to ensure rejection of disturbances, if any, during the transition. Furthermore, for ensuring the optimality of the selected control structure, the transition policy and control configuration should be optimized simultaneously, and not sequentially.

In the MOO of LDPE tubular reactors, when number-average molecular weight is constrained to lie exactly at the desired value, global optimal solutions could not obtained using the NSGA-II and its JG adaptations. Thus, it poses a challenging problem to the research community to work on new MOO algorithms and constraint handling techniques. Also, the gray-coding can be implemented instead of binary-coding in these algorithms to check the improvements. In gray-coding, the usual binary string is converted into an equivalent sequence of 1's and 0's, and it has the unique property of representing any two neighboring integers in the gray space by the difference of one bit only (Chakraborti, 2004). Caruana and Schaffer (1988) and Schaffer et al. (1989) showed empirically that gray encoding usually performs better than binary encoding for some cases.

During MOO, some chromosomes were generated for which the simulation of tubular reactor model was taking excessive time due to stiffness of model equations. Thus, the limits of decision variables (for instance, solvent flow rate, F_S) were

shortened to speed up the optimization. However, these solutions could be of importance considering the failure of NSGA-II and its JG adaptations for the equality constraints and therefore it is recommended that these solutions should be studied for the reactor performance by more powerful integrating techniques so as to overcome the stiffness of model equations.

Guria et al. (2005) observed that NSGA-II-aJG with the best set of computational parameters is the most rapidly converging technique for the MOO of reverse osmosis desalination units. Kachhap and Guria (2005) showed that NSGA-II-JG is superior to NSGA-II-aJG and NSGA-II in the MOO of copoly(ethylene-polyoxyethylene terephthalate) batch reactor. In the present study, NSGA-II-aJG and NSGA-II-JG were comparable for operation optimization but the former is better than the latter for design optimization. Hence, these algorithms should be thoroughly evaluated on both benchmark and application problems to establish their relative superiority, if any.

References

Agrawal, N., Rangaiah, G.P., Ray, A.K., Gupta, S.K., 2006. Multi-objective optimization of the operation of an industrial low-density polyethylene tubular reactor using genetic algorithm and its jumping gene adaptations. Industrial and Engineering Chemical Research 45, 3182–3199.

Agrawal, N., Rangaiah, G.P., Ray, A.K., Gupta, S.K., 2007. Design stage optimization of an industrial low-density polyethylene tubular reactor for multiple objectives using NSGA-II and its jumping gene adaptations. Chemical Engineering Science 62(9), 2346–2365.

Agrawal, S.C., Han, C.D., 1975. Analysis of the high-pressure polyethylene tubular reactor with axial mixing. American Institute of Chemical Engineering Journal 21, 449–465.

Anspon, H.D. in Smith, W.M., 1964. Manufacture of Plastics, vol. I, Reinhold: New York.

Asteasuain, M., Pereda, Brandolin, A., 2008. Modeling and optimization of a high-pressure ethylene polymerization reactor using gPROMS. Computers and Chemical Engineering 32(3), 396–408.

Asteasuain, M., Pereda, S., Lacunza, M.H., Ugrin, P.E., Brandolin, A., 2001a. Industrial high-pressure ethylene polymerization initiated by peroxide mixtures: A reduced mathematical model for parameter adjustment. Polymer Engineering and Science 41, 711–726.

Asteasuain, M., Tonelli, S.M., Brandolin, A., Bandoni, J.A., 2001b. Dynamic simulation and optimization of tubular polymerization reactors in gPROMS. Computers and Chemical Engineering 25, 509–515.

Asteasuain, M., Ugrin, P.E., Lacunza, M.H., Brandolin, A., 2001c. Effects of multiple feedings in the operation of a high-pressure polymerization reactor for ethylene polymerization. Polymer Reaction Engineering 9(3), 163–182.

Asteasuain, M., Bandoni, A., Sarmoria, C., Brandolin, A., 2006. Simultaneous process and control system design for grade transition in styrene polymerization. Chemical Engineering Science 61, 3362–3378.

Babu, B.V., Chakole, P.G., Mubeen, J.H.S., 2005. Multiobjective differential evolution (MODE) for optimization of adiabatic styrene reactor. Chemical Engineering Science 60, 4822–4837.

Bhaskar, V., Gupta, S.K., Ray, A.K., 2000. Applications of multiobjective optimization in chemical engineering, Review in Chemical Engineering 16, 1–54.

Bhaskar, V., Gupta, S.K., Ray, A.K., 2001. Modeling of an industrial wiped film poly (ethylene terephthalate) reactor. Polymer Reaction Engineering 9, 71–99.

Bhaskar, V., Gupta, S.K., Ray, A.K., 2001. Multi-objective optimization of an industrial wiped film poly (ethylene terephthalate) reactor: some further insights. Computers and Chemical Engineering 25, 391–407.

Brandolin, A., Capiati, N.J., Farber, J.N., Valles, E.M., 1988. Mathematical model for high-pressure tubular reactor for ethylene polymerization. Industrial and Engineering Chemical Research 27, 784–790.

Brandolin, A., Valles, E.M., Farber, J.N., 1991. High-pressure tubular reactors for ethylene polymerization optimization aspects. Polymer and Engineering Science 31, 381–390.

Brandolin, A., Lacunza, M.H., Ugrin, P.E., Capiati, N.J., 1996. High-pressure polymerization of ethylene. an improved mathematical model for industrial tubular reactors. Polymer Reaction Engineering 4, 193–241.

Buback, M., 1980. High-pressure polymerization of pure ethylene. Makromolekulare Chemie-Macromolecular Chemistry and Physics 181(2), 373–382.

Buchelli, A., Call, M. L., Brown, A. L., Bird, A., Hearn, S., Hannon, J., 2005a. Modeling fouling effects in LDPE tubular polymerization reactors. 1. Fouling thickness determination. Industrial and Engineering Chemical Research 44, 1474–1479.

Buchelli, A., Call, M. L., Brown, A. L., Bird, A., Hearn, S., Hannon, J., 2005b. Modeling fouling effects in LDPE tubular polymerization reactors. 2. Heat transfer, computational fluid dynamics, and phase equilibria. Industrial and Engineering Chemical Research 44, 1480–1493.

Buchelli, A., Call, M. L., Brown, A. L., Bird, A., Hearn, S., Hannon, J., 2005c. Modeling fouling effects in LDPE tubular polymerization reactors. 3. Computational fluid dynamics analysis of a reacting zone. Industrial and Engineering Chemical Research 44, 1493–1501.

Caruana, R.A., Schaffer, J.D., 1988. Representation and hidden bias: gray vs. binary coding for genetic algorithms, In: Proceedings of Fifth International Conference on Machine Learning, p. 153.

Cervantes, A., Tonelli, S., Brandolin, A., Bandoni, A., Beigler, L., 2000. Large-scale dynamic optimization of a low density polyethylene plant. Computers and Chemical Engineering 24, 983–989.

Chakraborti, N., 2004. Differential Evolution: the real-parameter genetic algorithm applied to materials and metallurgy, International Materials Reviews 49, 259–260.

Chankong, V., Haimes, Y.Y., 1983. Multiobjective Decision Making – Theory and Methodology, Elsevier: New York.

Chatzidoukas, C., Perkins, J.D., Pistikopoulos, E.N., Kiparissides, C., 2003. Optimal grade transition and selection of closed-loop in a gas-phase olefin polymerization fluidized bed reactor. Chemical Engineering Science 58, 3643–3658.

Chen, C.H., Vermeychuk, J.G., Howell, J.A., Ehrlich, P., 1976. Computer model for tubular high-pressure polyethylene reactors. American Institute of Chemical Engineering Journal 21, 463–471.

Coello, C.A.C., Christiansen, A.D., 1999. MOSES: A multi-objective optimization tool for engineering design. Engineering Optimization 31(3), 337–368.

Coello, C.A.C., Veldhuizen, V.D.A., Lamont, G.B., 2002. Evolutionary Algorithms for Solving Multi-objective Problems, Kluwer Academic: New York.

Coulson, J.M., Richardson, J.F., Backhurst, J.R., Harker, J.H., 1996. Coulson & Richardson's Chemical Engineering: Fluid Flow, Heat Transfer and Mass Transfer, vol. I, 5th Ed., Butterworth-Heinemann: Oxford, UK.

Deb. K., 2000. An efficient constraint handling method for genetic algorithms. Computer Methods in Applied Mechanics and Engineering 186, 311–338.

Deb, K., 2001. Multiobjective Optimization Using Evolutionary Algorithms, Wiley: Chichester, UK.

Deb. K., Pratap, A., Agarwal, A., Meyarivan, T., 2002. A fast and elitist multiobjective genetic algorithm: NSGA-II. IEEE Transactions on Evolutionary Computation 6, 182–197.

Donati, G., Marini, L., Marziano, G., Mazzaferri, C., Spampinato, M., Langianni, E., 1981. Mathematical model of low-density polyethylene tubular reactor. In Wei, J., Georgakis, C., Eds., Chemical Reaction Engineering. American Chemical Society Symposium Series. Vol. 196, p. 579.

Edgar, T.F., Himmelblau, D.M., Lasdon, L.S., 2001. Optimization of Chemical Processes, 2nd Ed., McGraw Hill: Boston.

Ehrlich, P., Mortimer, G.A., 1970. Fundamentals of the free radical polymerization of ethylene. Advance Polymer Science 7, 386–448.

Fonseca, C.M., Fleming, P.J., 1993. Genetic algorithms for multiobjective optimization: formulation, discussion and generalization. In Forrest, S. (Ed.), Proceedings of the Fifth International Conference on Genetic Algorithms. Morgan Kaufmann : San Mateo, CA, p. 416.

Gaylord, H.G., Mark, H.F., 1959. Linear and Stereoregular Addition Polymers, Wiley: New York.

Goldberg, D.E., 1989. Genetic Algorithms in Search, Optimization and Machine Learning, Addison-Wesley: Reading, MA.

Goto, S., Yamamoto, K., Furui, S., Sugimoto, M., 1981. Computer model for commercial high-pressure polyethylene reactor based on elementary reaction rates obtained experimentally. Journal of Applied Polymer Science 36, 21–40.

Gupta, S.K., Kumar, A., Krishnamurthy, M.V.G., 1985. Simulation of tubular low-density polyethylene. Polymer and Engineering Science 25, 37–47.

Gupta, S.K., 1995. Numerical Methods for Engineers; Wiley Eastern: New Delhi.

Guria, C., Bhattacharya, P.K., Gupta, S.K., 2005. Multi-objective optimization of reverse osmosis desalination units using different adaptations of the non-dominated genetic algorithm (NSGA), Computers and Chemical Engineering 29, 1977–1995.

Hafele, M., Kienle, A., Boll, M., Schmidt, C.-U., Schwibach, M., 2005. Dynamic simulation of a tubular reactor for the production of low-density polyethylene using adaptive method of lines, Journal of Computational and Applied Mathematics 183, 288–300.

Hafele, M., Kienle, A., Boll, M., Schmidt, C.-U., Schwibach, M., 2006. Modeling and analysis of a plant for the production of low-density polyethylene, Computers and Chemical Engineering 31, 51–65.

Haimes, Y.Y., 1977. Hierarchical Analysis of Water Resources Systems: Modeling and Optimization, McGraw Hill: New York.

Holland, J.H., 1975. Adaptation in Natural and Artificial Systems, University of Michigan Press: Ann Arbor, MI.

Hollar, W., Ehrlich, P., 1983. An improved model for temperature and conversion profiles in tubular high pressure polyethylene reactors. Chemical Engineering Communications 24, 57.

Homaifar, A, Lai, S.H.-V., Qi, X., 1994. Constrained optimization via genetic algorithms, Simulation 62 (4), 242–254.

Horn. J., Nafpliotis, N., Goldberg, D.E., 1994. A niched Pareto genetic algorithm for multiobjective optimization. Proceedings of the First IEEE Conference on Evolutionary Computation, p. 82.

Joines, J.A., Houck, C.R., 1994. On the use of nonstationary penalty functions to solve nonlinear constrained optimization problems with GAs, In: Michalewicz Z., (Ed.), Proceedings of the International Conference on Evolutionary Computation, IEEE Press: Piscataway, p. 579.

Kachhap, R., Guria, C., 2005. Multi-objective optimization of a batch copoly(ethylene-polyoxyethylene terephthalate) reactor using different adaptations of non-dominated sorting genetic algorithms. Macromolecular Theory and Simulations 14, 358–373.

Kalyon D.M., Chiou, Y.N., Kovenklioglu, S., Bouaffar, A., 1994. High pressure polymerization of ethylene and rheological behavior of polyethylene product. Polymer and Engineering Science 33, 804–814.

Kasat, R.B., Gupta, S.K., 2003. Multi-objective optimization of an industrial fluidized bed catalytic cracking unit (FCCU) using genetic algorithm with the jumping genes operator. Computers and Chemical Engineering 27, 1785–1800.

Katz S., Saidel, G.M., 1967. Moments of the size distribution in radical polymerization. American Institute of Chemical Engineering Journal 13, 319–326.

Kiparissides, C., Baltsas, A., Papadopoulos, S., John P., Congalidis, Richards, J. R., Kelly, M. B., Ye, Y., 2005. Mathematical Modeling of Free-Radical Ethylene Copolymerization in High-Pressure Tubular Reactors. Industrial and Engineering Chemical Research 44, 2592–2605.

Kiparissides, C., Verros, G., MacGregor, J.F., 1993a. Mathematical modeling, optimization, and quality control of high pressure ethylene polymerization reactors. Journal of Macromolecular Science-Reviews in Macromolecular Chemistry and Physics C33, 437–527.

Kiparissides, C., Verros, G., Kalfas, G., Koutoudi, M., Kantzia, C., 1993b. A comprehensive mathematical model for a multi-zone tubular high pressure LDPE reactor. Chemical Engineering Communications 121, 193–217.

Kiparissides, C., Verros, G., Pertsinidis, A., 1994. On-line optimization of a high-pressure low-density polyethylene tubular reactor. Chemical Engineering Science 49, 5011–5024.

Kiparissides, C., Verros, G., Pertsinidis, A., 1996. On-line parameter estimation in a high-pressure low-density polyethylene tubular reactor. American Institute of Chemical Engineering Journal 42(2), 440–454.

Kim, D., Iedema, P. D., 2004. Molecular weight distribution in low-density polyethylene polymerization; impact of scission mechanisms in the case of a tubular reactor. Chemical Engineering Science 59, 2039–2052.

Kondratiev, J.N., Ivanchev, S.S., 2005. Possibilities for optimization of technological modes for ethylene polymerization in autoclave and tubular reactors. Chemical Engineering Journal 107, 221–226.

Lacunza, M.H., Ugrin, P.E., Brandolin, A., Capiati, N.J., 1998. Heat transfer in a high pressure tubular reactor for ethylene polymerization. Polymer Engineering and Science 36, 992–1013.

Lee, K.H., Marano, J.P., 1979. Free-radical polymerization: sensitivity of conversion and molecular weights to reactor conditions. In Henderson, J.N., Bouton, T.C., Eds. Polymerization Reactors and Processes, American Chemical Society Symposium Series, vol. 104, p. 221.

Luft, G., Kampf, R., Seidl, H., 1982. Synthesis conditions and structure of low density polyethylene i. short and long chain branching. Die Angewandte Makromolekulare Chemie 108, 203–217.

Luft, G., Kampf, R., Seidl, H., 1983. synthesis conditions and structure of low density polyethylene ii. average molar mass and molar mass distribution. Die Angewandte Makromolekulare Chemie 111, 133–147.

Machi, S., Tamura, T., Hagiwara, M., Gotoda, M., Kagiya, T., 1966. Short-chain branching in γ-radiation-induced polymerization of ethylene. Journal of Polymer Science Part A-1 (4), 283–291.

Machi, S., Kawakami, W., Yamaguchi, K., Hosaki, Y., Hagiwara, M., Sugo, T., 1968. Structure and properties of polyethylene produced by γ-radiation polymerization in flow system. Journal of Applied Polymer Science 12, 2639–2647.

Man, K.F., Chan, T.M., Tang, K.S., Kwong, S., 2004. Jumping genes in evolutionary computing. Proceedings of the Thirtieth Annual Conference of the IEEE Industrial Electronics Society (IECON) [at Busan, Korea; 2 – 6 Nov, 2004]. vol. 2, IEEE: Piscataway, NJ, p.1268.

Mavridis, H., Kiparissides, C., 1985. Optimization of a high-pressure polyethylene tubular reactor. Polymer Process Engineering 3, 263–290.

McKlintock, B., 1987. The discovery and characterization of transposable elements. In The Collected Papers of Barbara McClintock, New York: Garland.

Michalewicz, Z., 1992. Genetic Algorithms + Data Structure = Evolution Programs. Springer-Verlag: Berlin.

Michalewicz, Z., Attia, N., 1994. Evolutionary optimization of constrained problems, In: Sebald, A.V., Fogel, L.J. (Eds.), Proceedings of the Third Annual Conference on Evolutionary Programming, World Scientific: Singapore, p. 98.

Michalewicz, Z., Schoenauer, M., 1996. Evolutionary algorithms for constrained parameter optimization problems. Evolutionary Computation 4(1), 1–32.

Micheles, A., Geldermans, M., 1942. Isotherms of ethylene up to 3000 atmospheres between 0° and 150°C. Physica 9, 967–973.

Musselman, K., Talavage, J., 1980. A Trade-off Cut Approach to Multiple Objective Optimization. Operations Research 28(6), 1424–1435.

Nandasana, A.D., Ray, A.K., Gupta, S.K., 2003. Dynamic model of an industrial steam reformer and its use for multiobjective optimization. Industrial and Engineering Chemical Research 42, 4028–4042.

Padhiyar, N., Bhartiya, S., Gudi, R.D., 2006. Optimal grade transition in polymerization reactors: A comparative case study. Industrial and Engineering Chemical Research 45, 3583–3592.

Parks, W., Richards, R.B., 1948. The effect of pressure on the volume, thermodynamic properties and crystallinity of polyethylene. Transactions in Faraday Society 45, 203–211.

Pladis, P., Kiparissides, C., 1998. A comprehensive model for the calculation of molecular weight-long chain branching distribution in free-radical polymerizations. Chemical Engineering Science 53(18), 3315–3333.

Poling, B.E., Prausnitz, J.M., O'Connel, J.P., 2001. The Properties of Gases and Liquids, 5th Ed., McGraw Hill: New York.

Rajesh, J.K., Gupta, S.K., Rangaiah, G.P., Ray, A.K., 2000. Multi-objective optimization of steam reformer performance using genetic algorithm. Industrial and Engineering Chemical Research 39, 706–717.

Rangaiah, G.P., 2007. Multi-Objective optimization techniques and applications in chemical engineering (Advances in Process Systems Engineering - Vol. 1), in preparation, World Scientific: Singapore.

Ray, A.K., Gupta, S.K., 2001. Mathematical Methods in Chemical and Environmental Engineering, Thomson Learning: Singapore.

Ray, T., Tai, K., Seow, C., 2001. An Evolutionary Algorithm for Multiobjective optimization. Engineering Optimization 33, 399–424.

Rodel, M.J., 1953. The molecular structure of polyethylene I. chain branching in polyethylene during polymerizations. Journal of American Chemical Society 75, 6110.

Rudolph, G., 1996. Convergence of evolutionary algorithms in general search spaces. In Proceedings of the Third IEEE conference on Evolutionary Computation, p. 50.

Rudolph, G., 2001. Evolutionary search under partially ordered fitness sets. In Proceedings of the International Symposium on Information Science Innovations in Engineering of Natural and Artificial Intelligent Systems (ISI 2001), p. 818.

Schaffer, J.D., 1984. Some experiments in machine learning using vector evaluated genetic algorithms. Ph.D. Thesis, Vanderbilt University, Nashville, TN.

Schaffer, J.D., Caruana, R.A., Eshelman, L.J., Das, R., 1989. A Study of control parameters affecting online performance of genetic algorithms for function optimization, In: Proceedings of 3rd International Conference on Genetic Algorithms (ICGA-1989), p. 81.

Simoes, A., Costas, E., 1999. Transposition: A biologically inspired mechanism to use with genetic algorithm. In: Dobnikar, A., Steele, N., Pearson, D. (Ed.), Proceedings of the Fourth International Conference on Neural Networks and Genetic Algorithms (ICANNGA99), Springer-Verlag: Portoroz, Slovenia, p. 178.

Srinivas, N., Deb, K., 1995. Multiobjective function optimization using nondominated sorting genetic algorithms. Evolutionary Computation 2, 221–248.

Tanaka, M., 1995. GA-based Decision Support System for Multicriteria Optimization. Proceedings of IEEE International Conference Systems, Man and Cybernetics, vol. 2, pp. 1556.

Tarafder, A., Rangaiah, G.P., Ray, A.K., 2005. Multiobjective optimization of an Industrial styrene monomer manufacturing process. Chemical Engineering Science 60, 347–363.

Tarafder, A., Lee, B.C.S., Ray, A.K., Rangaiah, G.P., 2006. Multiobjective optimization of an industrial ethylene reactor using nondominated sorting genetic algorithm. Industrial and Engineering Chemical Research 44, 124–141.

Tatsukami, Y., Takahashi, T., Yoshioka, H., 1980. Reaction mechanism of oxygen-initiated ethylene polymerization at high-pressure. Makromolekulare Chemie-Macromolecular Chemistry and Physics 181(5), 1107–1114.

Wajge, R.M., Rao, S.S., Gupta, S.K., 1994. Multi-objective dynamic optimization of a nonvaporizing nylon-6 batch reactor. Polymer Engineering and Science 34, 1161–1172.

Woodbrey, J.C., Ehrlich, P., 1963. The free radical high pressure polymerization of ethylene. ii. The evidence for side reactions from polymer structure and number average molecular weights. Journal of American Chemical Society 85, 1580–1589.

Yao, F.Z., Lohi A., Upreti, S.R., Dhib, R., 2004. Modeling, simulation and optimal control of ethylene polymerization in non-isothermal, high-pressure tubular reactors. International Journal of Chemical Reactor Engineering 2, 1–25.

Yee, A.K.Y., Ray, A.K., Rangaiah, G.P., 2003. Multi-objective optimization of an industrial styrene reactor. Computers and Chemical Engineering 27, 111–130.

Yoon, B.J., Rhee, H.K., 1985. A study of the high-pressure polyethylene tubular reactor. Chemical Engineering Communications 24, 253–256.

Zabisky, R.C.M., Chan, W.M., Gloor, P.E., Hamielec, A.E., 1992. A kinetic model for olefin polymerization in high-pressure tubular reactors: a review and update. Polymer 33, 2243–2261.

Zitzler, E., Deb, K., Thiele, L., 2000. Comparison of multiobjective evolutionary algorithms: empirical results. Evolutionary Computation 8, 173.

Zhou, F., Gupta, S.K., Ray, A.K., 2000. Multiobjective optimization of the continuous casting process for poly (methyl methacrylate) using adapted genetic algorithm, Journal of Applied Polymer Science 78, 1439–1458.

Appendix A

Moment Closure Technique by Assuming a Log-Normal Distribution

The moment closure technique has been adapted from Zabisky et al. (1992). If the molecular-weight distribution is assumed to be log-normal then the moment closure problem can be solved by expressing any integer moment of the distribution ($r > 2$) as a function of its lower moments. Thus, the log-normal distribution is defined as:

$$f(x) = \frac{1}{\left(\sqrt{(2\pi)}\sigma\right)x} \exp\left(-\frac{(\ln \mathbf{x} - \mu)^2}{2\sigma^2}\right) H(x) \tag{A.1}$$

Here, $H(x)$ is the unit step function (i.e., $H(x) = 1$ when $x > 0$ and $H(x) = 0$ for $x \leq 0$), and μ and σ are parameters.

The r^{th} moment of a variable x about the origin is defined as:

$$m_r = \int_{-\infty}^{\infty} x^r f(x)\, dx \tag{A.2}$$

For log-normal distribution, Equation (A.2) turns out to be:

$$m_r = \frac{1}{\left(\sqrt{(2\pi)}\sigma\right)} \int_0^{\infty} x^{r-1} \exp\left(-\frac{(\ln \mathbf{x} - \mu)^2}{2\sigma^2}\right) dx \tag{A.3}$$

By using appropriate variable changes, the integral in Equation (A.3) gives:

$$\int_0^{\infty} x^{r-1} \exp\left(-\frac{(\ln \mathbf{x} - \mu)^2}{2\sigma^2}\right) dx = \sqrt{(2\pi)}\sigma \exp\left(\mu r + \frac{\sigma^2 r^2}{2}\right)$$

Thus, substituting the equivalent of the integral in Equation A.3, the r^{th} moment of a variable x for log-normal distribution becomes:

$$m_r = \exp\left(\mu r + \frac{\sigma^2 r^2}{2}\right) \tag{A.4}$$

Note that the zeroth moment ($r = 0$) calculated from Equation (A.4) is unity due to probability density function $f(x)$. In order to satisfy this condition, the zeroth moment

of the molecular-weight distribution need to be normalized and the general result is given by:

$$Q_i^* = \frac{Q_i}{Q_o} \tag{A.5}$$

where the superscript * denotes the normalized moment. Thus, Equation (A.4) for the i^{th} moment is defined by:

$$m_i = Q_i^* = \frac{Q_i}{Q_0} \tag{A.6}$$

It should be noted that:

$$\frac{m_i}{m_j} = \frac{Q_i^*}{Q_j^*} = \frac{Q_i}{Q_j} \quad \text{for all } i, j \tag{A.7}$$

Now, the parameters, μ and σ^2, defined in Equation (A.1) are obtained in terms of the moments using Equation (A.6), which are given below.

$$\mu = \ln\left(\frac{Q_1^{*2}}{\sqrt{Q_2^*}}\right) \tag{A.8}$$

$$\sigma^2 = \ln\left(\frac{Q_2^*}{Q_1^{*2}}\right) \tag{A.9}$$

In order to express any integer moment ($r > 2$) as a function of its lower moments, we need to find a relationship among the moments. From Equation (A.4):

$$\frac{Q_3^*}{Q_2^*} = \frac{\exp\left(3\mu + \frac{9\sigma^2}{2}\right)}{\exp\left(2\mu + 2\sigma^2\right)} = \exp\left(\mu + \frac{5\sigma^2}{2}\right) \tag{A.10}$$

Substituting Equations (A.8), (A.9) and then (A.6) into Equation (A.10), the third order moment is obtained as follows:

$$Q_3 = \left(\frac{Q_2}{Q1}\right)^3 Q_0 \tag{A.11}$$

This equation is used for bi-variate moments in our study in the following forms:

$$Q_{03} = Q_{00}\left(\frac{Q_{02}}{Q_{01}}\right)^3 \tag{A.12}$$

$$Q_{13} = Q_{10}\left(\frac{Q_{12}}{Q_{11}}\right)^3 \tag{A.13}$$

Appendix B

Publications and Presentations of this Author

- Optimal Design of Chemical Processes for Multiple Economic and Environmental Objectives. In Multi-Objective Optimization Techniques and Applications in Chemical Engineering (Advances in Process Systems Engineering-Vol. 1), in preparation, Ed. by G.P. Rangaiah, World Scientific, Singapore, **2008**.
- Dynamic Model of an Industrial LDPE Tubular Reactor and its use for Optimal Grade-change for Multiple Criteria. ***Industrial and Engineering Chemical Research***, In reviews, **2008**.
- Design Stage Optimization of an Industrial Low-Density Polyethylene Tubular Reactor for Multiple Objectives using NSGA-II and its Jumping Gene Adaptations. ***Chemical Engineering Science,*** 62, 2346–2365, **2007**.
- Multi-objective Optimization of the Operation of an Industrial LDPE Tubular Reactor using Genetic Algorithms and its JG Adaptations. ***Industrial and Engineering Chemical Research,*** 45, 3182–3199, **2006**.
- Multi-Objective Design Optimization of an Industrial LDPE Tubular Reactor Using Jumping Gene Adaptations of NSGA and Constraint Handling Principle. Presented in ***AIChE Annual Meeting***, San Francisco, CA, USA, **2006**.
- An Effective Transformation for Enhancing Stochastic Global Optimization. Presented in ***AIChE Annual Meeting***, San Francisco, CA, USA, **2006**.
- Operation Optimization of an Industrial Polyethylene Reactor using Multi-objective Evolutionary Algorithms. Presented in ***CIRAS 2005***, Singapore, **2005**.

- Modeling and Multi-objective Optimal Operation of Ethylene Polymerization in an Industrial High-Pressure Tubular Reactor, Presented in ***CHEMCON 2005***, New Delhi, India, **2005**.